Dissertation

On

SHAPE OPTIMIZATION FOR GRINDING NOZZLE BY MULTI-FLUID SIMULATION AND EXPERIMENTAL VALIDATION

Submitted in partial fulfillment of the requirement for

the award of degree of

Master of Engineering

IN

CAD/CAM & Robotics

Submitted By

SAHIL SINGLA

Roll No. 800981020

Under the Guidance of

ANIRBAN BHATTACHARYA

Assistant Professor

Department of Mechanical Engineering

Thapar University, Patiala

DEPARTMENT OF MECHANICAL ENGINEERING

THAPAR UNIVERSITY

PATIALA-147004, INDIA,

ACKNOWLEDGEMENT

Words are often less to revels one's deep regards. With an understanding that work like this can never be the outcome of a single person, I take this opportunity to express my profound sense of gratitude and respect to all those who directly or indirectly helped me through the duration of this work.

I take the opportunity to express my heartfelt adulation and gratitude to my supervisor ***Anirban Bhattacharya*** *for his unreserved guidance, constructive suggestions, thought provoking discussions and unabashed inspiration in the nurturing work. It has been a benediction for me to spend many opportune moments under the guidance of the perfectionist at the acme of professionalism. The present work is testimony to his activity, inspiration and ardent personal interest, taken by him during the course of this work in its present form. I am grateful to* ***Dr. Ajay Batish****, Prof. & Head, MED for providing the facilities for the completion of the work.*

The non teaching staff, Mr. A.S. Cheema, Mr. Rajinder Kumar, Mr. R.K. Banerjee, Mr. Lalit Kumar and other members deserves special thanks for providing immense support in performing the practical work at mechanical workshop. No words acknowledge the support I received from my friends for their valorous help and co-operation.

I take pride of myself being son of ideal parents for their everlasting desire, sacrifice, affectionate blessings, and help, without which it would not have been possible for me to complete my studies.

I would like to thank to all the members and employees of Mechanical Engineering Department, Thapar University Patiala for their everlasting support. Above all, I express my indebtedness to the "ALMIGHTY" for all His blessing and kindness.

Sahil Singla

Reg. No.: 800981020

DECLARATION

I hereby declare that the work in this thesis report entitled **"SHAPE OPTIMIZATION FOR GRINDING NOZZLE BY MULTI-FLUID SIMULATION AND EXPERIMENTAL VALIDATION"** is an authentic record of my study carried out as requirement for the award of degree of **Master of Engineering (CAD/CAM & Robotics)** at **Thapar University, Patiala** under the guidance of **ANIRBAN BHATTACHARYA,** Assistant Professor, Department of Mechanical engineering, Thapar University, Patiala during **July 2010 to June 2011.** The matter embodied in this report has not been submitted in part or full to any other university or institute for the award of any other degree.

Sahil Singla

(Sahil Singla)
Reg. No. 800981020

This is to certify that above declaration made by the student concerned is correct to the best of my knowledge and belief.

Anirban Bhattacharya

(ANIRBAN BHATTACHARYA)
Assistant Professor,
Department of Mechanical Engineering,
Thapar University,
Patiala-147004

Countersigned by:

Dr. AJAY BATISH
Professor and Head,
Department of Mechanical Engineering,
Thapar University,
Patiala-147004

Dr. S.K. MOHAPATRA
Dean of Academic Affairs,
Thapar University,
Patiala-147004

ABSTRACT

Grinding is a vastly used manufacturing process in which abrasives are used to cut down the material of work piece .In grinding heat generation is very large which has some very bad effects like in can alter the dimensional accuracy, physical properties of workpiece (surface roughness, microhardness etc) and it can also reduce the life of grinding wheel. The present study has been carried out to refine the grinding process by optimized cooling system. Input parameters are varied and their effect is studied according to the desired response. Both software and experimental approaches have been adopted to achieve the goal. Multi-fluid simulation is used to know the behaviour of fluid flow through the nozzle and also to find the fluid flow behaviour in grinding zone with the help of Computational fluid dynamic software ANSYS CFX. Computer simulation is done on various nozzle geometries and on the bases of peak velocity and its distance from nozzle outlet three nozzles have been selected. Design of Experiment is used in this Taguchi L_9 orthogonal array is applied to carry out the grinding process simulation and experimental validation for four input parameters wheel speed, workpiece speed, nozzle angle and nozzle tip distance. An experimental setup is created to vary input parameters. The effect of these input parameters has been checked on output responses, velocity of fluid in grinding zone, dimensional control, surface hardness and surface cracks. ANOVA is used to analyse the results of taguchi design for input parameters with the help of significance graphs to study which input parameter effects more the output response.

INDEX

LIST OF FIGURES

LIST OF TABLES

ABBREVIATIONS AND NOTATION

ANOVA	Analysis of Variance
CAD	Computer Aided Designing
CBN	Cubic Boron Nitride
CFD	Computational Fluid Dynamics
CI	Confidence Interval
DOF	Degree of Freedom
FEA	Finite Element Analysis
HEDG	High Efficiency Deep Grinding
MS	Mean of Squares
OA	Orthogonal Array
S/N	Signal to Noise ratio
SS	Sum of Squares

CHAPTER 1
INTRODUCTION TO GRINDING PROCESS

1.1 PREAMBLE OF GRINDING PROCESS

Origin of grinding is more than 20 centuries old. In initial years Abrasive stones were used to give shapes to tools, weapons, for cutting and polishing gems, for cutting and shaping rocks and stones, for construction of buildings etc. Abrasives are used in most of today's industrial applications.

In Nineteenth century, Grinding developed as a manufacturing Process. Electronic devices, I.C engines and aeronautical tools and instruments were manufactured with the help of grinding process. In the second half of the twentieth century, it was recognised that grinding is a strategic process for high-technology applications. It was realised, for example, by manufacturers of aeronautic engines and missile guidance systems that grinding was the key to achieving the necessary quality. This provided the motivation for rapid development in the latter part of the twentieth century. More recently still, grinding has become a strategic process for the production of optical quality surfaces for communications and electronic devices [1].

In abrasive machining, material is removed as abrasive grits at high speed comes in contact with the work-piece (Figure. 1.1), with small penetration depths and the chips that are produced by other machining processes. The results of abrasive machining range from the finest and smoothest surfaces to coarse and rough surfaces depending upon different material removal rates and different abrasive grits.

Figure 1.1: Surface grinding machine [2]

1.2 ABRASIVES

An abrasive is a material that is used to shape or finish a work piece through rubbing which leads to part of the work piece being worn away. While finishing a material often means polishing it to gain a smooth, reflective surface it can also involve roughening as in satin, matte or beaded finishes. Abrasives are extremely commonplace and are used very extensively in a wide variety of industrial, domestic, and technological applications. This gives rise to a large variation in the physical and chemical composition of abrasives as well as the shape of the abrasive.

These minerals are either crushed or to small size (anywhere from macroscopic grains as large as about 2 mm to microscopic grains about 0.001 mm in diameter shown in figure. 1.2) to permit their use as an abrasive. These grains, commonly called grit, have rough edges, often terminating in points which will decrease the surface area in contact and increase the localised contact pressure.

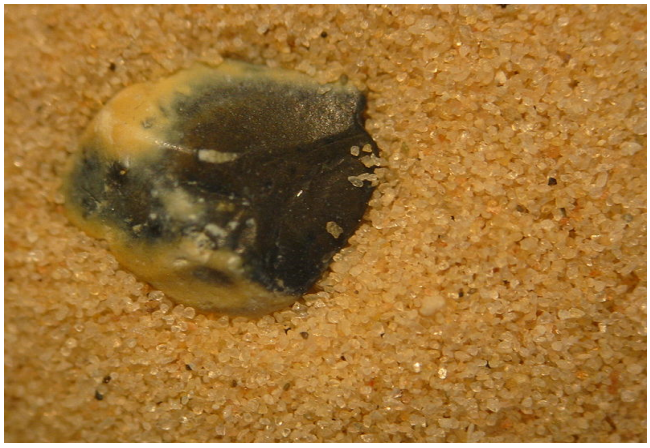

Figure 1.2: Differences in the size of sand [3]

Some typical abrasives provided by manufacturing are:

i. Super abrasives

- Diamond
- Cubic boron nitride

ii. Conventional abrasives

- Silicon carbide
- Aluminium oxide
- Quartz
- Glass

i. ***Diamond:*** Diamond is the hardest material and is used to grind the hardest ceramics. Main advantages of diamond as an abrasive, is the retention of hardness at high temperatures (up to 800°C). Diamond is a form of carbon and carbon is soluble with iron which makes it unsuitable for grinding steels. Diamond has very good thermal properties that help in reducing grinding temperatures. The highest thermal conductivity of any material lies between the values 600 and 2000 W/m-K at ambient temperatures, which falls to 70 W/m - K at 700°C. Diamond is vulnerable to thermal shocks, so sudden application of coolant to red hot diamond can increase its wear. Diamonds are used as single point dressing and cutting tool.

ii. ***Cubic Boron Nitride:*** It is second hardest material and is used to grind Steels. It is much more expensive than other conventional abrasives. Because of its low wear rate and ability to achieve high dimensional accuracy it is used for precision grinding of hardened steels Electroplated CBN is used these days for high efficiency deep grinding (HEDG). CBN is thermally efficient in inert atmospheres up to 1500°C. CBN forms a stable layer of boron oxide in air that prevents further oxidation up to 1300°C. This layer is dissolvable in water so wear rate of CBN is more with water miscible coolants.

iii. ***Silicon Carbide:*** It is hardest conventional abrasive. It is used primarily for grinding non ferrous materials, because it wear more when used for grinding material which have affinity for carbon like iron and nickel. It has low impact resistance than aluminium oxide. Because of its hardness it is used to grind less ductile materials. Black Silicon carbide is less hard so it used to grind ductile non-ferrous materials and ceramics.

iv. ***Aluminium Oxide:*** Also Know as corundum, is used for a wide range of ferrous materials including steels. Its grains may be either blocky or sharp according to preparation and purity. Blocky grains with high impact resistance are better for heavy stock removal operations. Tough grains like zirconia alumina are used for heavy removal rates in order to enhance micro-fracture. Adding 0.5-5.0% chromium oxide can increase friability and adding 2% titanium oxide (TiO,) increases toughness. Generally brown alumina is used in vitrified and resinoid wheels for rough grinding.

The abrasive particles (grains) can be mounted on a resin on a belt, or can be packed on stone wheels by bonding material.

Abrasive machining processes follow same metal removal process but the spacing of active grains creates the difference in finish of grinded surfaces [1, 3].

1.3 BONDED ABRASIVES

For high material removal rate abrasives grains are bonded together in different shapes, as single grain can remove very small amount of material. A bonded abrasive is composed of an abrasive material contained within a matrix. This matrix is called a binder and is often clay, a resin, a glass or a rubber. This mixture of binder and abrasive is typically shaped into blocks, sticks, or wheels. For cooling and chip clearance some porosity is required between the grains in bonded wheels [3, 4].

1.3.1 Types of Bonds

Organic bonds: These bonds are more elastic than other bonds. Elasticity can be useful for safety at high speeds. These bonds are used mainly with conventional abrasives to achieve extremely low roughness. The come in variety of bond types. Plastic include epoxy and polyurethane plastics and are used in burn sensitive applications such as knife grinding. phenolic bonds are used in heavy stock removal and also where grinding operation puts heavy twisting load on grinding wheel side walls. Organic bond wheels wear with high temperatures. Polyamide wheels were developed to improve this thermal resistance property. They can withstand heat upto 300^{o}C. Rubber wheels are used for cut-off wheels and control the wheels in centreless grinding. For finishing operations shellac wheels are used because they softer and more flexible so there is less risk of scratching while polishing [1].

Vitrified Bonds: These bonds are much harder than organic bonds are softer than metal bonds. Its favourable property is that it can be trued to produce the various profiles and also to sharpen the wheel when it gets blunt. In conventional grinding most common is vitrified alumina Wheel. In superabrasive grinding most common is vitrified CBN Wheel. They are made from mix of glass frits, clays, and fluxes such as feldspar and borax. This bond material is then mixed with a binder dextrin and water then this mixture is moulded in a mould. Wheel is then heated in a controlled temperature and cooling cycle upto 1300^{o}C [1].

Metalic Bonds: These bonds are used for superabrasives. Diamonds or CBN grains can be mounted in a single layer onto a metal disk or as a multi-layer abrasive in a sintered cast iron bond. In single-layer wheels much time is required to set the grains accurately on the surface, this thing makes them very expensive. Electroplating is commonly used to fix the grains onto the wheel disk as an alternative, or this can be done by brazing. But temperature needed in this process is much higher than electroplating so there is a risk of damaging the grains. As grains are larger in single layer superabrasive wheels, that makes it very reliable for grinding

hardest materials. Electroplated CBN wheels are more commonly used for high removal rates, high speed precision grinding and long wheel life. They are used for grinding ceramics and highly brittle abrasive materials. Multi layer superabrasives have small grains in size so they are used for high surface finish and high accuracy. Electrolytic in-process dressing system is used to maintain the sharpness of multi layer wheels [1].

1.4 GRINDING WHEEL

A grinding wheel is an expendable wheel used in grinding machine that is made of an abrasive compound (matrix of coarse particles pressed and bonded together) used for various grinding operations to form a solid, circular shape, various profiles and cross sections depending on the usage for the wheel (Figure 1.3). They can be made from a solid steel or aluminium disc with particles bonded to the surface. These wheels are manufactured in a very precise and tightly controlled process, because of the inherent safety risks of a spinning disc, and also the composition and uniformity which is required to prevent that disc from exploding due to the high stresses produced on rotation [5].

Figure 1.3: Grinding wheels [5]

1.5 GRINDING WHEEL SPECIFICATIONS

Grinding wheels are specified by different parameters like wheel types, sizes and other properties of abrasive wheels:

According To the Type of Wheels [6]

i. ***Straight grinding wheel:*** Straight grinding wheel are the most common mode of wheel widely used for centreless & cylindrical surface grinding operations. As it is used only on the periphery, it forms a little concave surface on the piece. The size of these wheels (width & diameter of its face) varies depending on the category of work, machines grinding power.

ii. ***Cylinder or wheel ring:*** A cylinder wheel is used to produce flat surface, it has no centre mounting support but has a long & wide surface. Their width varies up to 12 inches and is used only in horizontal or vertical spindle grinders.

iii. ***Tapered grinding wheel:*** Tapered Grinding wheel is a straight wheel that tapers externally towards the midpoint of the wheel. As this pact is stronger than straight wheels, it accepts advanced lateral loads. Straight wheel with tapered face is chiefly used for gear teeth, grinding thread, etc.

iv. ***Straight cup:*** This Straight cup wheels forms an option for cup wheels in cutter and tool grinders, having an extra radial surface of grinding is favourable.

v. ***Dish cup:*** This is used primarily in jig grinding and cutter grinding. It is a very thin cup-style grinding wheel which permits grinding in crevices and slot.

vi. ***Saucer grinding wheel:*** Saucer Grinding Wheel is used for grinding twist drills and milling cutters. So it has wide usage in non-machining areas, as this saw filers are used by saucer wheels to maintain saw blades.

vii. ***Diamond grinding wheel:*** Diamond wheel is used to grind hard materials like concrete, gemstones & carbide tips. In diamond wheels industrial diamonds remain bonded to the edge.

According to the Standard Marking System for Grinding Wheel [4]

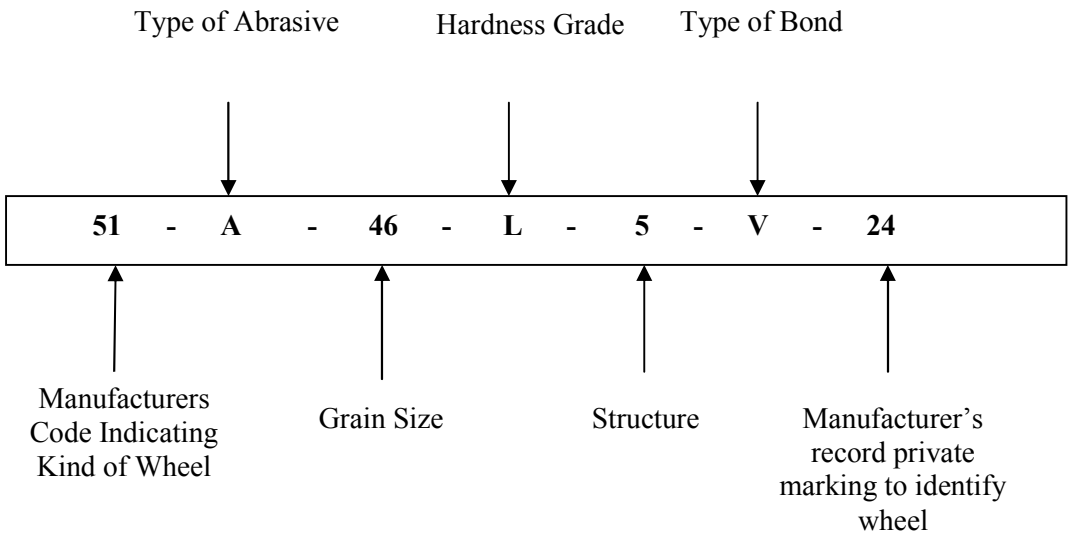

Figure 1.4: Standard marking systems for grinding wheel [4]

Code Specifications [4]:

Type of Abrasive:	A - Aluminium oxide
	C – Silicon Carbide
Grain Size:	Course - 8,10,12,14,16,20,24
	Medium – 30, 36, 46, 54, 60
	Fine – 70, 80, 90, 100, 120, 150, 180
	Very Fine – 220, 240, 280, 320, 280, 320, 400, 500, 600
Hardness Grade:	Soft – ABCDEFGH
	Medium – IJKLMNOP
	Hard – QRSTUVWXZ
Structure:	Dense to Open
	1 to 16
Type of Bond:	B – Resinoid
	BF – Resinoid Reinfoced
	E – Shellac
	O – Oxychloride
	R – Rubber
	RF – Rubber Reinforced
	S – Silicate
	V - Vitrified

1.6 GRINDING MECHANICS

A grinding wheel removes material in a similar way to a micro-milling cutter. In micro-milling, the cutting tools are identical in shape. The situation is quite different in grinding. The cutting tools in a grinding wheel are the grains, and material removal depends on their shape and position. The shapes and positions are both random distributions that change with wear. Grinding forces, accuracy, and wheel wear all depend on the amount of material removed by individual grains. Blunt worn grains are much less efficient than sharp grains. Material removal by grains provides a basis for understanding forces, power, roughness, and temperature with different grinding geometries and abrasives.

Major factors that differentiate the action of a single grain from that of a single point tool are as follow:

a) Grains have highly negative (-60^0 or even lower) average rake angle, so the shear angles are very low too.

b) Geometry of an individual grain is not regular and grains are randomly spaced over the surface of wheel.

c) As compared to turning operation in grinding the temperature generation is much higher that can lead to the surface burn of the work piece.

d) Grinding wheels operate at very high cutting speeds, typically 30m/sec.

e) In grinding operation depth of cut given is low (10-20 microns) and cutting force and power consumption is much higher.

Consider a surface grinding operation shown in Figure 1.5 to understand the Mechanics of Grinding. In this figure,

Diameter of grinding wheel cutting a layer of a metal is D

Wheel depth of cut is d.

Tangential velocity of an individual grain of the wheel is V.

Working piece is moving at a velocity v.

Thickness and length of undeformed chip removed by the grain is t, l.

Diameter of the work piece is D_w.

The undeformed chip length is approximately $\mathbf{l} \approx \sqrt{D.d}$, for **v<<V**

For external (cylindrical) grinding $\mathbf{l} = \sqrt{\frac{D.d}{l+(\frac{D}{Dw})}}$

And for internal grinding $\mathbf{l} = \sqrt{\frac{D.d}{l-(\frac{D}{Dw})}}$,

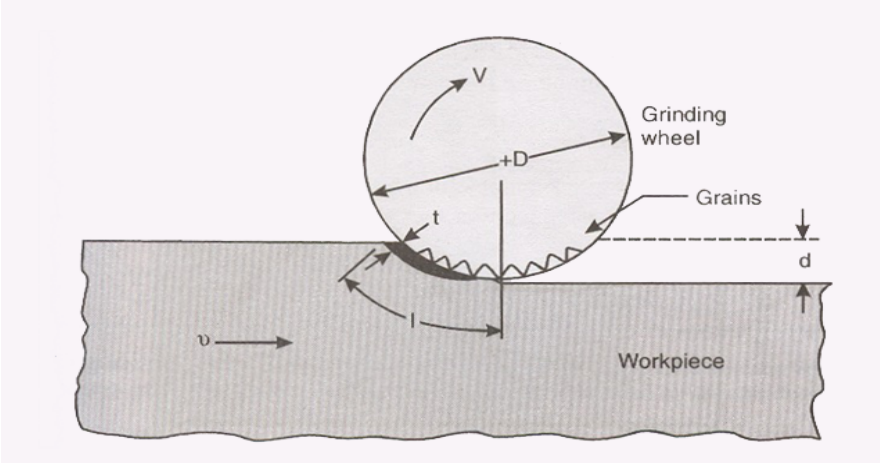

Figure 1.5: Variables in Surface Grinding [4]

The relationship between t and other process variables:

Let the width of work piece is unity and number of cutting points per unit area of the wheel surface are C. Let the Ratio of the chip width w to the average chip thickness is r. Then

The number of chips produced per unit time is V.C

Volume of the material removed per unit time is vd.

The volume of the chip with rectangular cross-sectional area and constant width is

$\mathbf{Vol_{chip}} = \frac{\mathbf{w.t.l}}{\mathbf{2}} = \frac{\mathbf{r.t^2.l}}{\mathbf{4}}$.

The volume of material removed per unit time **vd** =**VC.** $\frac{\mathbf{r.t^2.l}}{\mathbf{4}}$

The undeformed chip thickness $\mathbf{t} = \sqrt{\frac{4v}{VCr}}\sqrt{\frac{d}{D}}$ (because $\mathbf{l}=\sqrt{D.d}$,) [1, 3, 4, 7, 8].

1.6.1 Grinding Forces and Power

It is very useful to know about the grinding forces involved in grinding process for the design of grinding machine and its power. Grinding power can be calculated from the grinding forces. Grinding force resolved into three components: tangential force F_t, normal force F_n, and axial force F_a. as shown in figure 1.6.

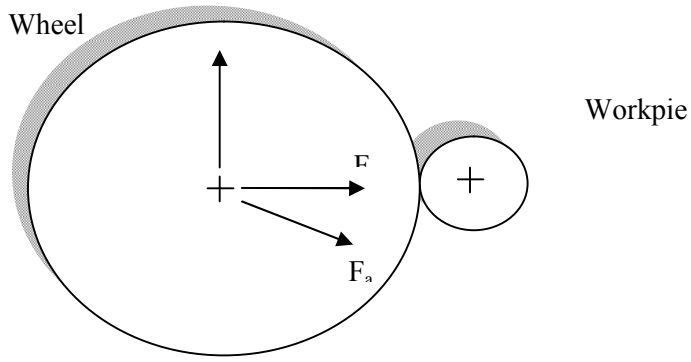

Figure 1.6: Grinding forces components [1]

Grinding Power $\mathbf{P} = F_t.(V \pm v) + F_n.v_{fn}, + Fa.v_{fa}$

Where v_{fn} is normal feed speed and v_{fa} is axial feed speed

Plus sign in tangential power component is for up cut grinding and minus sign is for down cut grinding. As V>>v and normal and axial feed speeds v_{fn} and v_{fa}, respectively, are much smaller than the wheel speed, so that grinding power is given quite closely by F_t. The normal and axial feed speeds are much smaller than the wheel speed V, so that grinding power is given quite closely by $F_t.V$ [1].

1.6.2 Grinding Force Ratio

There is another useful parameter 'Grinding force ratio' which provides information about the efficiency of grinding.

The force ratio is defined as $\boldsymbol{\mu} = F_t / F_n$

When grinding wheel is sharp, then grinding force ratio is high as the $F_n < F_t$

When grinding wheel gets blunt, then grinding force ratio is low.

Because of similarities in the mechanics of friction and grinding the grinding force ratio is similar to friction coefficient [1].

1.7 GRINDING TEMPERATURE

In grinding during metal cutting very high temperature is achieved than other machining processes. Temperature rise can be too excessive that it can unfavourably influence the surface properties and cause residual stresses on the work piece. Also, differential thermal expansion and contraction due to temperature gradients can cause the distortions in workpiece, so difficult to control dimensional accuracy.

The surface temperature rise, ΔT, is a function of ratio of the total energy input to the surface area ground. $\Delta \mathbf{T} \boldsymbol{\alpha} \frac{\boldsymbol{uwLd}}{\boldsymbol{wL}} \boldsymbol{\alpha}$ **ud (**L is the length of the surface area ground and w is the width).

Temperatures rise in the chip generation during grinding can reach as high as 1650^0C. Sparks are seen during grinding because of the exothermic reaction of the hot chips with oxygen in the atmosphere.

Effects of Temperature in Grinding

The following list describes briefly the major effects of temperature in grinding:

i. ***Temperature:*** Excessive temperature rise caused by grinding can temper and soften the surfaces of steel components, which are often ground in the hardened state. The use of grinding fluids can effectively control temperatures.

ii. ***Burning:*** The surface may burn if the temperature is excessive. The thermal cracks can appear on surface of workpiece or it can experience metallurgical burn, which is due to the martensite formation in high carbon steels from reaustenization followed by rapid cooling.

iii. ***Residual stress:*** Another severs effect of temperature gradients within the workpiece is generation of residual stress in grinding which decreases fatigue strength. The application of the grinding fluid also has a significant effect on the residual stresses. [4, 8].

1.8 TYPES OF GRINDING PROCESSES

1.8.1 Surface Grinding

Surface grinding uses a rotating abrasive wheel to smooth the flat surface of metallic or nonmetallic materials to give them a more refined look or to attain a desired surface for a functional purpose (Figure 1.7).

Figure 1.7: Surface grinding [10]

There are four basic types of grinding machines:

1. Horizontal spindle and reciprocating table
2. Vertical spindle and reciprocating table
3. Horizontal spindle and rotary table
4. Vertical spindle and rotary table.

1. Horizontal spindle and reciprocating table: It is the most common type of surface grinding. The table has longitudinal reciprocating motion. The wheelhead has transverse motion at the end of each table motion, these motions can be controlled manual handwheel or by hydraulic power feed using limiting switch.

2. Vertical spindle and reciprocating table: These grinders are different from horizontal spindles only because their spindles are vertical and wheel diameter must exceed the width of the surface to be ground. These machines are able to produce very flat surface**.**

3. Horizontal spindle and rotary table: They are not used in great extent because the type of the work a horizontal spindle can accommodate is very limited.

4. ***Vertical spindle and rotary table:*** They are primarily production type machines. Because these grinders have more than one grinding heads, therefore both rough and finish grinding can be achieved in one rotation of the work-piece [4, 9].

1.8.2 Cylindrical Grinding

Cylindrical grinding (also called centre-type grinding) is used in the removing the cylindrical surfaces and shoulders of the workpiece. The workpiece is mounted and rotated by a workpiece holder, also known as a grinding dog or canter driver. Both the grinding wheel and the workpiece are rotated by separate motors and at different speeds in opposite directions (Figure 1.8). Grinding wheel normally rotates at 23 to 40 m/s. The axes of rotation tool can be adjusted to produce a variety of shapes.

Figure 1.8: Cylindrical grinding [11]

In plain centre type grinder work-piece is mounted between the headstock and tailstock centres. The table assembly can be Slide, mostly, by hydraulic drive. Its speed can be varied and dog carrier can be used to control the length of movement. Workpiece can be held in chuck or between headstock and tailstock centres. Tailstock can move in longitudinal direction to hold the workpieces of different length. Wheel head moves in perpendicular direction to the table to provide infeed. Workpiece chuck and grinding wheel spindle is rotated by two separate electric motors. There speeds can be varied by pulley system or by voltage regulators. The infeed can be provided by manual feeding system with least amount of 0.01 mm. Most machines have automatic infeed system which can be used to produce required size of workpiece. These machines also have self dressing diamond turning system.

Long workpieces are held using dog carriers the shape of ground surface depends upon the shape in which grinding wheel is dressed.

In universal grinders, taper parts can be ground because both the work-piece and the wheel axis can be moved and Rotate around a horizontal plane [4].

1.8.3 Centreless Grinding

In this type of grinding cylindrical workpiece is not mounted between centres or chuck and can grind both cylindrical and external surface of workpiece. It reduces the cycle time because no need to mount the job in chuck and no need to make centre holes in work piece. Workpiece is grinded with the help of two wheels as shown figure1.9. The larger wheel is grinding wheel which does actual grinding. Grinding wheel can rotate with speed upto 10000 m/min. The smaller wheel is the regulating wheel (at speed usually 16 to 60 m/min) which controls the rotation and longitudinal motion of workpiece.

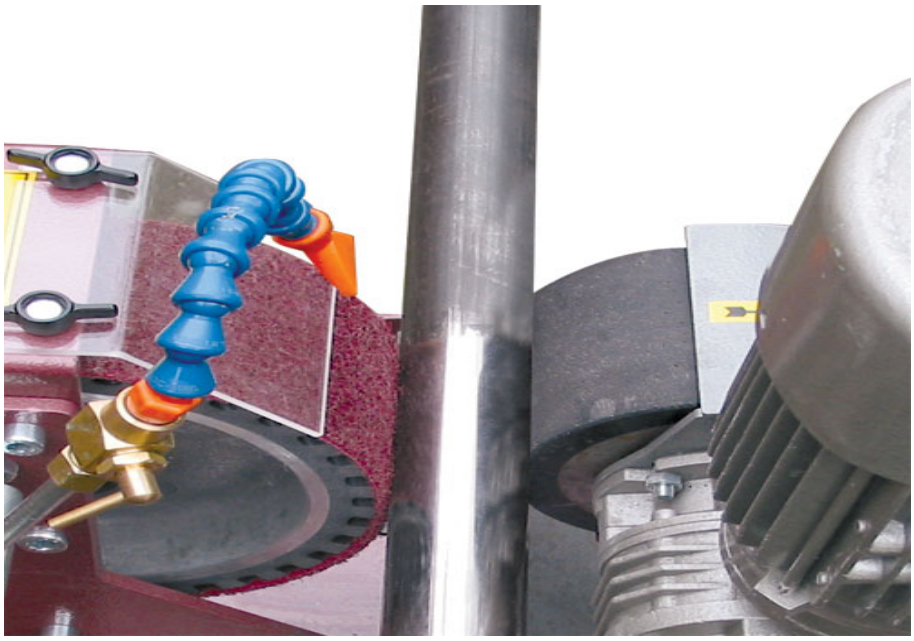

Figure 1.9: Centreless grinding [12]

1.8.4 Internal Grinding

These type of grinders are used to grind the inside diameter of a part such as bushings and bearing races. A small size grinding wheel is used for that purpose. Grinding wheel speed can be varied from 30,000 rpm to 1,00,000 rpm. Different profiles can be ground inside the workpiece with profile-dressed wheels. Taper holes can be ground by swirling the headstock [4].

1.9 CUTTING FLUIDS

Cutting fluids are very important in grinding process to keep the temperature under control during grinding because excessive heat can damage the microstructure of metals. They are also used to reduce the effects of friction. Proper use of coolants can make higher metal removal rates possible. Coolants can also help improve part quality and dimensional accuracy.

1.9.1 Need of Cutting Fluid

i. ***Cooling:*** Grinding operations create heat. This heat must be removed from the process. The chip helps carry away heat from the tool and work piece. Coolant takes heat from the chips, tool, and work piece. To be effective the fluid must be able to transfer heat very rapidly. The fluid absorbs the heat and carries it away.

ii. ***Lubrication:*** In a grinding operation, two-thirds of the heat is created by the resistance of the work piece atoms to being sheared. The friction of the chip sliding over the cutting tool face creates the other one-third of the heat. Cutting fluid with good lubrication qualities can reduce the friction of the chip sliding over the tool face. The lubrication actually changes the shear angle, which reduces the shear path and produces a thinner chip. Good lubrication also reduces internal friction and heat through less molecular disturbance [13].

1.9.2. Effects of Cutting Fluids

i. ***Improve Part Quality:*** The removal of the heat prevents the work piece from expanding during the machining operation, which would cause size variation as well as damage to the material's microstructure.

ii. ***Reduce tooling costs:*** Proper use of cutting fluids increases tool life, which reduces the tooling costs.

iii. ***Increase Cutting Speeds and Feeds:*** This allows high speeds and feeds to be used to achieve optimal cutting conditions.

iv. ***Improved Surface Finishes:*** Effective use of cutting fluids helps remove the chips. This prevents the chip from being caught between the tool and work piece where it causes scratches and a poor surface finish.

v. ***Rust and Corrosion Prevention:*** Cutting fluids should protect the tooling, machine, and work piece against rust and corrosion. Cutting fluids should leave a small residual film that remains after the water has evaporated [13].

1.9.3 Types of Cutting Fluids

Cutting fluids can be broken into four main categories:

i. Water miscible fluid

ii. Straight cutting oils

iii. Gas jet cooling

iv. Paste or solid lubricants.

Water is the best fluid for cooling. It has the best ability to carry heat away. Water quality has a large effect on the coolant. Water can be deionized to remove the impurities and minerals. Water that is very hard (high mineral content) can cause rust, stains, and corrosion of machines and work pieces, so it is a poor lubricant. Oil is great for lubrication but very poor for cooling. Oil is also flammable.

a) Water Miscible Fluids

Pure water can be used as a grinding fluid for occasional operation where only a small quantity of water is required. Example of Water based cutting is shown in figure 1.10.

Figure1.10: Water-miscible cutting fluid application [14].

i. ***Emulsions:*** Emulsion is a term that describes soluble oils. An emulsion is a suspension of oil droplets in water. Soluble oils are mineral oils that contain emulsifiers. Emulsifiers are soap-like materials that allow the oil to mix with water. Emulsions (soluble oils) when mixed with water produce a milky white coolant. Lean concentrations (more water-less oil) provide better cooling but less lubrication. Rich concentrations (less water- more oil) have better lubrication qualities but poorer cooling. There are different types of soluble cutting fluids available including extreme pressure soluble oils. These should be used for extreme machining conditions where it is necessary to reduce friction where the tool and work piece contact each other [13].

ii. ***Chemical fluids:*** Chemical coolants are also water miscible cutting fluids. Chemical cutting fluids are pre-concentrated emulsions that contain very little oil. Chemical fluids mix very easily with water. The chemical components in the fluid are used to enhance the lubrication, bacterial control, rust, and corrosion characteristics. There are several types of chemical coolants available, including coolants for extreme cutting conditions. Inactive chemical cutting fluids are usually clear fluids with high rust inhibition, high cooling, and low lubrication qualities. Active chemical fluids include wetting agents. They have excellent rust inhibition and moderate lubrication and cooling properties. Some contain sulphur or chlorine additives for extreme pressure cutting applications [13].

iii. ***Semi-chemical coolants:*** Semi-chemical fluids are a combination of a chemical fluid and an emulsion. They have lower oil content but more emulsifier. This makes the oil droplets much smaller. They have moderate lubrication and cooling and high rust inhibition properties. Sulphur, chlorine, and phosphorous are sometimes added to improve the extreme pressure characteristics [13].

b) Straight Cutting Oils

Straight cutting oils are not mixed with water so can be called as neat oils. Cutting oils are generally mixtures of mineral oil and animal, vegetable, or marine oils to improve the wetting and lubricating properties. Sulphur, chlorine, and phosphorous compounds are sometimes added to improve the lubrication qualities of the fluid for extreme pressure applications. There are two main types of straight oils: active and inactive.

The main advantage of neat oils when compare to water based fluids is reduced wheel wear. This is due to improved lubrication. The use of neat oil greatly reduces the tendency for the wheel loading and in this respect it is better than water –based fluid for reducing the buildup of wear flats.

Neat oil is thermally stable at temperatures up to approximately 200^0C but can withstand burn-out at temperature up to 300^0C neat oils may be mineral oils or synthetic oils [1].

i. ***Synthetic Oils:*** Synthetic oil may be derived from hydro carbons or from other chemicals. Synthetic oil tends to be considerably more expensive than mineral oils. This oil tends to be purer and is produced for particular properties such as high temperature stability. Synthetic oil may be hydrocarbons. Type of synthetic oil may include organic esters, silicon, and halogenated organic compound [1].

ii. ***Mineral Oils:*** Mineral oil is refined petroleum-based hydrocarbons. Mineral oil is combinations of paraffin, napthene, and aromatic oils. A wide variety of mineral oil compositions are employed in cutting and grinding fluids. A lubrication property is modified for different purposes [1].

c) Gas-Jet Cooling

Cutting oils and water miscible types of cutting fluids are the most common but compressed air and inert gasses are also used where direct water miscible or oil cannot be as in medical applications. Carbon dioxide, Freon, and nitrogen are also used sometimes.

i. ***Mist Cooling:*** A new method proposed involves injecting a small quantity of water mist into an air jet. This method has virtue of simplicity and low risk. Early result encouraging although the limitation is probably similar to these of other MQL methods [1].

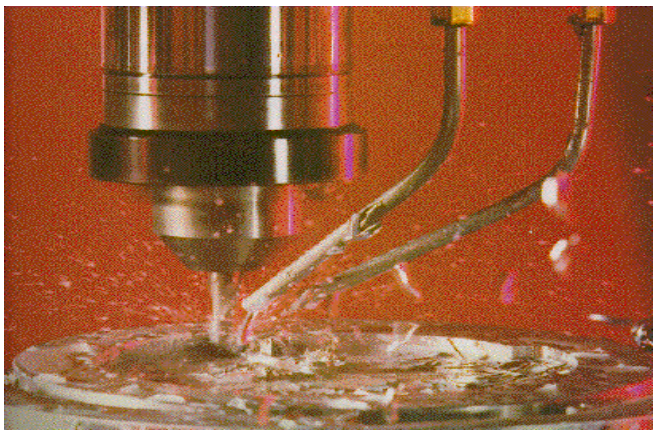

Figure1.11: Mist cooling application [15]

ii. ***Ice-Air Jet Blasting:*** The very fine ice particle can be used to safely clean surfaces for medical or other application where solvent are not permissible. This raises the question of possible development for a range of applications including wheel cleaning. An application demonstrated was the removal of glue from the rubber surface without damage to the rubber surface [1].

d) Paste and Solid Lubricants

Waxes, pastes, soaps, graphite, and molybdenum disulfide can also be used as lubricants. These are generally applied directly to the work piece or tool, or in some cases, impregnated directly into a tool, such as a grinding wheel. One example is lard and is recommended for tapping by many researchers [13].

CHAPTER 2

LITERATURE REVIEW

2.1 INTRODUCTION

Grinding is a machining process which has played consistently an important role in Metal manufacturing industry from early times. Because of increasing need of manufacturing complex components with strict geometrical dimensions and tolerances, there are many advancements have been done so far in grinding process to improve the quality of components being manufactured. Some of the Literature review is presented here.

2.2 CATEGORISATION OF LITERATURE

Literature is categorised as following:

i. Grinding process and fluid applications
ii. Experimental and simulation work
iii. Optimization of fluid flow in grinding

2.2.1 Grinding Process and Fluid Applications

Oliveira *et al.* [16] presented the industrial importance and necessity of grinding research. It is analysed that automotive industry is one of the main users of ground components. Study started with analysis of efficient engines. And trends are analysed that how changes in their main components can affect the grinding performance .Different sources of information on industrial challenges in grinding are explored. 23 machine tool builder's perspectives are presented. The Motive of gathered information, is illustrate several phases of the main trends that can represent opportunities for grinding research. It has been analysed that there are many areas which can be researched for advancement of grinding such as Energy control, use of electroplated wheels, process reliability, increasing CBN applications, cost analysis etc.

Malkin *et al.* [17] provided outline of analytical methods to calculate grinding temperatures and their effect on thermal damage. Modelling of the grinding zone as a heat source which moves along the work-piece surface is included in the approach. Energy partition is a critical factor for calculating grinding temperatures, which is the fraction of the grinding energy transported as heat to the work-piece at the grinding zone. The energy partition was only about 5% for creep-feed grinding with slow work speeds and large depths of cut. The energy partition was found to be typically 60%–85% for shallow cut grinding with conventional

abrasive wheels. CBN like abrasives which have high thermal conductivity can conduct to the grains which also can reduce the energy partition. In High Efficiency Deep Grinding (HEDG) using CBN wheels, preheated material ahead of the grinding zone is removed together with the chips, thereby lowering the temperature on the finished surface. An analytical modal is developed which can take all of these effects into account.

Jin *et al.* [18] have predicted the convection heat transfer Coefficient of fluids under different grinding conditions by coupled fluid dynamic and thermal modelling. A special test rig, with thermocouples implanted at different distances to the grinding surface, has been used to measure the heat flux to the workpiece, which is used to calculate the CHTCs of grinding fluids. The theoretical modal shows good concurrence with the experimental results. It has been found that, under forced convection conditions due to the high grinding wheel speeds the CHTCs are much higher than the values previously reported. The CHTC values change with wheel speed and are also influenced by the value of the fluid film thickness. This film thickness in turn can be a function of wheel speed, porosity, grain size, coolant viscosity and flow rate. For deep grinding conditions (creep feed and HEDG), the upper bound value of fluid film thickness can be achieved due to the high coolant supply pressure and flow rate.

Tawakoli *et al*. [19] have analysed that according to economical and ecological point of view dry grinding is very much liked. But due to method of operation of grinding a great deal of heat is introduced. That is very harmful for surface properties of work piece and abrasives. Cutting fluids were introduced to reduce the effect of heat generated during grinding. But cutting fluids have cost and environment hazard related issues. A method is observed to reduce or obsolete the use of harmful fluids and reducing heat generated. According to the method change in grinding wheel properties (abrasive size, porosity etc.) and grinding parameters (wheel speed, depth of cut, feed rate etc) can reduce the heat generation in grinding process. To reduce heat generation, the reduction of cutting edges by definite conditioning of the grinding wheel using a single-point diamond dressing tool produced a specific structure on the wheel surface.

Schumack *et al.* [20] used a perturbation scheme to model a fluid flow under a grinding wheel. In this initial effort to understand the flow characteristics, they concentrate on the case of a smooth wheel with slight clearance between the wheel and work-piece. Comparison of experimental and analytical pressure profiles was done to validate the model. Lubrication

theory provided fine agreement with low Reynolds number flows and the perturbation scheme provided sound agreement with moderate Reynolds number flows but fails at high Reynolds numbers. Results from experiments demonstrated that the ignoring upstream and downstream conditions significantly affect the flow characteristics, implying that only a model based on the fully two- (or three-) dimensional Navier-Stokes equations will accurately predict the flow. They made one comparison between an experiment with a grinding wheel and the model incorporating a one-dimensional sinusoidal roughness term. For this case, lubrication theory surprisingly provides good agreement with experiment.

Kiyak *et al.* [21] did comparison of dry and cutting fluid application (wet) in grinding in terms to obtain the best possible surface quality and dimensionally accurate of ground machine parts. The grinding parameters (ground work-piece material, wheel type, wheel speed, work-piece speed, depth of cut and feed) have a significant effect on surface finish of work-piece. The application of cutting fluid is usually carried out and the influence of selected cutting fluid on surface roughness is extensively accepted positive. It was observed that the dry grinding surprisingly produced a better surface quality in the external cylindrical grinding of AISI 1040 steel. The selected grinding parameters such as depth of cut, feed and wheel speed had very high influence on surface roughness. Material removal rates for dry and wet grinding processes were also examined.

Ebbrell *et al.* [22] presented the effect of air boundary layer on cutting fluid application. They proposed a positioning for placement of nozzle. They measured the velocity of air boundary layer around the grinding wheel and observed a reversed airflow against the direction of rotating boundary layer. They found that flow reversal is most severing just before the wheel work-piece contact and above the work-piece surface. So, an intermediate nozzle position for most effective cutting fluid application was proposed. This was opposing the common method of applying fluid jet, as tangential to the grinding wheel periphery and parallel to the work-piece surface, in anticipation the rotating wheel will aid in driving the fluid through grinding zone.

Webster *et al.* [23] analyzed the ongoing coolant application in grinding systems and observed its limitations and used fluid mechanics to develop flow conditioners to compensate for bends in pipes. New nozzle designs were presented to maximize the application of fluid

into the grinding zone. They showed the effect of nozzle position, jet velocity, and distance from the grinding zone. It is reported that optimized coolant application can increase the wheel life by 26.5% during grinding of an aerospace component.

Alves *et al.* **[24]** have investigated the method of reducing the amount of cutting fluid used in grinding process without affecting the surface properties, geometric and dimensional parameters. Due to increasing need of producing complex geometries in grinding operations with good surface finish strict geometrical tolerances. Cutting Fluid application is of great concern but the chemicals additives in cutting fluids are hazards for environment. So cutting fluids can be recycled instead of releasing them in environment, but recycling of fluid is also a costly process. Or the amount of cutting fluids can be reduced to a good extent. This is done by plunge cylindrical grinding of ABNT D6 steel, using a superabrasive CBN (cubic boron nitride) grinding wheel with vitrified binder ,two cutting fluids and varying the plunge velocity to evaluate the output parameters of tangential cutting force, acoustic emission, roundness, tool wear, residual stress and surface integrity, using scanning electron microscopy (SEM) to examine the test specimens. For different plunge velocities cutting fluid and grinding wheel performances were examined to find out a best grinding condition to reducing the cutting fluid amount used in grinding without altering the dimensional and geometrical accuracies or workpiece.

Cakir *et al.* [25] examined that heat generated due to friction have affects like shorter tool life, higher surface roughness and lower dimensional sensitiveness of work material. Their study is more important when machining of hard materials, due to generation of higher heat. To reduce this heat generation, methods have been reported. The selection of coated cutting tools is an expensive alternative and also it is a suitable approach only for machining some materials such as titanium alloys, heat resistance alloys etc. Alternatively apply cutting fluids in machining operation is more appropriate and cheap method. They provide lubrication and cooling effects between cutting tool and work-piece and chip removal during machining operation resulting in reduction of heat generation. In benefit longer tool life, easy chip flow and higher machining quality in the machining processes is observed. The selection of cutting fluids is very crucial to obtain optimum result in machining processes. Selection of cutting fluid type in machining operation depends upon the factors such as type of work-piece materials, cutting tool material and the method of machining processes. In their study, the

selection of cutting fluids for machining processes was examined. Suitable cutting fluids for various material machining processes have been determined according to cutting tool materials.

Choi *et al.* [26] have explained that cooling effect can be increased in grinding process using Mist type coolant in comparison of other coolants. Mostly coolants contain environment polluting extreme pressure additives like chlorine, sulphur and phosphorus to improve the grinding efficiency. A grinding experiment using mist type coolant is performed to overcome the environmental problems of coolants. The surface integrity of workpiece (surface roughness, residual stress and energy ratio into workpiece) was measured to analyze the grinding characteristic of mist type coolant. And then, the grinding experiments according to the supply method of mist type coolant and grinding condition like wheel speed were performed. Through these experiments, it is concluded that the cooling effect in grinding using mist type coolant could be increased as much as that of coolant or even better. The energy ratio into the workpiece in the grinding using mist type coolant is 31.04% where in the grinding using coolant was 26.83%.Residual stresses using mist type coolant are lesser than coolants.

Gviniashvili *et al.* [27] has found that the conventional methods of cooling are not much effective in achieving the useful flowrate in the grinding zone. It was found that useful flowrate depends upon different parameters wheel speed, delivery-nozzle jet velocity and spindle power for fluid acceleration. A modal is developed for useful flowrate in grinding contact zone. For this modal it is required that the grinding wheel and fluid delivery type have less than one loss coefficients. The model relates important parameters such as power, wheel speed, nozzle flowrate, jet velocity, jet power and the required nozzle outlet gap. This modal is verified experimentally. For optimisation of the jet velocity in relation to the power required to accelerate the fluid and the particular velocity of the wheel A guide is given. A rig was manufactured to separate the useful flow rate that had passed through the contact zone from the non-useful flow for varying jet flowrate and wheel speed.

Irani *et al.* [28] analysed that heat generation is most sever and important factor in grinding process which can cause thermal damage to the work piece grinding wheel. Cutting fluids are often applied to the operation avoid the heat transfer to the workpiece. They considered some

common cutting fluid systems and some more rare cutting fluid systems that have been used in recent years with an emphasis on creep-feed applications. These cutting fluids remove or reduce the amount of energy transferred to the work-piece through debris flushing, lubrication and the cooling effects of the liquid. They suggested possible avenues of future research in cutting fluid application for the grinding process.

Powel [29] worked on increasing the amount of useful flow through the grinding zone it is done by applying shoe between the fluid supply and the wheel surface for creep feed grinding to force fluid to penetrate the wheel pores. The maximum depth of fluid penetration into the wheel was estimated. It was assumed that radial pressure inside the shoe was the important parameter in penetration of fluid in grinding wheel pores. Important parameters of the model are the wheel speed, radius, porosity and permeability. The depth of penetration is usually small in comparison to the grain size of the wheel and it was concluded that fluid does not flow deep into the pores and remains mainly on the surface of the wheel.

Hryniewicz *et al.* [30] employed nonporous wheels to model the fluid flow in grinding. A smooth wheel was used to simplify the analysis. Reynolds equation of lubrication and a modified Reynolds equation for turbulent flows were used to inspect fluid flow for laminar and turbulent systems. Hydrodynamic pressure was predicted for experimental validation of type of flow. It was seen that if the Reynolds number Re is less than 300 then classical Reynolds equation is suitable to predicts the hydrodynamic pressure and if Re is between 300 and 1500, that suggests that the flow is turbulent.

Cameron *et al.* [31] examined the influence of speed, flowrate and orientation of the cleaning jet on wheel cleaning. A duller wheel gives a smoother surface finish, but was more prone to cause thermal damage to the workpiece if not properly cooled. During grinding, some of the material being cut may not be flushed away with the coolant and can get fused to the surface of the grinding wheel. This phenomenon, called wheel loading, can clog the pores of the grinding wheel and accelerate thermal damage to the workpiece. A separate high speed cleaning-jet systems was applied to the grinding process to reduce the wheel loading. Wheel cleaning resulted increase in the critical specific material removal rate of up to 100% and a decrease in the critical specific energy by 33% compared with experiments with no wheel cleaning. The experimental results showed that- As the wheel-cleaning-jet speed increased,

the CSMRR increased up to the point at which the cleaning jet itself began to damage the grinding wheel.

Sinot *et al*. [32] defined the parameters which are influential in maintaining a clean wheel. A cleaning criterion was proposed to estimate the efficiency of the cleaning process. An experimental set was created and some parameters like influence of the nozzle position, the flow rate and pressure, the boundary layer of air around the rotating wheel and the particle rate contained in the fluid were measured. As a result it was found that the fluid temperature has no significant effect, the distance from the nozzle to the wheel should be taken least possible, flow rate should be high and the cleaning pressure should be low, particle rate in fluid should be minimum and boundary layer of air have significant effect.

2.2.2 Experimental and Simulation Work

Rowe *et al.* [33] worked on cost effectiveness of grinding process for repeat batch production. Costs involved in precision cylindrical grinding for different abrasives, machines and grinding conditions were calculated. Machine cost and abrasive cost were the main parameters. With the help of experiments it was shown that wheel speed affects production rate through acceptable values of re-dress life, removal rate and dwell time. Vitrified CBN rotated and conventional abrasive at conventional speed and at high speed to grind material were used. It was found that Vitrified CBN wheels at high speed, gave better quality at lower cost than conventional abrasives and results in negligible wheel costs and highly reduced labour costs. Re-dress life trials are found to be essential to reduce costs and maintain quality.

Li *et al.* [34] have observed that in the grinding process, due to the high surface speeds of the wheel, causes a boundary layer of air around the wheel periphery. The boundary layer restricts the flow of cutting fluid into the grinding zone. Conventional methods of delivering grinding fluid that flood delivery via a shoe or jet delivery tangential to the wheel via a nozzle, are not could to fully penetrate the boundary layer and, thus, the majority of the grinding fluid is deflected away from the grinding zone. So the required flowrate of fluid is not achieved in effect reducing the performance of grinding process. Conventional flood delivery are useful for achieving bulk cooling of the work surface, but are often ineffective in achieving sufficient useful flow-rate through the grinding contact zone at high speeds. They have presented a theoretical model for flow of grinding fluid through the grinding zone. The model shows that the flow rate through the contact zone between the wheel and the work

surface depends on wheel porosity and wheel speed as well as depends on nozzle position, design, and fluid jet velocity.

Monici *et al.* [35] have examined the form and amount of cutting fluid in grinding. Chemicals in fluids can have a severe effect on environment and human health and also the amount of cutting fluid enhance the purchasing cost and maintenance costs due to improper handling. Some crucial parameters such as specific grinding energy, tangential cutting force, residual stress, acoustic emission, diametrical wear, roughness, and scanning electron microscopy are greatly affect by the amount of fluid used. To find the optimal amount of coolant rounded nozzles of 3, 4 and 5 mm diameter, were employed without affecting output parameters.Neat oil and 5% synthetic emulsion were used as cutting fluids and two abrasives CBN and Aluminium oxide were used for this purpose. Based on this analysis, a new form of applying cutting fluid is investigated, aimed at improving the performance of the process with regard to the main output variables.

Morgan *et al.* [36] have done experimentation to reduce the waste of flow rate the waste occurs because supplied flowrate does not to reach inside the grinding contact and useful flow rate is decreased causing diverse effects like high surface roughness, wheel loading and excessive temperature at grinding surface. And also if the high speed jet and greater amount of fluid is used that increases the machining cost and power consumption. So an experiment is done to measure the actual flow rate. With the help of scraper board and nozzle simulation the effect of nozzle position on useful flowrate was measured experimentally. It was shown that wheel speed, jet velocity and nozzle flowrate were of greatest importance for actual useful flowrate. It was confirmed that jet speed should be approximately 80% -100% of wheel speed to match achievable useful flowrate. The jet speed should not be higher as this does not significantly increase useful flowrate and the jet flowrate needs to be of the order of 4 times larger than achievable useful flowrate.

Salonitis *et al.* [37] has suggested the utilization of heat generated during grinding to grind harden the work piece. In grind harden process; grinding and hardening are done simultaneously. This is accomplished as the dissipated heat and the quenching of the workpiece inducing metallurgical transformation on the surface of workpiece. The work piece temperature is increased above the austenitisation temperature with the help of heat dissipated in the grinding area and subsequently is self-quenched by taking the heat away from the

surface with the application of cutting fluid to achieve the expected surface hardening. The utilization of cutting fluid is examined. Considering the rapid heating of the workpiece and the short austenitising time, hardness penetration depth (HPD) and hardness profile are estimated. For this specific case a finite element analyses modal is developed and experimentally verified.

Engineer *et al***.** [38] disclosed a method to measure directly the useful fluid flow through the grinding zone using conventional fluid application by separating and collecting all the fluid that passes through the grinding zone during straight plunge grinding. A experimental test rig was developed to measure the amount of grinding fluid which flows through the grinding zone in straight plunge grinding. Proportional relationships were obtained between the flow rate from the nozzle and the useful flow rate of fluid passing through the grinding zone. The percentage of applied fluid passing through the grinding zone was found to depend mainly on the bulk porosity of the grinding wheel and the nozzle position. Wheel dressing has only a secondary influence, which is attributed to its influence on the surface porosity of the wheel. The work speed and wheel depth of cut have virtually no influence.

Brinksmeier *et al.* [39] explained different methods for modelling and optimization of grinding processes. First the process and product quality characterizing quantities were measured. Secondly different model types, e.g. physical–empirical basic grinding models as well as empirical process models based on neural networks, fuzzy set theory and standard multiple regression methods, were discussed for an off-line process conceptualization and optimization using a genetic algorithm. The evaluation of grinding process results was carried out using a target tree method. These methods were integrated into an existing grinding information system, as part of a three control loop system for quality assurance.

Sakakura *et al.* [40] have explained that in grinding process with large no of abrasive grains the finishing of workpiece is carried out. But due to the irregular shapes and random distribution of abrasive grains it is difficult to analyse the grinding process. To resolve this problem Monte Carlo method is used to carry out different computer simulations. This software calculates geometric interference between a grain and a workpiece statically, till now no computer simulation program is developed based on elastic behaviour modal of grains. The focus program is on the generation of a workpiece surface, and simulating the interaction of grains and a workpiece which embraces the elastic and plastic deformation and the removal

of workpiece material. A three dimensional graphics technique is use to display the simulation results as an animated image. The simulation facilitates to understand the microscopic grinding phenomena, and makes it possible to analyze the surface generation process quantitatively. Thus, it could be used to predict the grinding results such as surface roughness, and for optimizing grinding parameters such as infeed rate.

Nguyen *et al.* [41] carried out the research in two parts describing the kinematic simulation of the grinding process. The firstly researchers were concerned with the generation of the grinding wheel surface. For effectively generating the grinding wheel topography a numerical procedure was suggested. The procedure was based on the transformation of a random field. To illustrate the viability of the approach numerical examples were used. It was found that the generated and measured grinding wheel topography share the same probabilistic characteristics.

Mandeep *et al.* [8, 42] have used a computational fluid simulation (ANSYS CFX) approach to analyse the fluid Behaviour of Nozzles. He has taken six different nozzles for this purpose and done simulation to find the best appropriate nozzle in terms of high peak velocity to send it to the cutting zone to displace the rotating air layer around the grinding wheel. The rotating air layer with the grinding wheel does not allow the cutting fluid to enter the cutting zone and cause excessive heat generation. This air layer can be successfully eliminated if the fluid jet velocity becomes equal or greater than the grinding wheel surface speed, then cutting fluid can reach cutting zone causing an effective cooling, and eliminating scraper board usage. This ensures effective cooling to reduce thermal damage to work piece to be ground and produces the enhanced surface and dimensional quality, which is required for precision manufacturing. Experimental validation was done and process capabilities are found out in turms of C_p and C_{pk} for dimensional accuracy, surface finish and microhardness.

Devillez *et al.* [43] provided the results of an experimental design performed with an industrial grinder during the manufacturing of automotive workpieces. The aim of this investigation is to define the significant parameters of the grinding process, especially concerning lubrication. Taguchi method was used to define the experiment. Significance of parameters was obtained by the use of Principal Components Analysis (PCA,). It was found that nozzle geometry and the coolant temperature are not important factors. The control of the roughness is better when the wheel speed was at its low level and cleaning pressure has a

weak effect on the roughness .This study gave a global approach of lubrication parameters for high speed grinding.

Chryssolouris *et al.* [44] reported that in grind hardening, the heat dissipated in the cutting area during grinding can used for the heat treatment of the work-piece. They employed analytical and numerical techniques to understand the grind-hardening mechanisms as well as the working conditions during the process. Parameters considered include work-piece speed and depth of cut at a constant cutting speed. The hardness penetration depth has been calculated, for a given set of process parameters, and compared with experimental data from a cylindrical dry grind hardening process. Their model shows that the flow rate through the contact zone between the wheel and the work surface depends on wheel porosity and wheel speed as well as depends on nozzle position, design, and fluid jet velocity. Furthermore, the model was tested by a surface grinding machine in order to correlate between experiment and theory. Consequently, the useful flow rate model was found to give a good description of the experimental results and the model can well forecast the useful flow-rate in flood delivery grinding.

2.2.3 Optimization of Fluid Flow in Grinding

Banerjee *et al.* [45] examined the formation of thin but stiff air boundary layer that rotates along with the grinding wheel produces most detrimental effect on the flowrate of coolant through grinding zone. A special twin jet nozzle was designed to break the air boundary layer and to improve effective flow rate because the use of scrapper plate, coating the side surfaces of grinding wheel by silicon rubber or positioning the nozzle at some specific theoretical location poses difficulties in practical applications. To monitor the effective flow rate at different locations and geometrical orientations of the designed nozzle a special attachment is designed to control the horizontal, vertical and angular movements of the new nozzle. A special work-piece-cum-fluid collecting chute is designed to separate and collect the fluid passing only through the grinding zone; Effective Fluid flowrate measured through this process is compared with the previous flow rate of grinding machine. As a result is found that Maximum effective flowrate obtained using the developed nozzle for jet cooling is much better than that obtained with flood cooling condition.

Bains-Jones *et al.* [46] observed that for optimal coolant flow some coolant delivery parameters like optimal nozzle design and positioning are critical elements of the delivery system. Researchers analyzed that fluid delivery lesser or greater than that of optimal coolant delivery is not favorable. This paper gave the idea of work done on nozzle design. Importance of factors nozzle position, nozzle angle, and nozzle type and jet velocity was presented. Coolant system design considerations, based on the presently available research material included the use of two different types of nozzles. The primary nozzle or entry nozzle consisting of either a jet, slot or shoe nozzle, and the secondary nozzle or exit nozzle used for bulk cooling of the workpiece and cleaning of the wheel. Grinding tests indicated that secondary nozzle at a nominally low pressure was necessary for preventing thermal damage of the workpiece.

Shin'ichi *et al.* [47] designed and developed a nozzle naming floating nozzle to decrease the grinding temperature and wear of superabrasive grinding wheel. To attain the exact dimensional accuracy grinding temperature and wear of grinding wheel should be removed. A new nozzle made of the graphite and pressed to the grinding wheel by the spring mechanism so that the nozzle can wear and can get the shape of circumference of grinding wheel. Therefore between the grinding wheel and the nozzle a narrow gap was created and the grinding fluid sticks to the wheel because floating nozzle cuts off the airflow around the grinding wheel and the adhered coolant was always supplied just to the grinding point.

Morgan *et al.* [48] presented an analytical modal to calculate the coherent length of jet. For cooling, a nozzle must provide a required jet velocity and a accurate flow pattern which depends upon nozzle geometry. They examined that a required jet velocity through a nozzle should have appropriate coverage of grinding zone for efficient grinding and better surface finish. Coverage of grinding zone depends upon the coherent length of jet. For accurate coverage of the grinding contact, the distance between the nozzle orifice and the grinding contact zone should not exceed the length at which the nozzle covers the entire distance at this peak velocity (coherent length). Previously coherent length was observed with visual inspection. They provided a analytical modal for that purpose. Their paper has shown coherent lengths and inside nozzle flow of wide range of Nozzles.

Webster. [49] has provided a design which is very useful for the grinding of thermally sensitive materials and to minimize the scattering of coolant jet in different grinding applications for reducing thermal damage to the workpiece surface. A nozzle assembly is designed and configured with a method, to apply coherent jets in tangential direction to grinding wheel at required conditions like fluid flow rate, pressure and temperatures arcuate path in the first plane corresponding to a location of the work-piece that would be contacted first by the distal end during movement along the second arcuate path.

2.3 GAPS IN LITERATURE

Researchers have done lots of work in the grinding for coolant flow, type of coolant, grinding wheel material. Heat generation and its ill effect have been considered, Surface roughness, microhardness were measured. Less work is done on nozzle optimization for optimal coolant delivery and computational fluid dynamic simulation softwares to measure the coolant flow behaviour. Less work is done on systematic approach in varying nozzle angle nozzle tip distance for nozzle optimization and that could show that the parameters wheel speed, work piece speed nozzle angle; nozzle tip distance and type of nozzles all together can have effect on output response like dimensional accuracy, surface hardness, surface finish. Sufficient literature is not available on the use of Computer fluid simulation software ANSYS CFX to find out correct nozzle design to achieve optimal coolant delivery. Multi-fluid computer simulation has not yet been reported to predict the behaviour of coolant jet on atmospheric air in the grinding zone. Also little literature is available on nozzle orientation for optimum flowrate.

2.4 OBJECTIVE

After doing detailed study of literature on grinding process and cooling techniques to reduce heat in grinding zone, it is summarised that many experimentations have been done to improve grinding processes with grinding wheel dressing, varying grinding wheel and workpiece speed and nozzle geometry. ANSYS CFX software is used to simulate and analyse the fluid flow through different nozzles and Multi-fluid (coolant and atmospheric air) simulation is done on selected nozzles to analyse the behaviour of coolant jet through nozzle at different positions and orientations on atmospheric air around the wheel in the grinding region during cylindrical grinding operation. Optimum results are extracted through which maximum cooling can be achieved in grinding zone by removing the air layer formed around wheel with different nozzles jet velocity. Thereafter experimentation on these nozzles is done to validate the results of simulation in terms of cooling capability and by measuring dimensional control, surface hardness and surface cracks of work piece to be grounded, followed by finding process capabilities of best performing nozzles.

CHAPTER 3
METHODOLOGY

3.1 INTRODUCTION

Grinding is a very wildly used manufacturing process for high quality finished products. In this process very high amount of heat is generated and chips are formed, which can change the surface properties of the workpiece and can halt required surface finish. To eliminate the heat generation problem and to remove the chips formed during grinding an appropriate cooling is required so that the heat generated can be rejected to the environment. For this appropriate nozzles are required which can supply the coolant in the grinding zone at a required high velocity. To achieve the high velocity of coolant the design of nozzles and its position from the cutting is very important. Computational fluid dynamic (CFD) simulation is used to find out the best design of nozzles which can provide coolant at high speed for the better grinding. And also the complete grinding process Simulation is done to find out the behaviour of coolant in grinding zone. Then experimentation is done to validate the selection of nozzles.

3.2 SIMULATION METHODOLOGY

3.2.1 Introduction to ANSYS CFX

For the simulation of fluid behaviour through different nozzles, CFD simulation software ANSYS CFX 11 is used. ANSYS CFX 11 is a fluid analysis and simulation software which combines CAD automatic Meshing and Fast solution algorithms, which include Pre processing, Solving, Post processing.

Pre Processor includes modelling (CAD), meshing, applying boundary conditions,

Solver which is based on finite volume method Includes applying the solution algorithms and iterating and forming the results.

Post Processor Includes displaying the results, forming vector diagrams, contours graphs on display screen.

3.2.2 Simulation of Fluid Flow Through Nozzles

When the grinding of workpiece takes place, due to the high rotation speed of the grinding wheel a thin air layer is formed around the wheel which prevents the coolant to enter in the cutting zone which causes excessive heat generation, low surface finish and change in surface properties (micro hardness, cracks etc.). When the fluid coming out of nozzle has a velocity

greater than or equal to the air around the wheel then it can cut the air layer around the wheel and fluid can enter the cutting zone and, heat generated can be rejected to the environment and provides efficient cooling. For this purpose the simulations of different types of nozzles are done and three nozzles are considered for best performance. Inlet and outlet diameter of all nozzles is kept constant inlet diameter is 25mm and outlet diameter is 10mm. A taper Nozzle with taper angle of 4 degree is considered. After trying different spline profiles a best performing spline profile is considered. A convergent divergent nozzle with 7.5 degree is with 7.5 degree convergent angle and 10 degree divergent angle and 4 mm divergent length is considered. To understand the methodology of fluid flow through nozzles convergent divergent nozzle is taken. This is shown in Various Steps.

a) Boundary Conditions

S. No	Parameter	Value
1	Cutting fluid	Water
2	Inlet pressure	3.5 bar
3	Environment pressure	1 bar

b) Methodology of Nozzle Simulations:

Step1. Geometric modal of inside volume of nozzle is created using ANSYS CAD module and this geometric modal is imported to the ANSYS meshing module to generate the meshing of the nozzle volume. And a mesh file (.msh) is saved in working directory Physical boundary conditions are shown in figure 3.1.

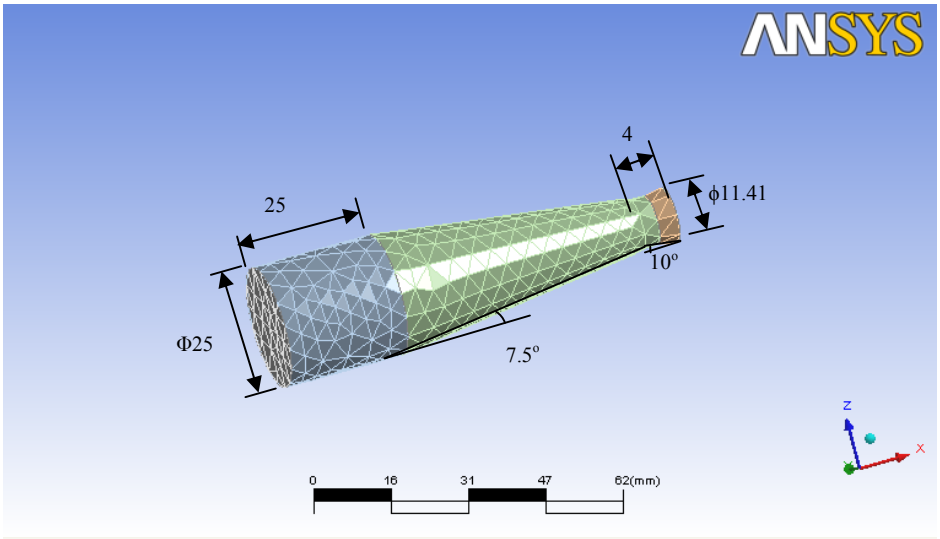

Figure 3.1: Convergent divergent nozzle dimensions and meshing (All dimensions in mm)

Mesh statistics

Total number of nodes	2351
Total number of tetrahedral	1888
Total Number of prisms	3520
Total Number of elements	5408

Step2. Geometric modal of environment at the outlet of nozzles is created using ANSYS CAD module and this geometric modal of environment is imported to the ANSYS meshing module to generate the volume mesh. And a mesh file (.msh) is saved in the working directory physical boundary conditions are shown in figure 3.2.

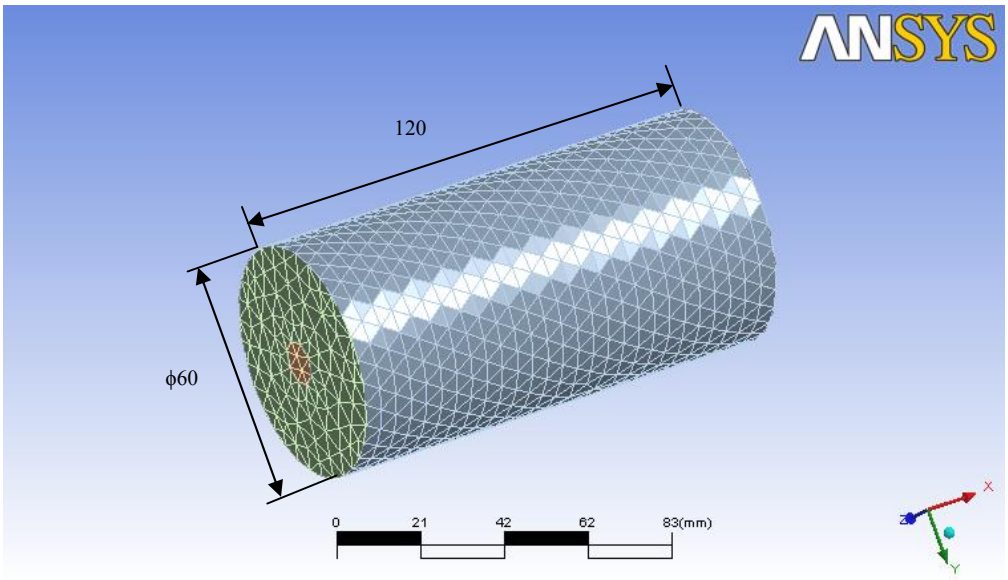

Figure 3.2: Environment dimensions and meshing

(All dimensions in mm)

Mesh statistics

Total Number of nodes	4539
Total number of tetrahedral	23251
Total Number of elements	23251

Step3. Mesh files of Nozzle and environment are then imported to the CFX Pre. Nozzle outlet is interfaced with environment. The physical and numerical parameters (type of fluid, inlet and outlet) and boundary conditions (inlet pressure, environment pressure etc.) of the models are set in CFX-Pre module. Figure3.3 shows the Pre processing.

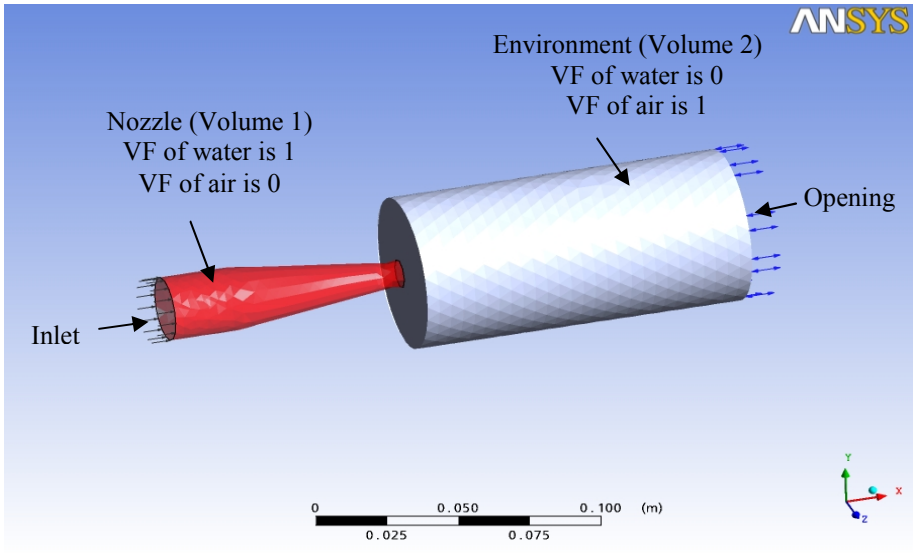

Figure 3.3: Nozzle environment simulation

Initial Condition:

Volume	Volume Fraction	
	Water	Air at 25^0 C
Volume 1	1	0
Volume 2	0	1

Step4. CFX Solver performs the iteration process when the iteration process comes to the end of convergence as shown in figure 3.4 it provides the results to the CFX Post Processor.

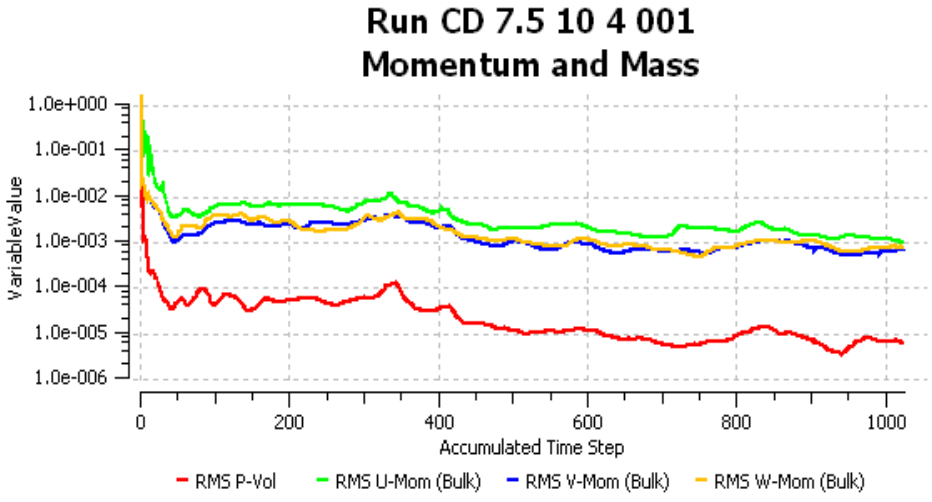

Figure 3.4: Convergence graph of fluid flow simulation

Step5. CFX Post Processor provides the results contours and velocity vector diagrams of fluid flowing through the nozzle. Results are shown in chapter 4.

3.2.3 Simulation of Grinding Process

Computer simulation of complete cylindrical grinding process is done using ANSYS CFX to analyse the behaviour of fluid (coming out of nozzle) in the cutting zone and on air layer around the grinding wheel. For the simulation purpose a large environment is created in which grinding wheel and work piece are placed and different nozzles are modelled at different positions and different angles to the contact point of grinding wheel and cylindrical workpiece. Roughness of grinding wheel is taken as 1mm. Diameter of grinding wheel is taken as 300 mm and diameter of work piece is taken as 17.750 mm. Air at 25^0 C is taken for the environment of grinding.

A Convergent divergent nozzle is considered in grinding process with following boundary conditions to understand the methodology.

a) Boundary Conditions

S. No	Parameters	Values
1.	Grinding wheel speed	1921 rpm
2.	Work piece speed	545 rpm
3.	Nozzle angle	23^o
4.	Nozzle tip distance	14mm

b) Methodology of Grinding Process Simulation

Step1. Geometric modal of grinding environment with grinding wheel and work piece is created using ANSYS CAD module and this geometric modal of grinding environment is imported to the ANSYS meshing module to generate the volume mesh. And a mesh file (.msh) is saved in the working directory. Grinding environment is shown in figure 3.5.

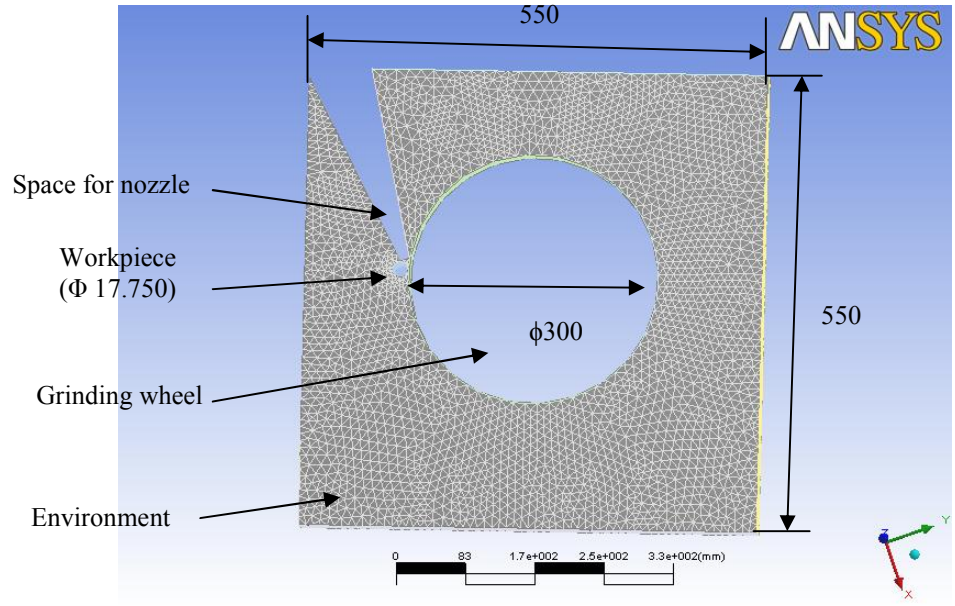

Figure 3.5: Grinding environment geometry and meshing

(All dimensions in mm)

Mesh statistics

Total number of nodes	44996
Total number of tetrahedral	31336
Total number of pyramids	20
Total number of prisms	67390

Step2. Mesh files of nozzle and environment are then imported to the CFX Pre. Nozzle outlet is interfaced with environment. The physical and numerical parameters (type of fluid, inlet and outlet) and boundary conditions (inlet pressure, environment pressure etc) of the models are set in CFX-PRE module.

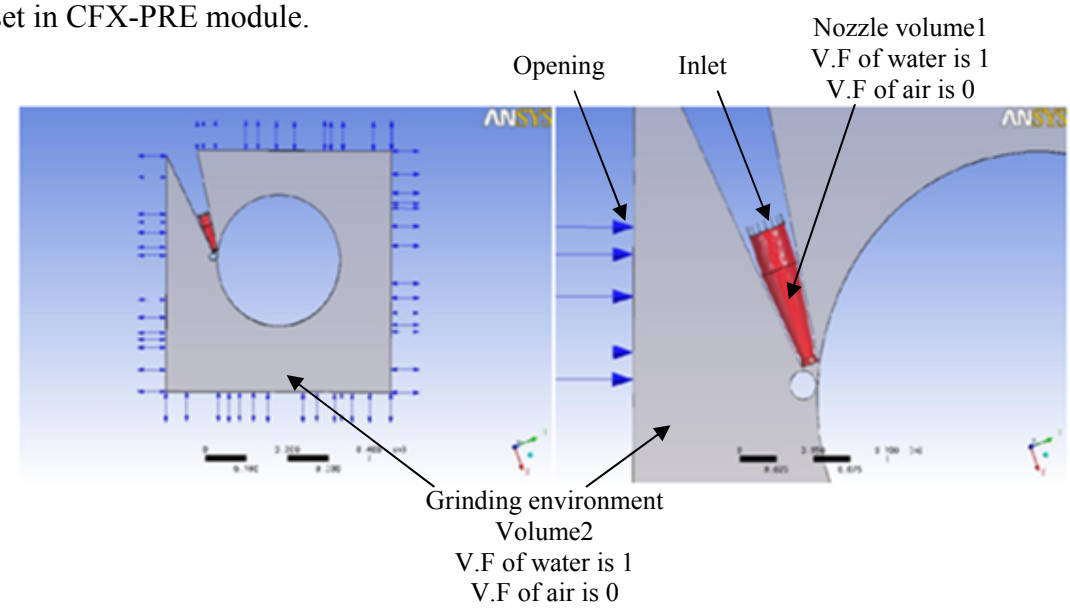

Figure 3.6: Complete grinding process simulations

Initial Condition:

Volume	Volume Fraction (V.F)	
	Water	Air at 25^0C
Volume 1	1	0
Volume 2	0	1

Step3. In CFX Solver the iteration process is process is performed, when the iteration process comes to the end of convergence criteria as shown in figure 3.7, it provides the results to the CFX Post Processor.

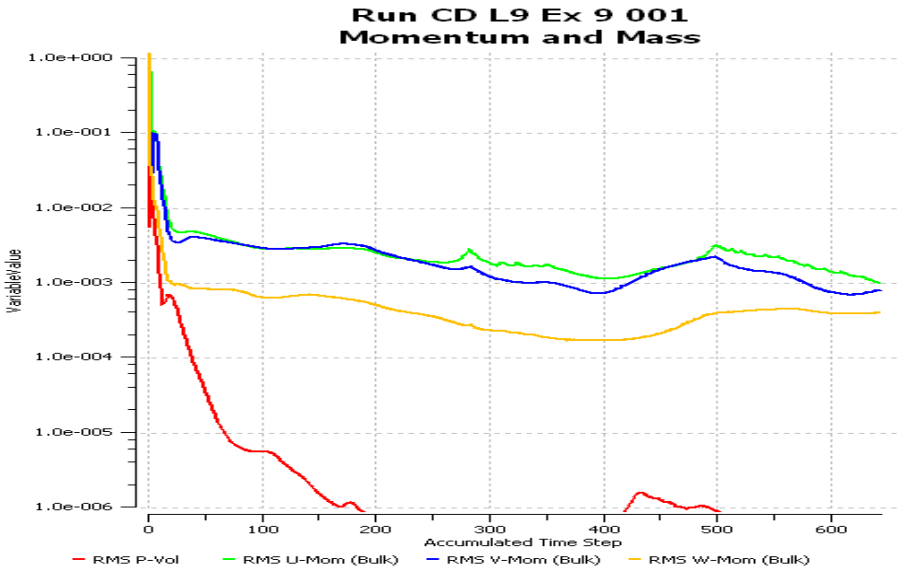

Figure 3.7: Convergence graph of grinding process simulation

Step4. CFX Post Processor provides the contours and velocity vector diagrams of fluid flowing through the nozzle. Results are shown in chapter 5.

3.3 EXPERIMENTAL METHODOLOGY

Experimentation is done to validate the simulation work. The design of experimentation technique is used to carry out the experiments. It is an organised and structured method which is used to determine the relationship between different factors. Fractional factorials analyses method is used. Taguchi technique is used to simplify the fractional factorial analysis and to overcome the limitations of full factorial design.

3.3.1 Objective Establishment

The goal of the study is to find out the minimum number of surface cracks, nominal dimensional control and to minimize the change in surface hardness by evaluating the effects grinding wheel speed, work-piece speed, nozzle tip distance and nozzle angle for all three nozzle types and their interactions during grinding operations. The surface roughness value, dimensional control and surface hardness were selected as output for the present investigation.

3.3.2 Factor, Their Levels and Response Parameters

Factors are divided into two categories first is constant factors such as grade of grinding wheel, work piece material, coolants type and coolant pressure. These factors were remained constant throughout the experimentation. Second is variable factors which are grinding wheel speed, work-piece speed, nozzle tip distance nozzle angle and the type of nozzles. The work piece speed levels and grinding wheel speed levels were selected as per the pulley arrangement available on the grinding machine. The internal geometry of nozzles is selected on the bases of proposed and developed by researchers. All the factors have 3 levels each. These factors are same for each of the three nozzles. The factors and there levels are show in Table 3.1.

Table 3.1: Factors and their levels

Factor	Level 1	Level 2	Level 3
Wheel speed (rpm)	1628	1795	1921
Workpiece speed (rpm)	245	375	545
Nozzle angle (degree)	18	23	28
Nozzle tip distance (mm)	14	18	22

Initial diameter of the workpiece is taken a 17.750 mm.

3.3.3 Orthogonal Array

Taguchi's orthogonal arrays are experimental designs designed to handle as many factors as possible in a certain number of runs compared to those dictated by full factorial design, So it usually require only a fraction of the full factorial combinations. All factor combinations occurs same number of times, in each pair of columns and effect of each factor on the response can be estimated independently of all other factors. It is mandatory to compute the total degree of freedom (*dof*) of all the factors to select an appropriate orthogonal array for experiments. The degrees of freedom are defined as the number of comparisons between process parameters that must be made to determine which level is better and, specifically, how much better it is. Degree of freedom of each factor is one less than the number of levels in the factor. And total degree of freedom is sum of degrees of freedom of all factors. Total degree of freedom is equal to the sum of degree of freedom of each factor. Total degree of freedom is shown in table 3.2.

Table 3.2: Degree of freedom for each factor of interest

Factor	***Dof***
Wheel speed	2
Workpiece speed	2
Nozzle angle	2
Nozzle tip distance	2
Total *dof*	8

Once the total degree of freedom is known the orthogonal array (OA) can be easily selected. The total degree of freedom required for the experiment is 8, and there are four factors of interest and all factors have three levels each. In the orthogonal array, the number of rows is equal to the number of treatment conditions and it must be equal to or greater than the total degrees of freedom. The most suitable orthogonal array that can be used for this experiment is L_9. In this experiment, the assignment of factors and interactions was carried out using 3 level L_9 orthogonal array. This array has eight degrees of freedom and it can handle four process parameters. Each grinding parameter was assigned to a column. According to L_9 orthogonal array nine parameter combinations are formed and so nine experiments were required to study the complete grinding parameter space. The L_9 orthogonal array for experimentation for these grinding parameters is shown in Table 3.3.

Table 3.3: L_9 experimental design

Exp. No.	Wheel Speed (rpm)	Work piece Speed (rpm)	Nozzle Angle (degree)	Nozzle Tip Distance (mm)
1	1628	245	18	14
2	1628	375	23	18
3	1628	545	28	22
4	1795	245	23	22
5	1795	375	28	14
6	1795	545	18	18
7	1921	245	28	18
8	1921	375	18	22
9	1921	545	23	14

Three L_9 table were formed for all three nozzles separately.

3.3.4 Experimental Details

The three nozzles (Spline, Convergent-divergent and Taper) designed in the ANSYS and their fluid flow behaviour is simulated in CFX module of ANSYS CFX. These nozzles are manufactured with the same dimensions as in simulation. The material used for manufacturing nozzles is aluminium. Boring operation is used to manufacture them and for finishing the inside of nozzle, tool is made of exact geometry as of nozzle. Six pieces of length 260 mm are cut from a 20 mm mild steel rod. Firstly the centres are marked on both faces of workpiece to hold them in dock carrier. Than they are initially rough turned on the lathe to reduce their diameter to 17.800 mm and then cylindrical grinder is used to finish the diameter to required 17.750 mm. Two workpieces are assigned for each L_9 array and nozzle. On one work-piece five cuts are applied and on second workpiece four cuts are applied. The first cut is of 100 microns and second cut is of 50 microns. For pumping the coolant to the required pressure 1 hp centrifugal pump is used. The fluid pressure is controlled with the help of a pressure regulating valve and the pressure is measured with the help of U-Tube mercury manometer and pressure gauge. A sump tank of capacity 100 litres was provided, from where the coolant was sucked by pump and gets collected again after filtering the chips. The total experimental set up and its schematic arrangement has been shown in Figure 3.8.

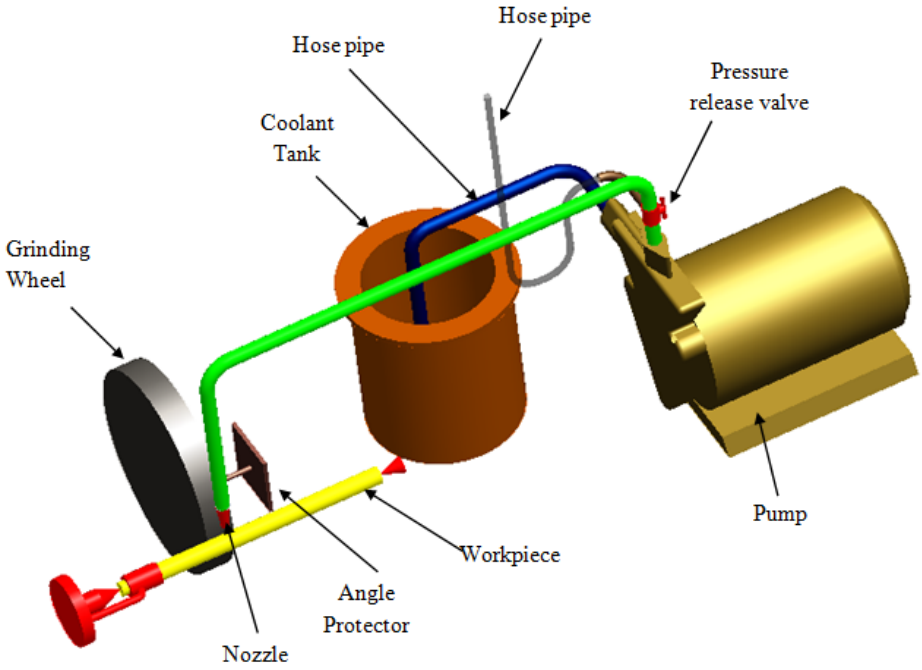

Figures 3.8: Schematic arrangement of complete setup

Pulley combination arrangement is used to vary the speed of the wheel and work-piece with the help of V belts. Nozzle angle is varied about horizontal axis parallel to the axis of workpiece with the help of screw arrangement. To measure the nozzle angle a scraper board is placed perpendicular to the workpiece axis. Nozzle tip distance is also varied with the help of another screw arrangement. Grinding wheel was dressed after every small intervals using dressing tool. In Figure 3.9 the setup of the arrangement is shown.

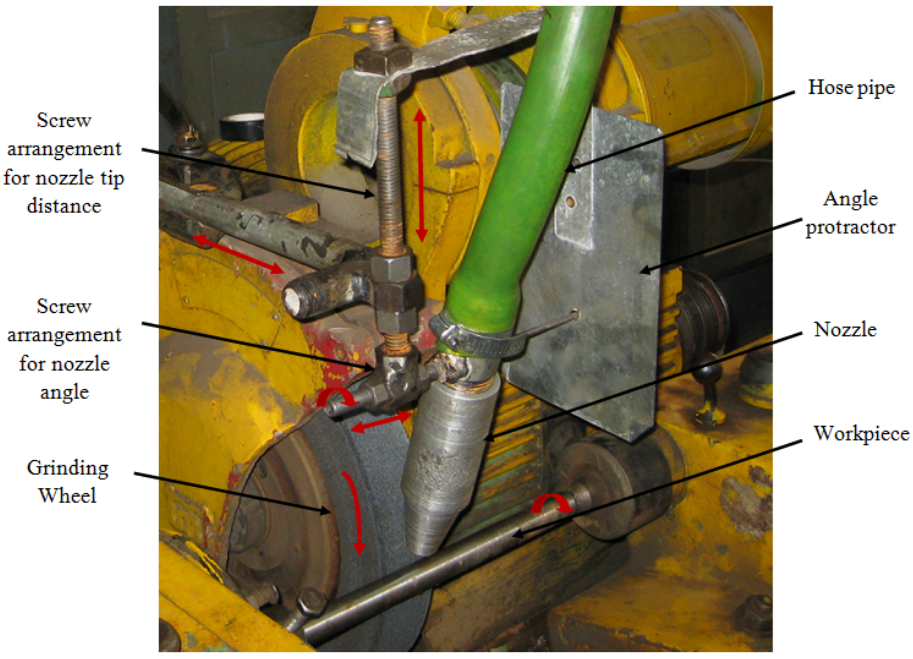

Figure 3.9: Setup of nozzle orientation arrangement

3.3.5 Machine Description

Universal cylindrical grinding machine (Make: TMT; Model: 600) is used to conduct the experiments, available at Central Workshop, Thapar University, Patiala and is shown in the figure 3.10. The main parts of the machine are control box panel, grinding wheel-head with driving motor, work head, hand traverse table, coolant tank, power traverse of table, in-feed of wheel-head and rapid movement of hand-wheel. A Control panel is provided to switch ON/OFF independently the motors attached to the workpiece, grinding wheels coolant pump.

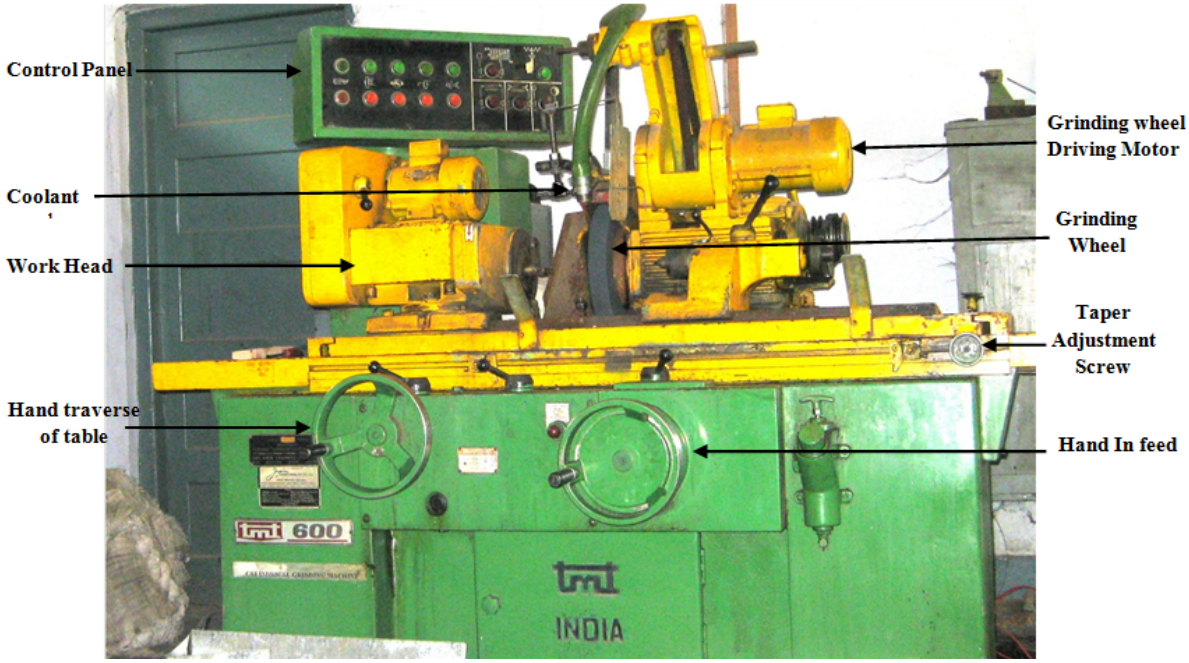

Figure 3.10: Universal grinding machine used for experimentation

Wheel and work-piece speeds are varied to three levels by changing position of V-Belts for different combinations of pulleys available on the machine. Control is provided on the machine for the in-feed of wheel-head and traverse table movement. Both manual and automatic movements are possible. In Table 3.4 technical specifications of the grinding machine are given.

Table 3.4: Technical parameters of grinding machine

Maximum Travel of Traverse table	600 mm
Maximum Taper of table	60° clockwise and 30° anti clockwise
Minimum In-feed of wheel-head	10 microns

3.3.6 Pressure Measurement

3.5 bar pressure of coolant is required to measured with the help of. U-tube mercury manometer is used to measure the pressure. In figure 3.11 U-tube mercury manometer is shown. The hydrostatic pressure equation, is used to measure the pressure exerted P.

$$P = hg\rho$$

h is height of column of fluid

ρ is density (13.534g/cm^3 for mercury)

Therefore in a U-tube manometer the pressure difference between the applied pressure P_a and the reference pressure P_0 can be found by equation,

$$P_a - P_0 = hg\rho$$

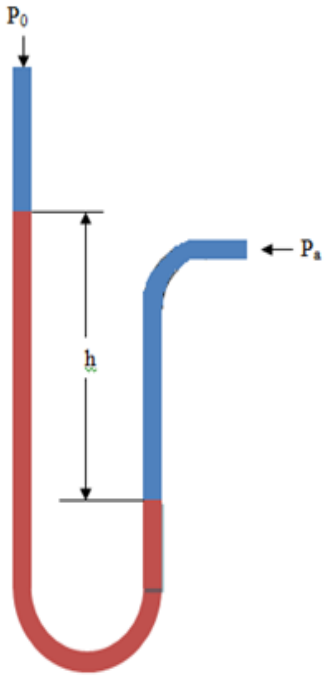

Figure 3.11: U- Tube mercury manometer for pressure measurement

3.3.7 Pulley Combination for Wheel Speeds

The driving motor and wheel spindle consists of two different diameters of pulleys each. Three set of combinations can be made from these pulleys. Schematic diagram is shown in figure 3.12.

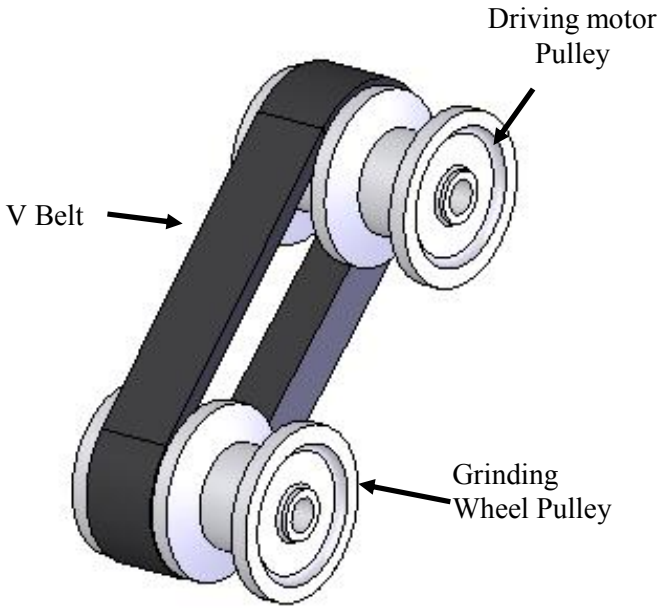

Figure 3.12: Schematic of pulleys arrangement of grinding wheel speed

Initial dimensions and parameters are shown in table 3.5. Calculations for wheel speeds are given in table 3.6.

Table 3.5: Initial dimensions and parameters

Parameter	Dimension/value
Diameter of pulley 1 of driving motor(P1)	100mm
Diameter of pulley 2 of driving motor(P2)	107mm
Diameter of pulley 1 of Wheel spindle (D1)	86mm
Diameter of pulley 2 of driving motor(D2)	78mm
Fixed rpm of Driving motor	1400 rpm
Diameter of the grinding wheel i.e. D	300 mm
Width of the wheel	38 mm

Table 3.6: Calculations for wheel speed

Arrangement\Factors	rpm	Wheel Speed $\frac{\pi.D.N}{60x1000}$ m/sec
P1 & D1	1628	25.98
P1 & D2	1795	28.65
P2 & D2	1921	30.66

3.3.8 Pulley Combination for Work Piece Speeds

The work head motor and work head spindle consists of two pulleys of different diameter on each. An intermediate spindle which consists of four different diameter of pulleys two are for dork head motor and two for work head spindle. The schematic of arrangement is shown in Figure 3.13. Initial dimensions and parameters are shown in table 3.7. The calculations for workpiece speed are done in table 3.8.

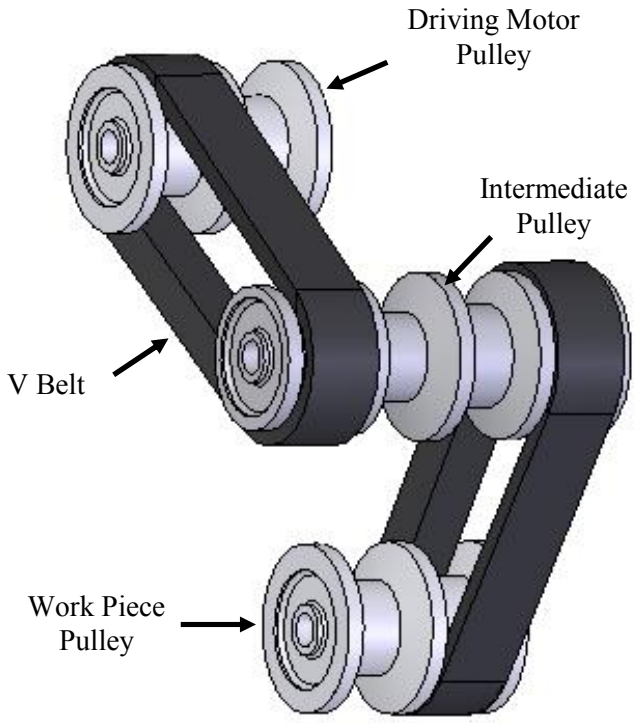

Figure 3.13: Schematic of pulleys arrangement for workpiece speeds

The work head motor has fixed 1380 rpm.

The diameter of the work-piece was 17.750mm.

Table 3.7: Initial dimensions and parameters

Parameter	Dimension/value
Diameter of pulley 1 of driving motor (p1)	50 mm
Diameter of pulley 2 of driving motor (p2)	60 mm
Diameter of Intermediate Pulley 1 (i1)	115 mm
Diameter of Intermediate Pulley 2 (i2)	95 mm
Diameter of Intermediate Pulley 3 (i3)	75 mm
Diameter of Intermediate Pulley 4 (i4)	55 mm
Diameter of pulley 1 of Wheel spindle (d1)	120 mm
Diameter of pulley 2 of driving motor(d2)	135 mm
Fixed rpm of driving motor	1380 rpm
Diameter of the worpiece i.e. d	17.750 mm

Table 3.8: Calculations for workpiece speed

Workpiece Speed	Arrangement\Factors	rpm	Wheel Speed $\frac{\pi.D.N}{60x1000}$ m/sec
1	p1 & i1 i4 &d2	245	$1.98x10^{-1}$
2	p1 & i1 i3 & d1	375	$3.04x10^{-1}$
2	p2 &i2 i3 & d1	545	$4.42x10^{-1}$

3.3.9 Grinding Wheel Specifications

The specifications of grinding wheel are A-60-L-5-V-10

The outside diameter of the grinding wheel is D = 300 mm

Width of grinding wheel is 38 mm

3.4 Experimental Setup

As stated before, L_9 array has been selected for the experimentation for each of three nozzles. Grinding wheel speed, work-piece speed, nozzle tip distance and nozzle angle are the factors of interest. L_9 array with actual factors level is shown in Table 3.3. The values of the input process parameters for the grinding are shown in table 3.1. Figure 3.14 shows the work-piece being ground on cylindrical grinding machine.

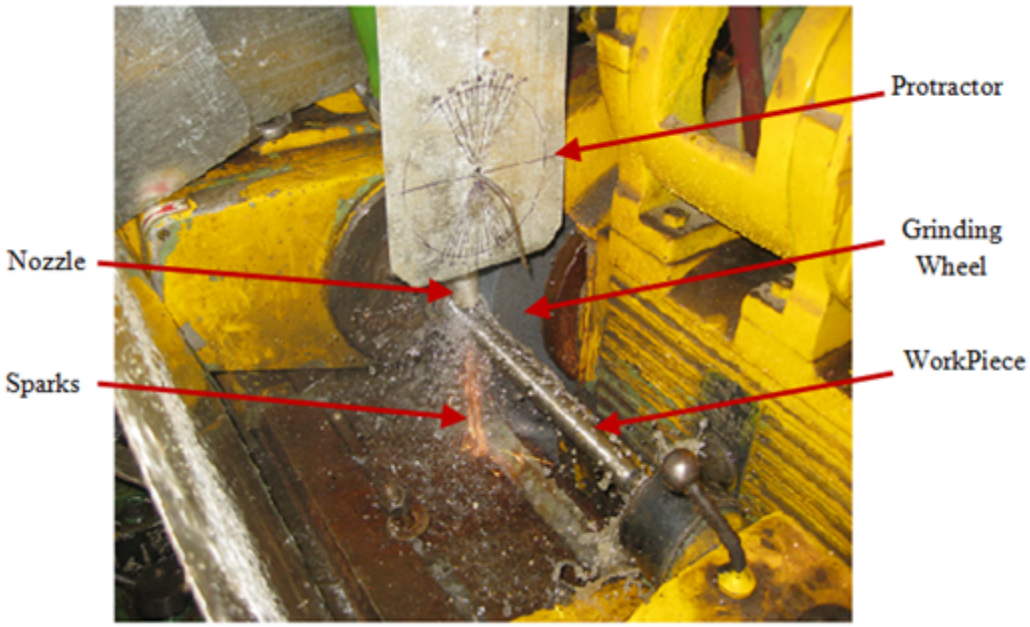

Figure 3.14: Grinding operation on machine

Mild Steel rod is taken for the workpiece to be ground. It is a 20 mm diameter rod which is finished to 17.750 mm first by rough turning and then by cylindrical grinding machine as an initial diameter for the workpiece. Length of work piece was taken as 260mm. Two workpieces are assigned for each L_9 array and Nozzle. On one work-piece five cuts are applied and on second workpiece four cuts are applied. The first cut is of 100 microns and second cut is of 50 microns.

Surface cracks are checked on the digital microscope with 200X zoom camera. Then dimensional control of each sample having 4 or 5 replications is measured with vernier micrometer. On each replication six readings are taken on different locations and then the C_p is calculated. The surface hardness was measured, after samples are etched with *2%* Nital solution (Alcohol + Nitric Acid) on each sample on each of 4 or 5 replications. Three readings on each replication are taken individually and then the mean of three is taken.

3.5 MEASURING EQUIPMENT

1) **Vernier micrometer:** Screw gauge type micrometer was used to check the dimensional control. It has range of 0 to 25mm with least count of 1 μm.
2) **Metallurgical microscope:** Surface Cracks are checked with metallurgical microscope available in the Central workshop, Thapar University, Patiala.
3) **Surface hardness tester:** Surface hardness tests are conducted on the Vickers hardness tester available at Central workshop, Thapar University, Patiala. Diamond indenter is used for the purpose (hardness measured is dependent on the Diagonal length of indentation on the sample. Load applied and dwell time for surface hardness testing was taken 50Kgf and 20 seconds respectively.

CHAPTER 4
RESULTS AND ANALYSIS

4.1 COMPUTATIONAL FLUID DYNAMIC SIMULATIONS

In grinding the effect of heat is very severe as change in surface finish, dimensional accuracy, surface properties (micro hardness, roughness etc.) of workpiece. So a cooling system with appropriate is needed which can successfully remove the heat generated during grinding operations preventing the diverse effects of heat on workpiece. Computational fluid dynamic (CFD) simulation approach is adopted to analyse the flow behaviour through different type nozzles so that suitable nozzle for cooling system can be chosen. Simulation of fluid flow is carried out using ANSYS CFX 11.0 software. Also the effect of coolant flow through selected nozzles is analysed in grinding zone through the same CFD approach.

4.2 FLUID FLOW SIMULATION THROUGH DIFFERENT TYPES NOZZLES

First, flow behaviour simulation of coolant is done through different type of nozzles described by different researchers, by varying there geometrical dimensions. Nozzle selected for fluid flow simulation analyses are Convergent divergent, Taper, Spline, Round, Step. Outlet diameter and inlet diameter of nozzles are kept constant. Nozzle selection for further grinding process simulation and for manufacturing for experimentation is done on the bases of peak velocity and its range from nozzle outlet. Fluid simulations through different types of nozzles are shown bellow.

4.2.1 Fluid Simulation Through Different Convergent Divergent Nozzles

Convergent and divergent angles are varied which are denoted as α1 and α2 respectively. Divergence length (y) is also varied. A schematic diagram of convergent divergent nozzle is shown in figure 4.1. Effect of dimensional variation is given in the form of table (table 4.1) and figures 4.2 to 4.8. Figure (a) of each figure set shows the velocity vectors of fluid flow through outlet of nozzle. Figure (b) shows that how velocity of fluid varies at the outlet of nozzle. In the graphs distance from outlet of nozzle is along abscissa and velocity of fluid (water) is along ordinate.

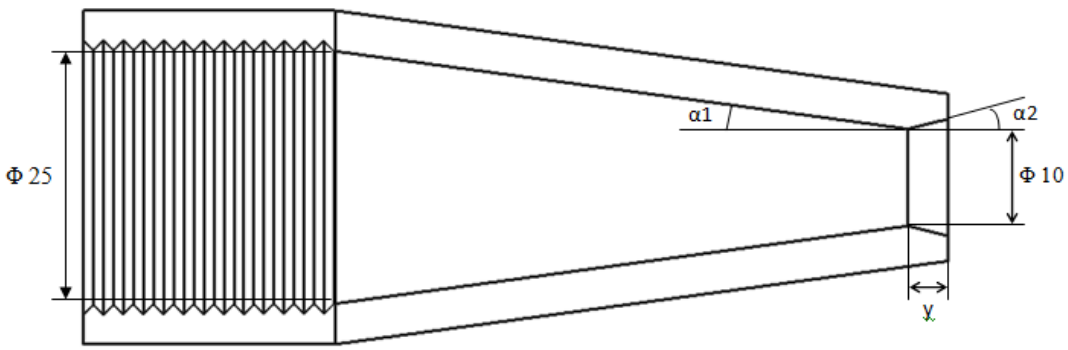

Figure 4.1: Schematic diagram of convergent divergent nozzle

(All dimensions in mm)

Table 4.1: Peak Velocities of different convergent divergent nozzles

S. No	Dimensions			Peak Velocity (m/s)	Figure No.
	Convergence angle α1 (degrees)	Divergence angle α2 (degrees)	Divergence length y (mm)		
1	5	5	2	22.31	Figure 4.2
2	5	5	4	22.69	Figure 4.3
3	5	7.5	4	23.84	Figure 4.4
4	5	10	4	24.19	Figure 4.5
5	7.5	7.5	2	22.40	Figure 4.6
6	7.5	7.5	4	23.86	Figure 4.7
7	7.5	10	4	24.50	Figure 4.8

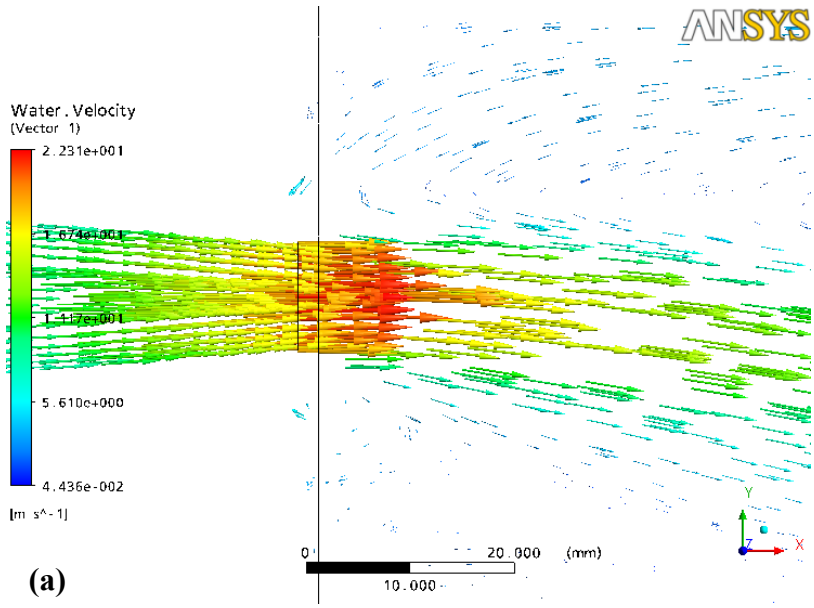

(a)

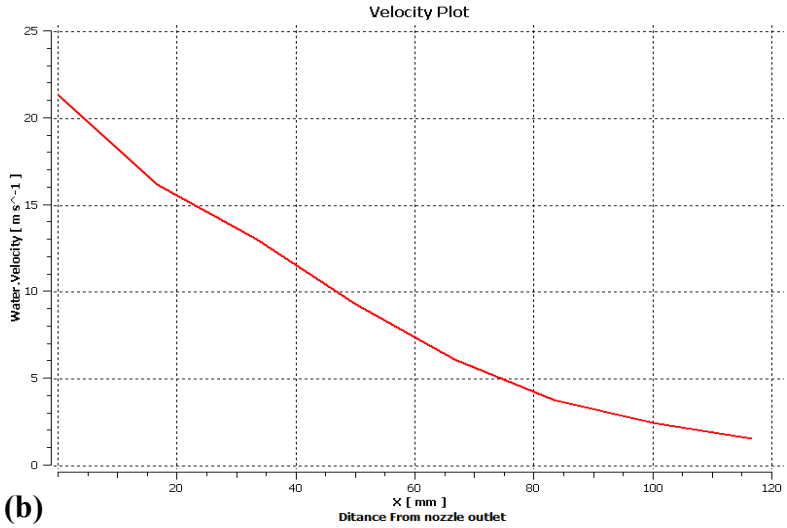

(b)

Figure 4.2: (a) Velocity vectors diagram of convergent divergent nozzle with α1 = 5^0, α2 = 5^0 and y = 2 mm (b) Velocity Plot

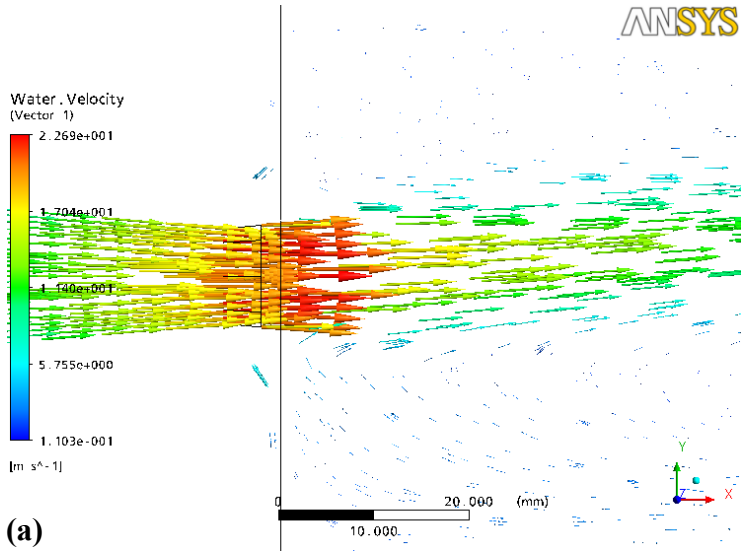

(a)

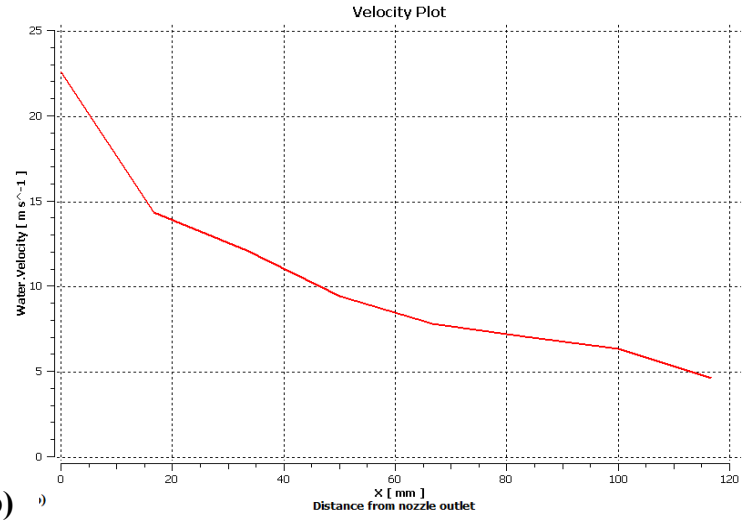

(b)

Figure 4.3: (a) Velocity vectors diagram of convergent divergent nozzle with α1 = 5^0, α2 = 5^0 and y = 4 mm (b) Velocity plot

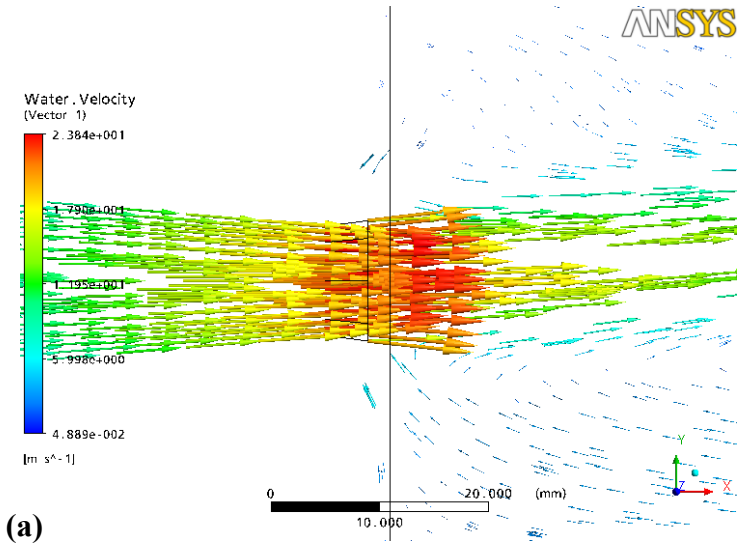

(a)

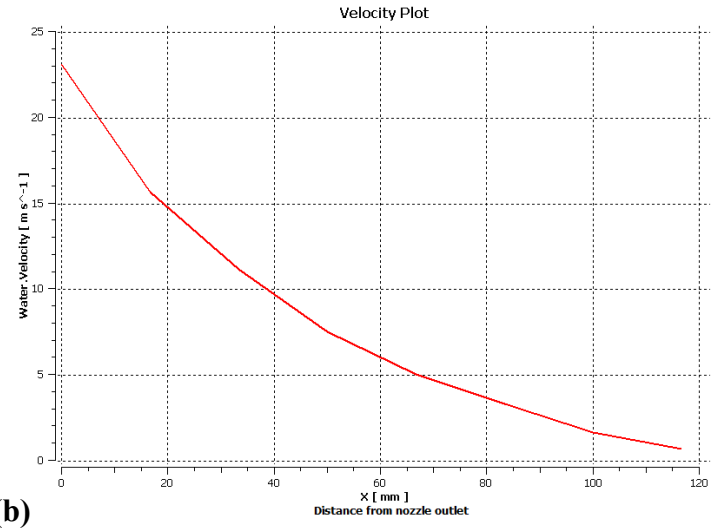

(b)

Figure 4.4: (a) Velocity vectors diagram of convergent divergent nozzle with α1 = 5^0, α2 = 7.5^0 and y = 4 mm (b) Velocity plot

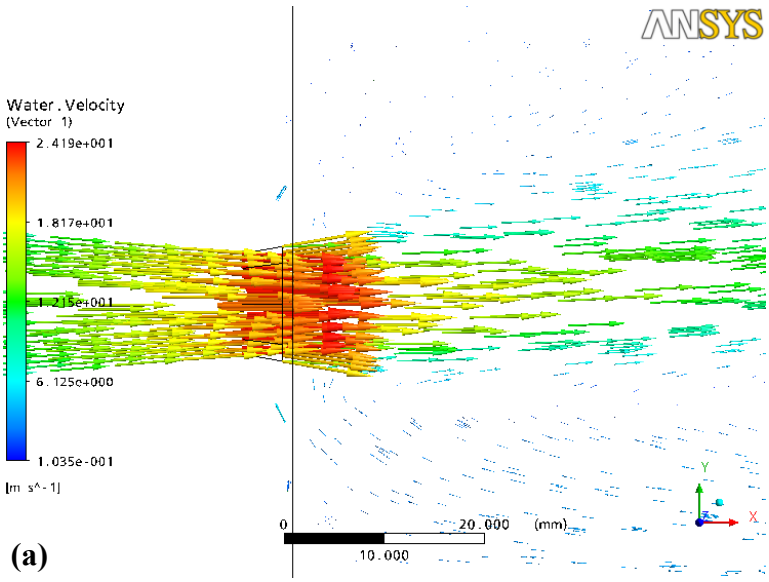

(a)

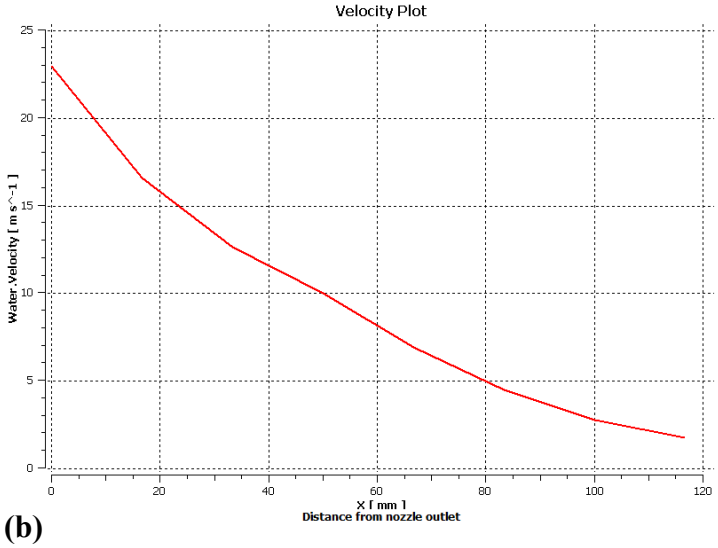

(b)

Figure 4.5: (a) Velocity vectors diagram of convergent divergent nozzle with α1 = 5^0, α2 = 10^0 and y = 4 mm (b) Velocity Plot

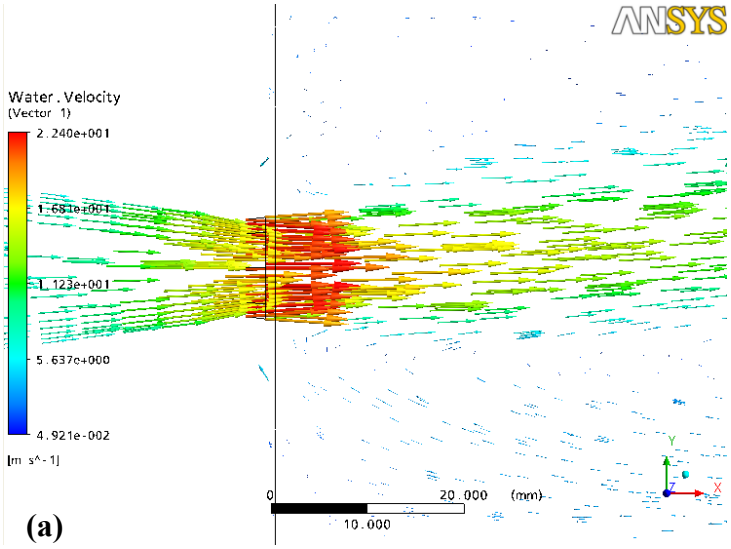

(a)

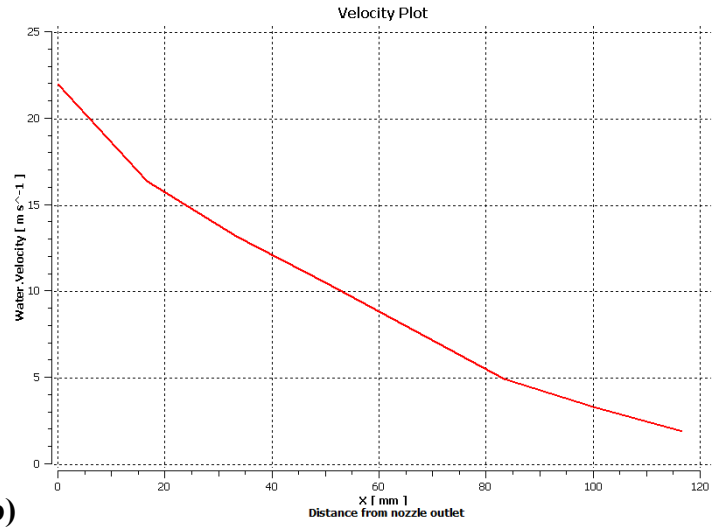

(b)

Figure 4.6: (a) Velocity vectors diagram of convergent divergent nozzle with α1 = 7.5^0, α2 = 7.5^0 and y = 2 mm (b) Velocity plot

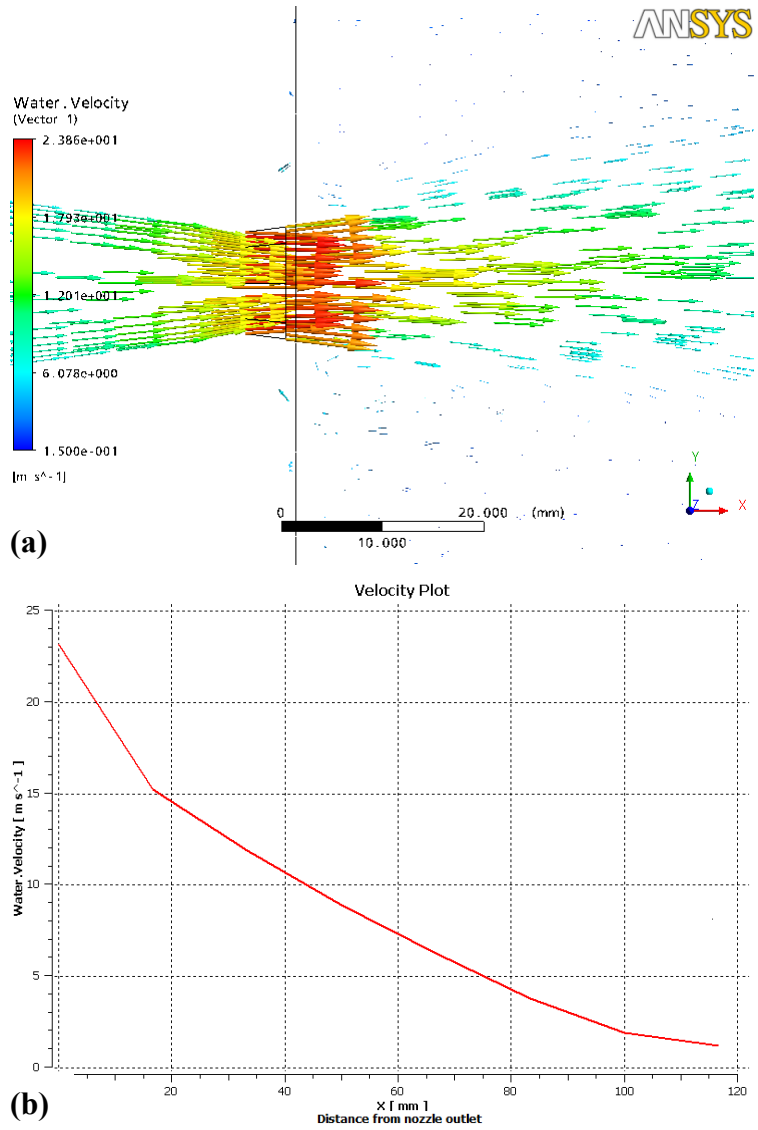

Figure 4.7: (a) Velocity vectors diagram of convergent divergent nozzle with α1 = 7.5^0, α2 = 7.5^0 and y = 4 mm (b) Velocity Plot

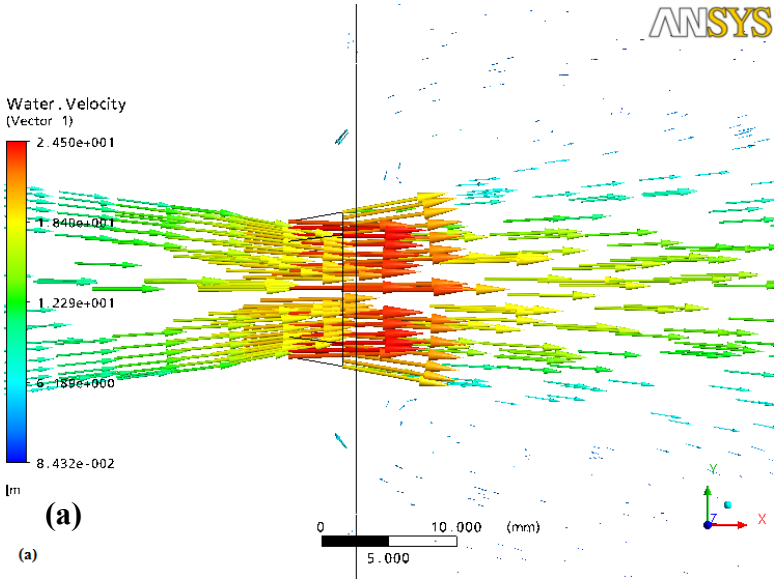

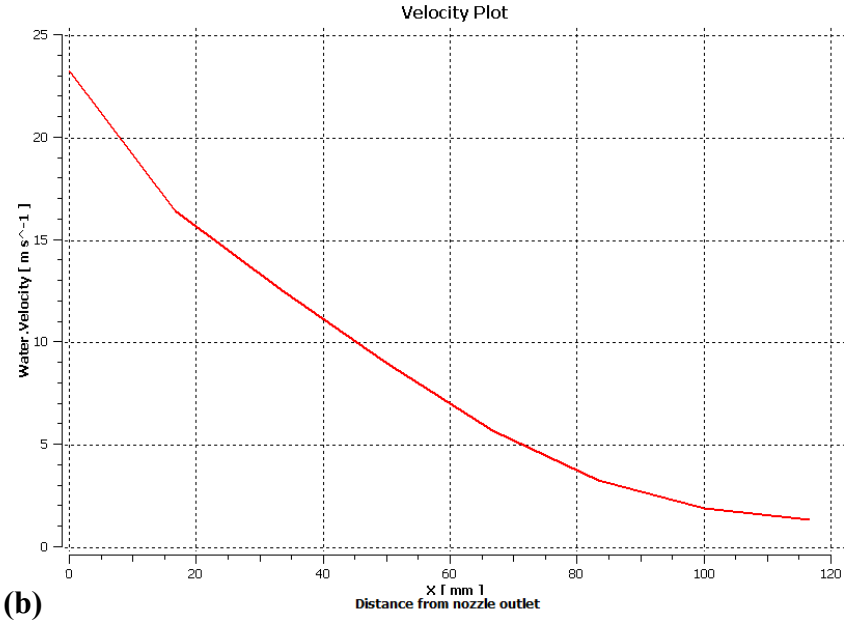

(b)

Figure 4.8: (a) Velocity vectors diagram of Convergent divergent nozzle with α1 = 7.5^0, α2 = 10^0 and y = 4 mm (b) Velocity Plot

4.2.2 Fluid Flow Simulation Through Different Taper Nozzles

Profile of Taper Nozzle is converging from inlet toward outlet. Taper angle is varied which is denoted by symbol α. A schematic diagram of Taper nozzle is shown in figure 4.9. Effect of dimensional variation on peak velocity is shown in table 4.2 and in figures from (4.10 to 4.13). Figure (a) of each figure set shows the velocity vectors of fluid flow and figure (b) shows the plot between velocity of fluid and distance from nozzle outlet.

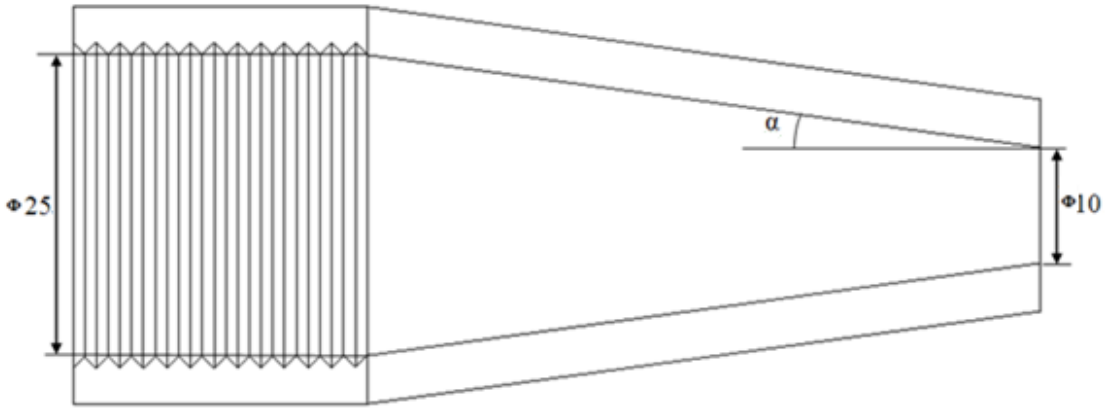

Figure 4.9: Schematic diagram of taper nozzle

(All dimensions in mm)

Table 4.2: Peak velocities of different taper nozzles

S. No.	Taper angle α (degrees)	Peak velocity (m/s)	Figure no.
1	4	21.76	Figure 4.10
2	7.5	21.56	Figure 4.11
3	10	20.96	Figure 4.12
4	15	20.33	Figure 4.13

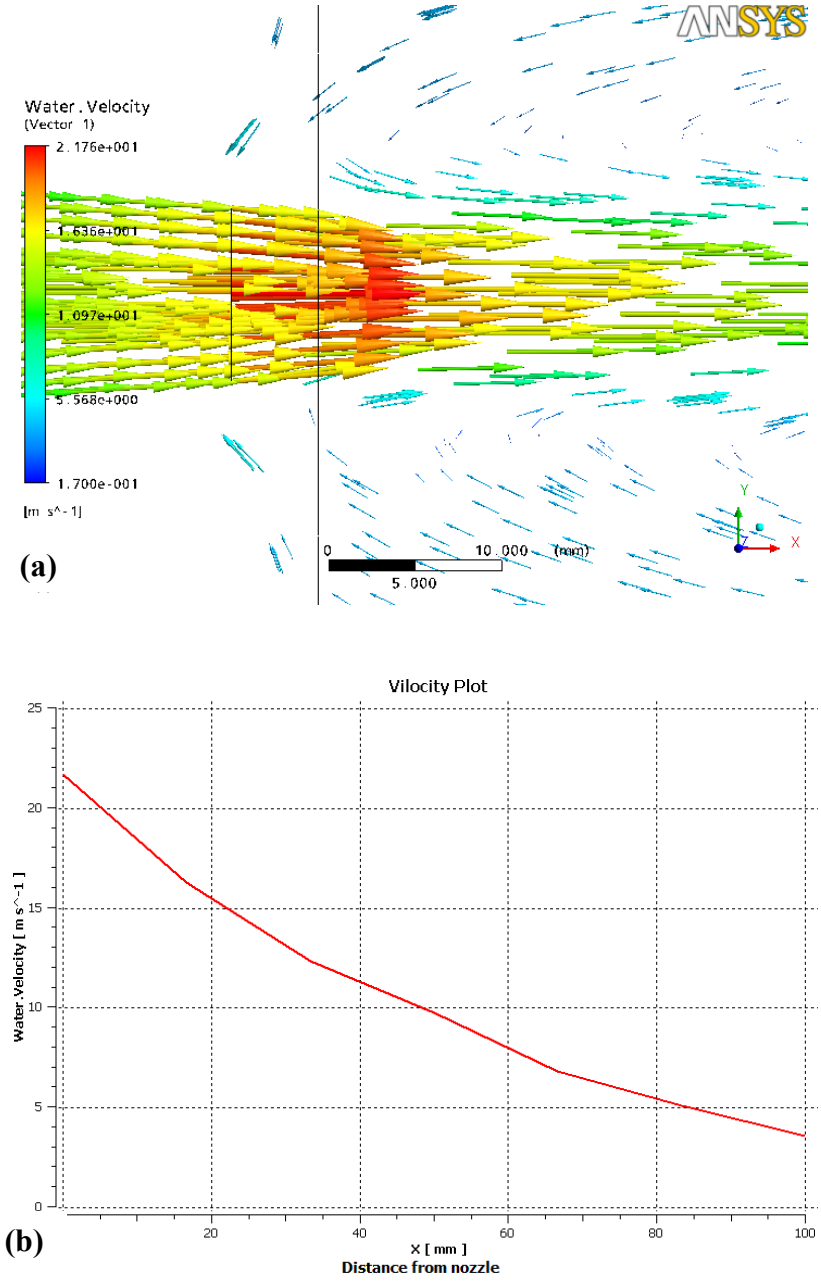

Figure 4.10: (a) Velocity vectors diagram of taper nozzle with α = 4^0 (b) Velocity Plot

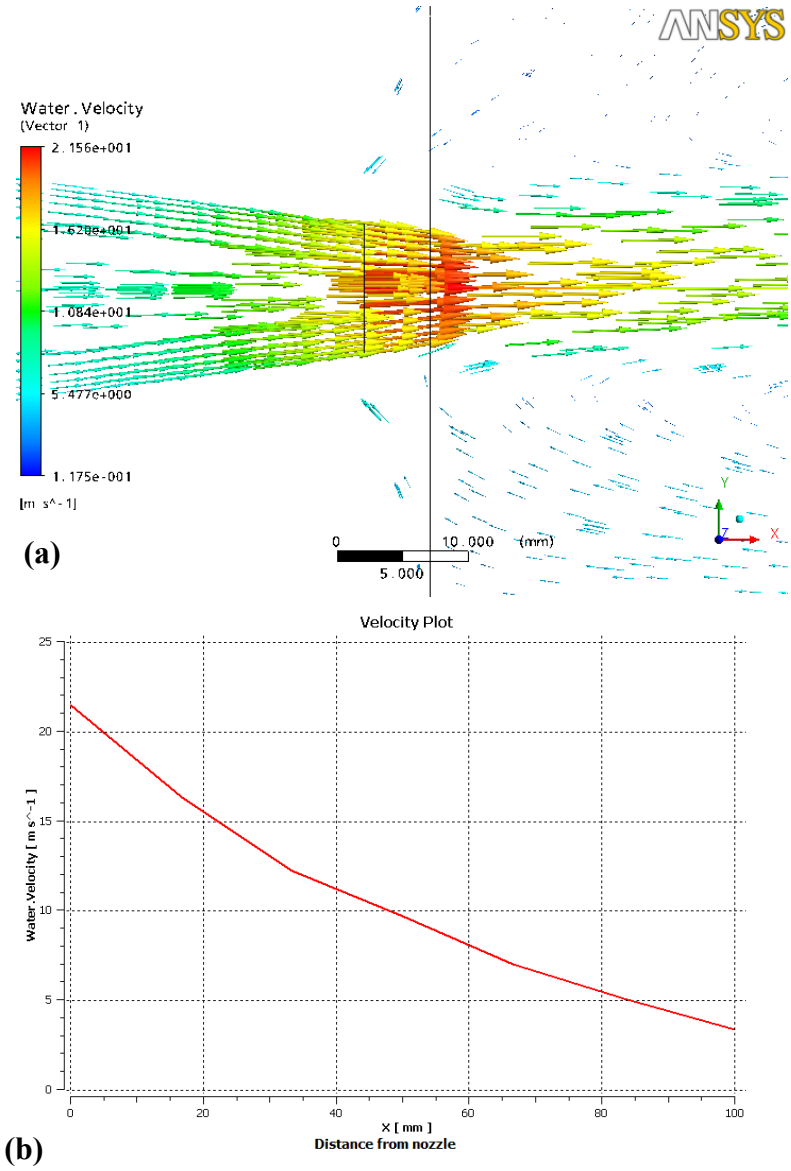

Figure 4.11 (a) Velocity vectors diagram of taper nozzle with α = 7.5^0 (b) Velocity Plot

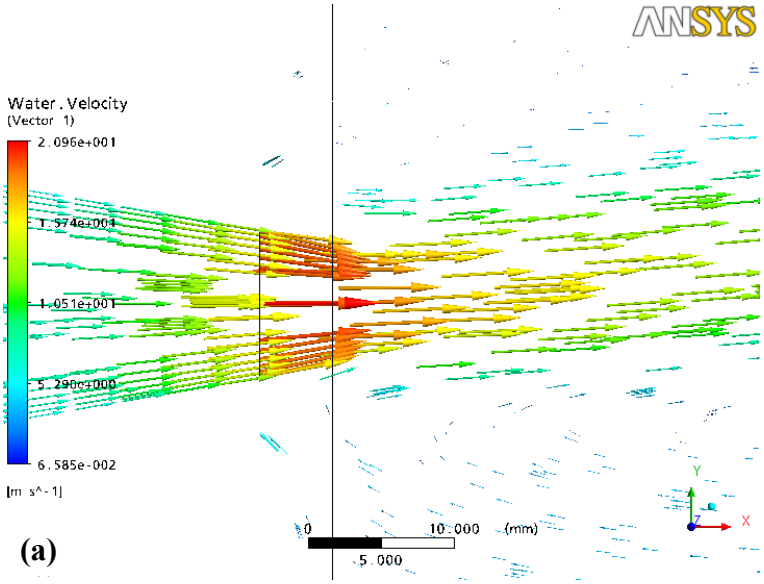

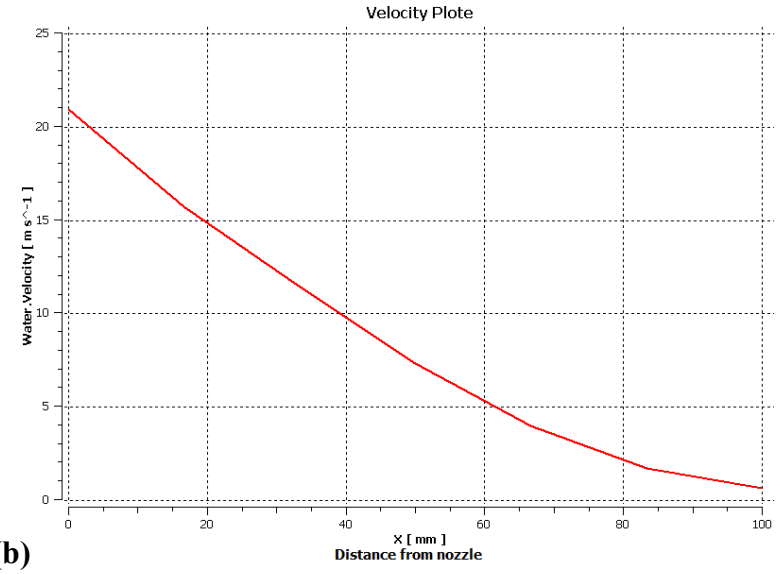

(b)

Figure 4.12: (a) Velocity vectors diagram of taper nozzle with α = 10^0 (b) Velocity plot

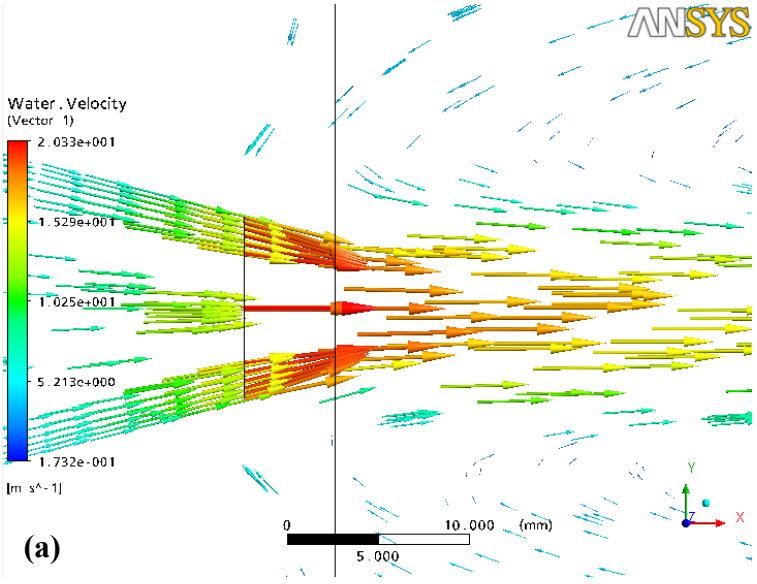

(a)

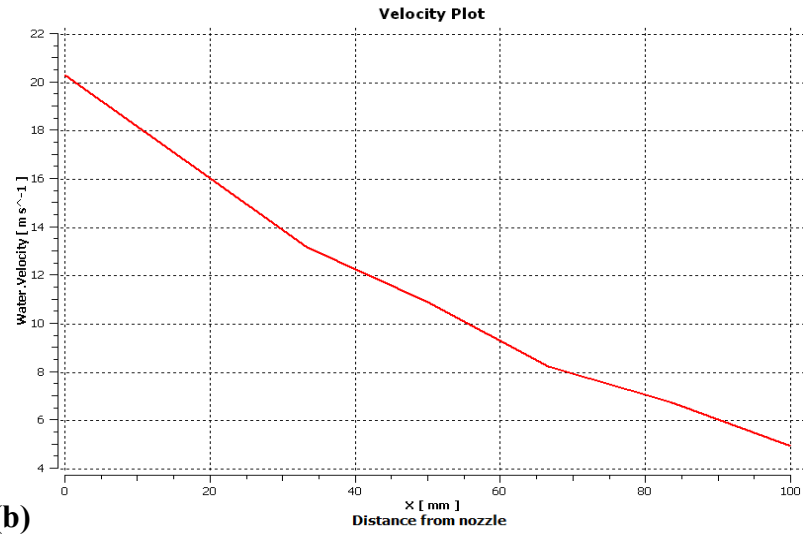

(b)

Figure 4.13 (a) Velocity vectors diagram of taper nozzle with α = 15^0 (b) Velocity plot

4.2.3 Fluid Flow Simulation Through Different Spline nozzles

Different Spline curve profiles are tried to make the nozzle to simulate the fluid flow. Their Peak velocity and length of peak velocity region at the outlet on nozzle are analysed. There velocity vector diagrams and velocity plot are shown in following figures. Peak velocities for different spline nozzles are shown in table 4.3. A schematic of Spline Nozzle is shown in figure 4.14. Velocity vectors of fluid flow and plot between velocity and distance from nozzle out let is shown in figure sets (4.15 to 4.17).

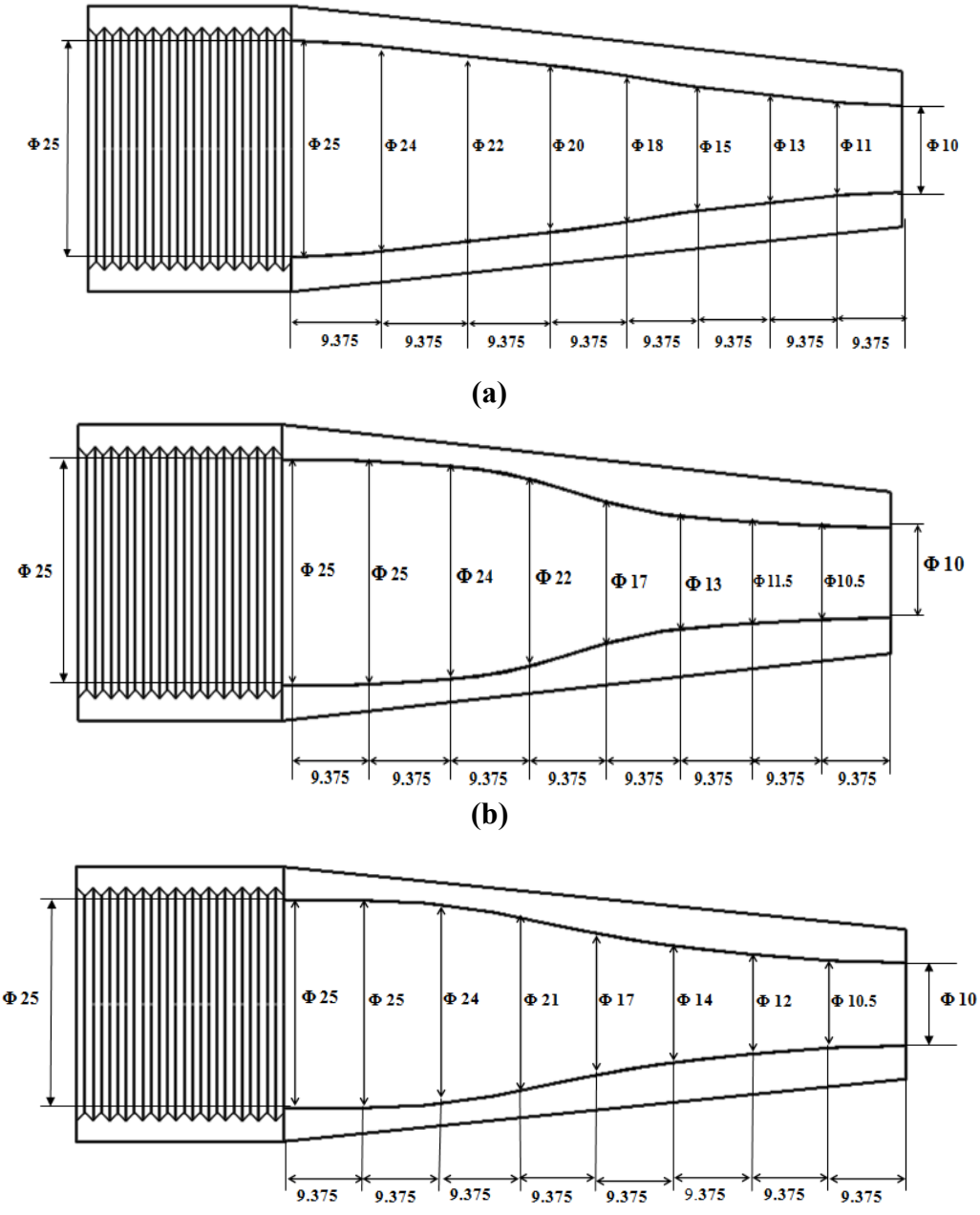

Figure 4.14: Schematic Diagrams of (a) Spline_1 nozzle (b) Spline_2 nozzle (c) Spline_3 nozzle (all dimensions in mm)

Table 4.3: Peak velocities of different spline nozzles

S. No.	Spline Name	Peak velocity (m/s)	Figure no.
1	Spline_1	22.20	Figure 4.15
2	Spline_2	22.44	Figure 4.16
3	Spline_3	22.32	Figure 4.17

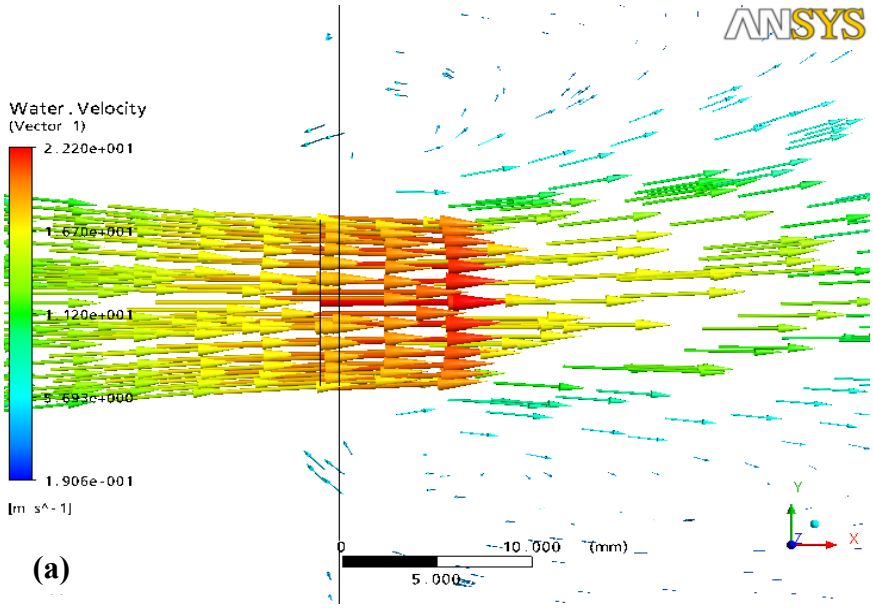

(a)

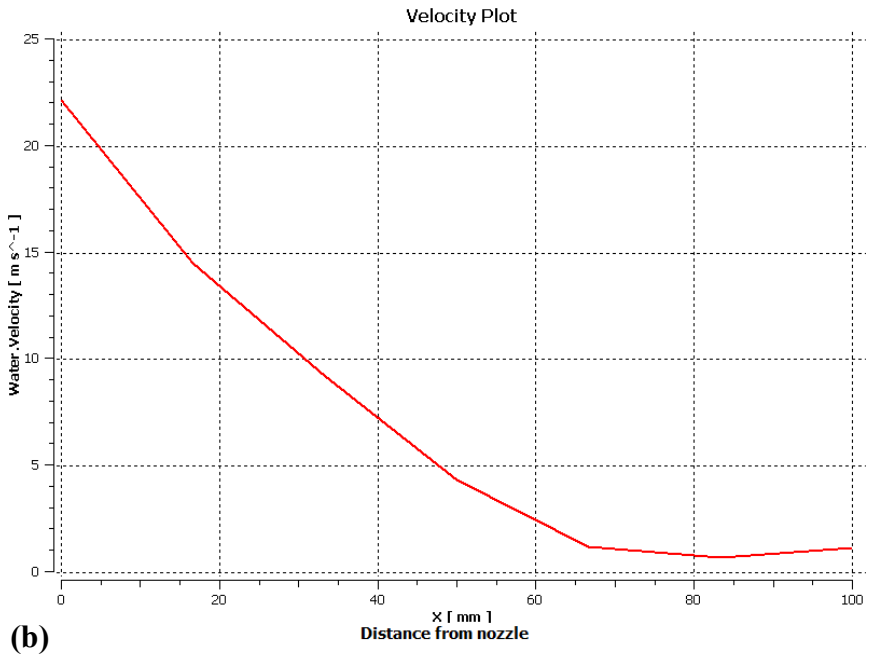

(b)

Figure 4.15: (a) Velocity vectors diagram of spline_1 nozzle (b) Velocity Plot

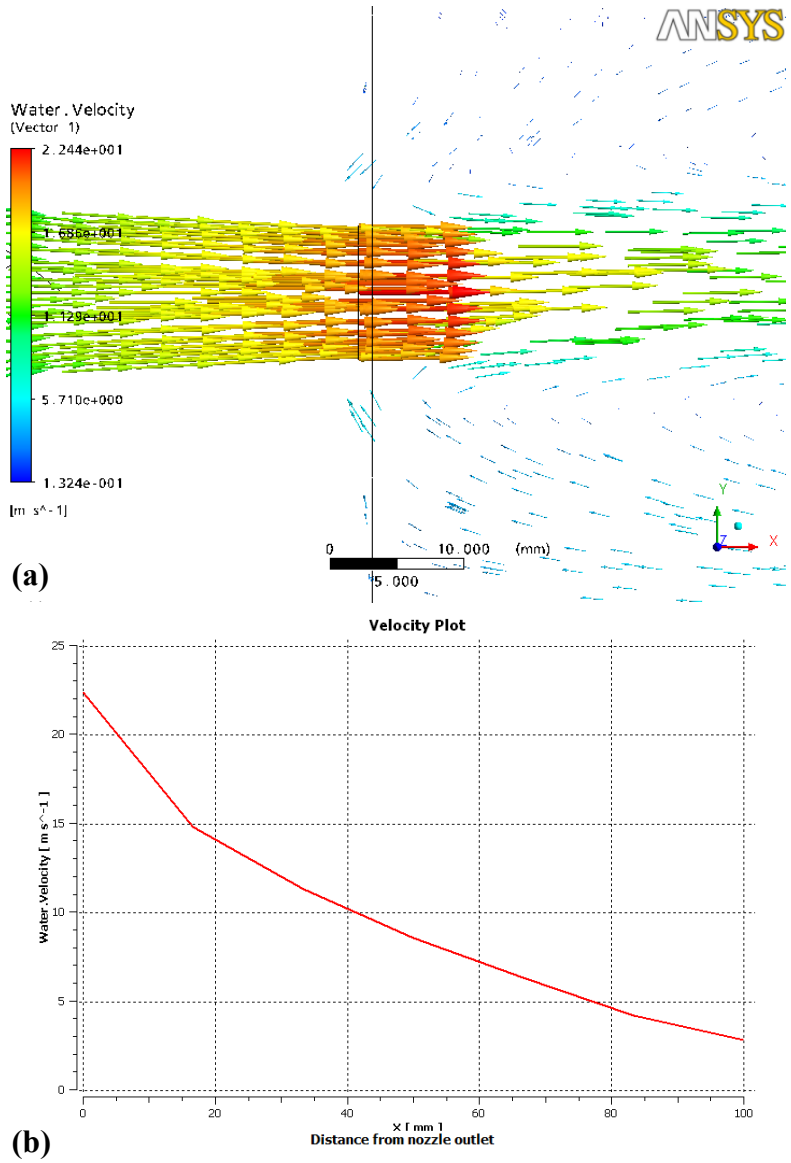

Figure 4.16: (a) Velocity vectors diagram of spline_2 nozzle (b) Velocity plot

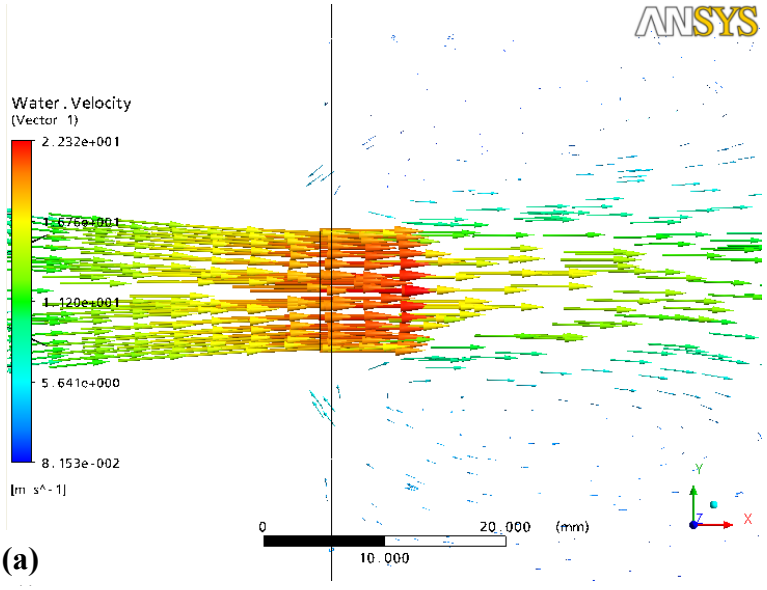

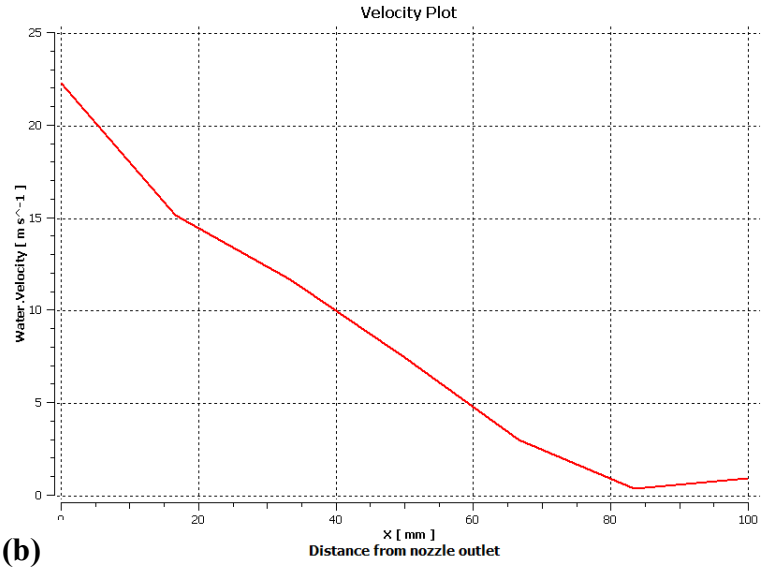

(b)

Figure 4.17: (a) Velocity vectors diagram of spline_3 nozzle (b) Velocity plot

4.2.4 Fluid Simulation Through Different Round Nozzles

Radius of round section and land length are varied which are denoted as r and l respectively. A schematic diagram of Round nozzle is shown in figure 4.18. Effect of dimensional variation on velocity of fluid flow is given in the table 4.4 and figures (4.19 to 4.21). In Figure (a) of each figure set Velocity vector diagram is shown and in figure (b) variation of velocity with respect to distance from nozzle outlet is drawn.

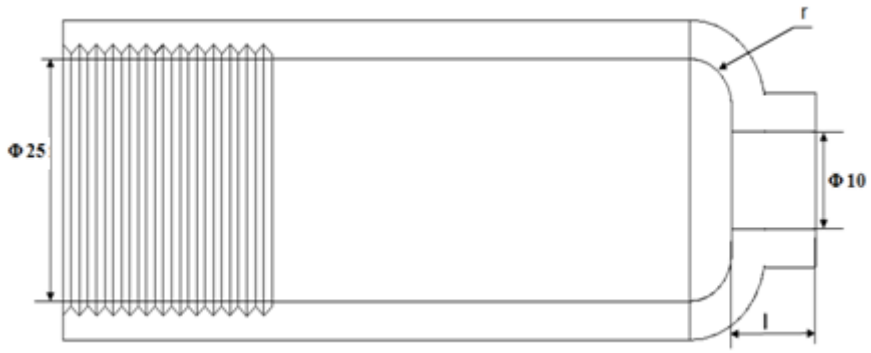

Figure 4.18: Schematic diagram of round nozzle

(All dimensions in mm)

Table 4.4: Peak velocities of different Round nozzles

S. No	Radius r (mm)	Land l (mm)	Peak Velocity (m/s)	Figure No.
1	5	10	20.24	Figure 4.19
2	5	15	20.02	Figure 4.20
3	22.5	10	22.25	Figure 4.21

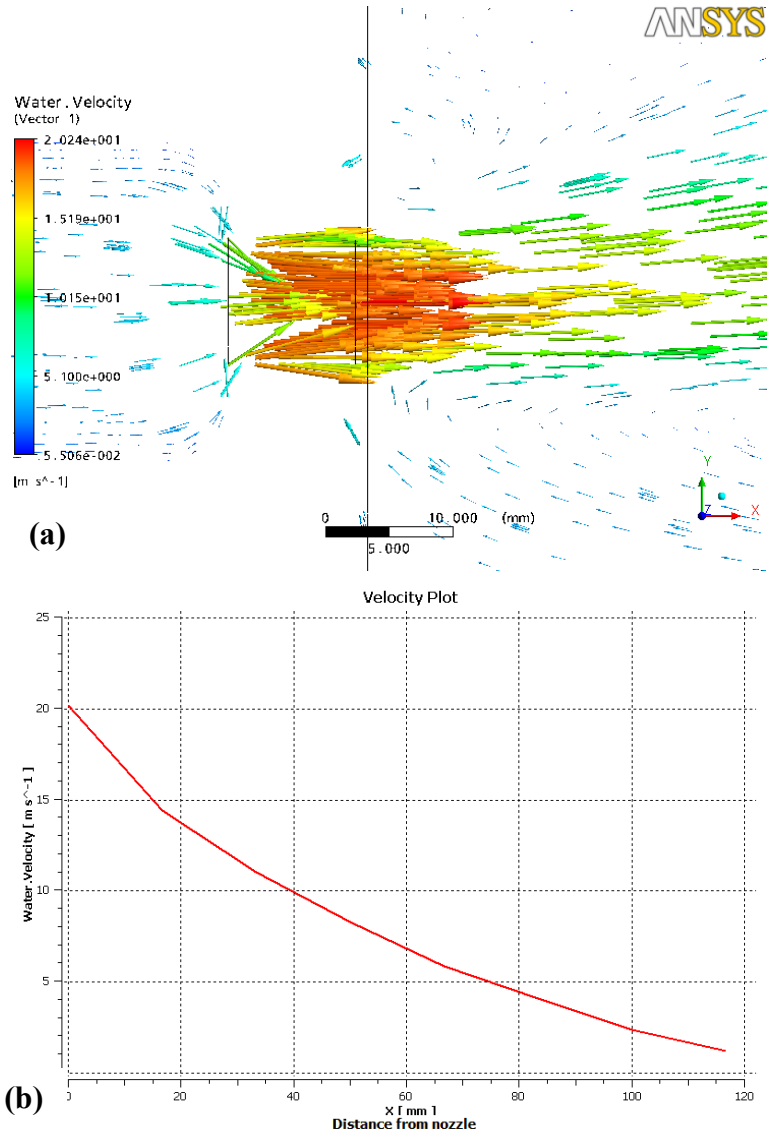

Figure 4.19: (a) Velocity vectors diagram of round nozzle with radius r=5 mm and land l=10 mm (b) Velocity Plot

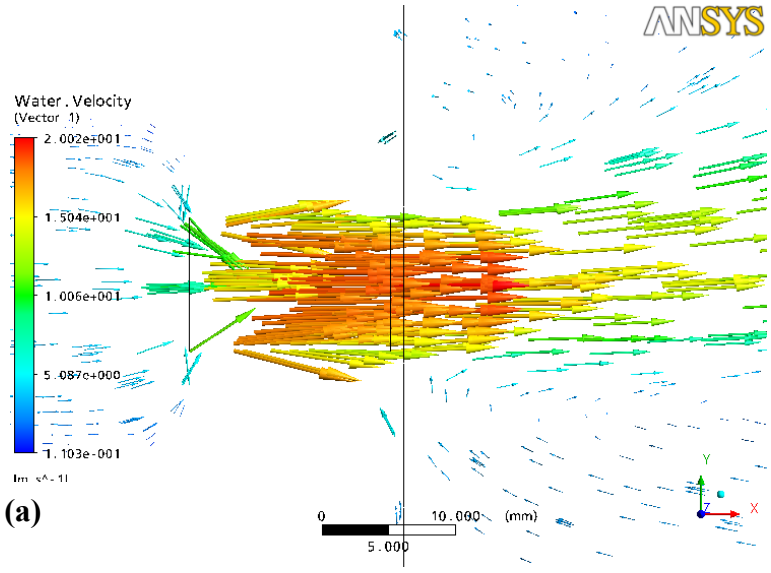

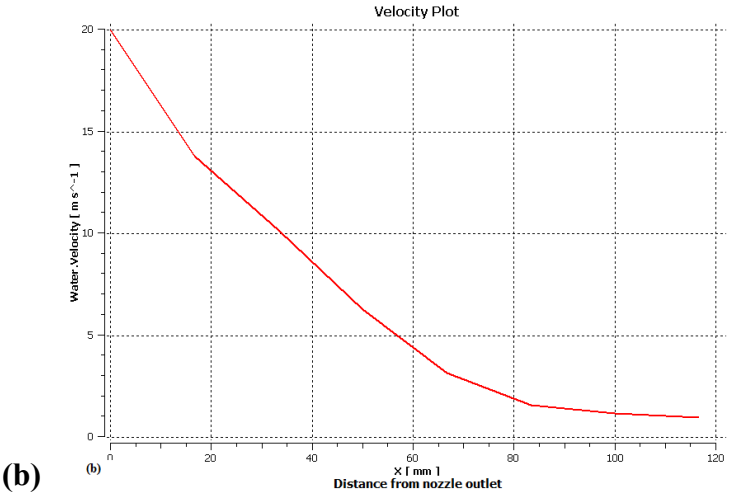

Figure 4.20: (a) Velocity vectors diagram of round nozzle with radius r=5 mm and land l=15 mm (b) Velocity plot

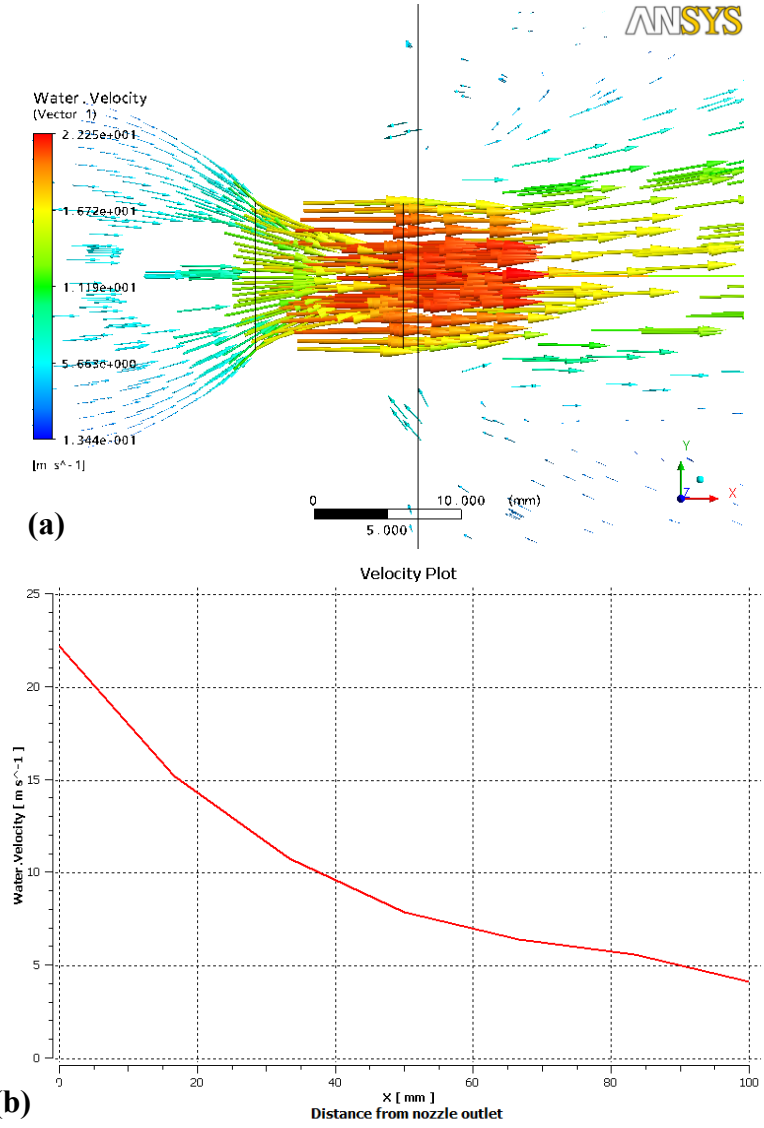

Figure 4.21: (a) Velocity vectors diagram of round nozzle with radius r=22.5 mm and land l=10 mm (b) Velocity plot

4.2.5 Fluid simulation Through Different Step Nozzles

Land length of step nozzles is varied which is denoted as l. A schematic diagram of Step nozzle is shown in figure 4.22. Variations in peak velocity of nozzle due to change in dimensions of land section of nozzle are given in the table 4.5 and in figure (4.23 and 4.24). Velocity vector diagram of fluid flow through outlet of nozzle and Plot between velocity and distance from nozzle outlet is shown in figure (a) and figure (b) of figure 4.23 and figure 4.24.

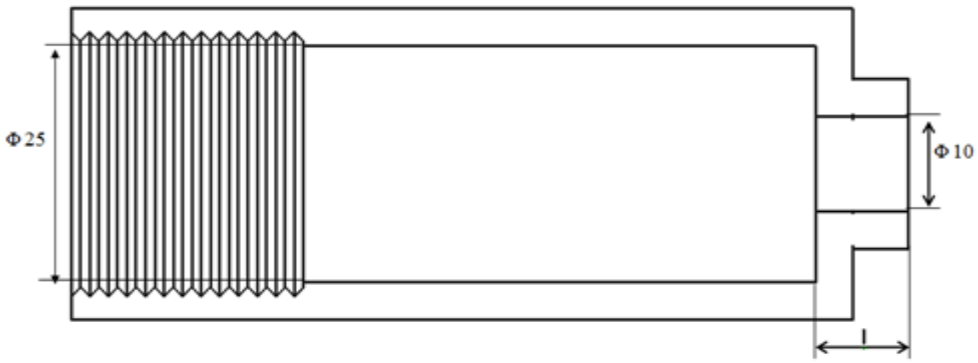

Figure 4.22: Schematic diagram of step nozzle

(All dimensions in mm)

Table 4.5: Peak velocities of different step nozzles

S. No	Land l (mm)	Peak Velocity (m/s)	Figure No.
1	10	23.44	Figure 4.23
2	15	22.81	Figure 4.24

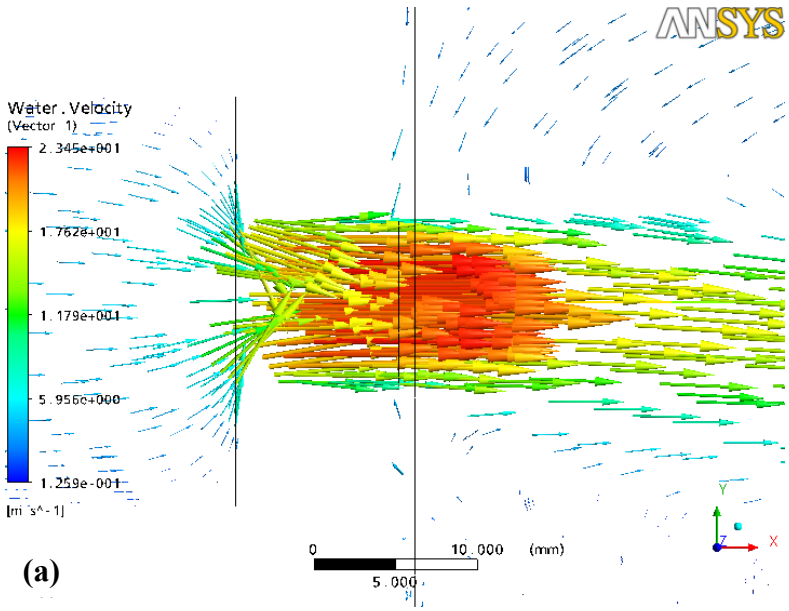

(a)

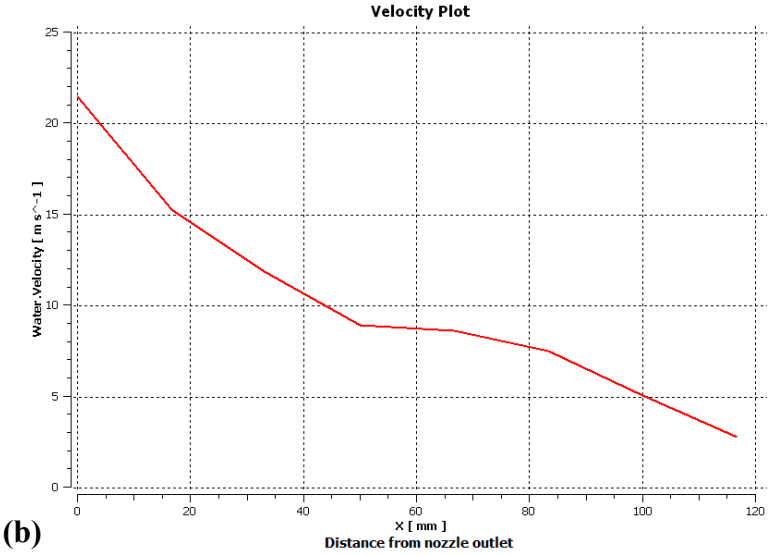

(b)

Figure 4.23: (a) Velocity vectors in Step nozzle with land l=10 mm (b) Velocity Plot

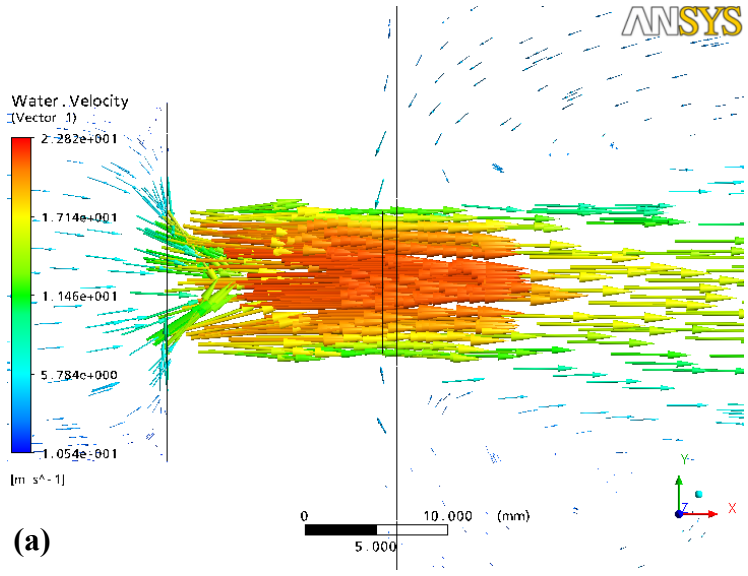

(a)

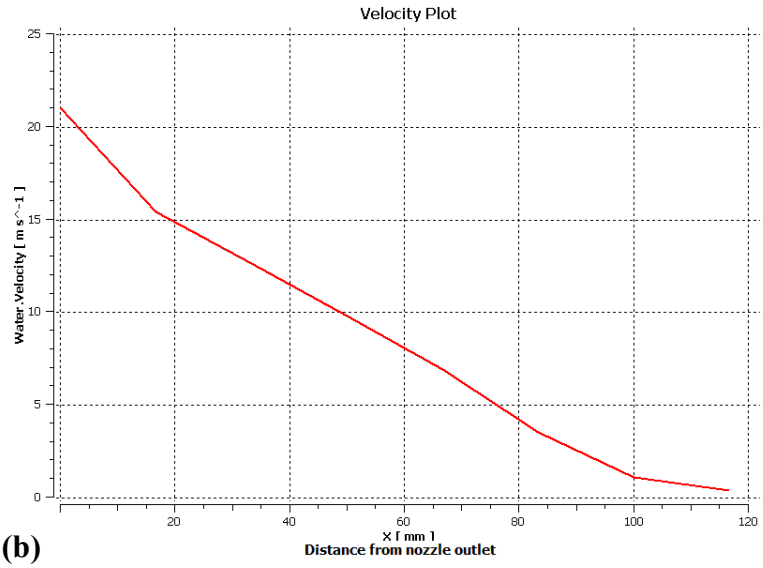

(b)

Figure 4.24: (a) Velocity vectors Step nozzle with land l=15 mm (b) Velocity Plot

After analysing the fluid flow through different types of nozzles and also by changing geometrical parameters of each type of nozzles three nozzles are selected for further simulation of grinding process and to be manufactured for experimentation work on the bases of their peak velocities and also on the bases of the region of peak velocities at the outlet of nozzles. These three nozzles are convergent divergent nozzle with convergent angle $\alpha1=7.5^0$, divergent angle $\alpha2=10^0$ and divergence length y= 4mm, Spline_2 nozzles, taper with taper angle $\alpha=4^0$. Geometrical diagrams of these three nozzles are shown in figure 4.25 (a to c).

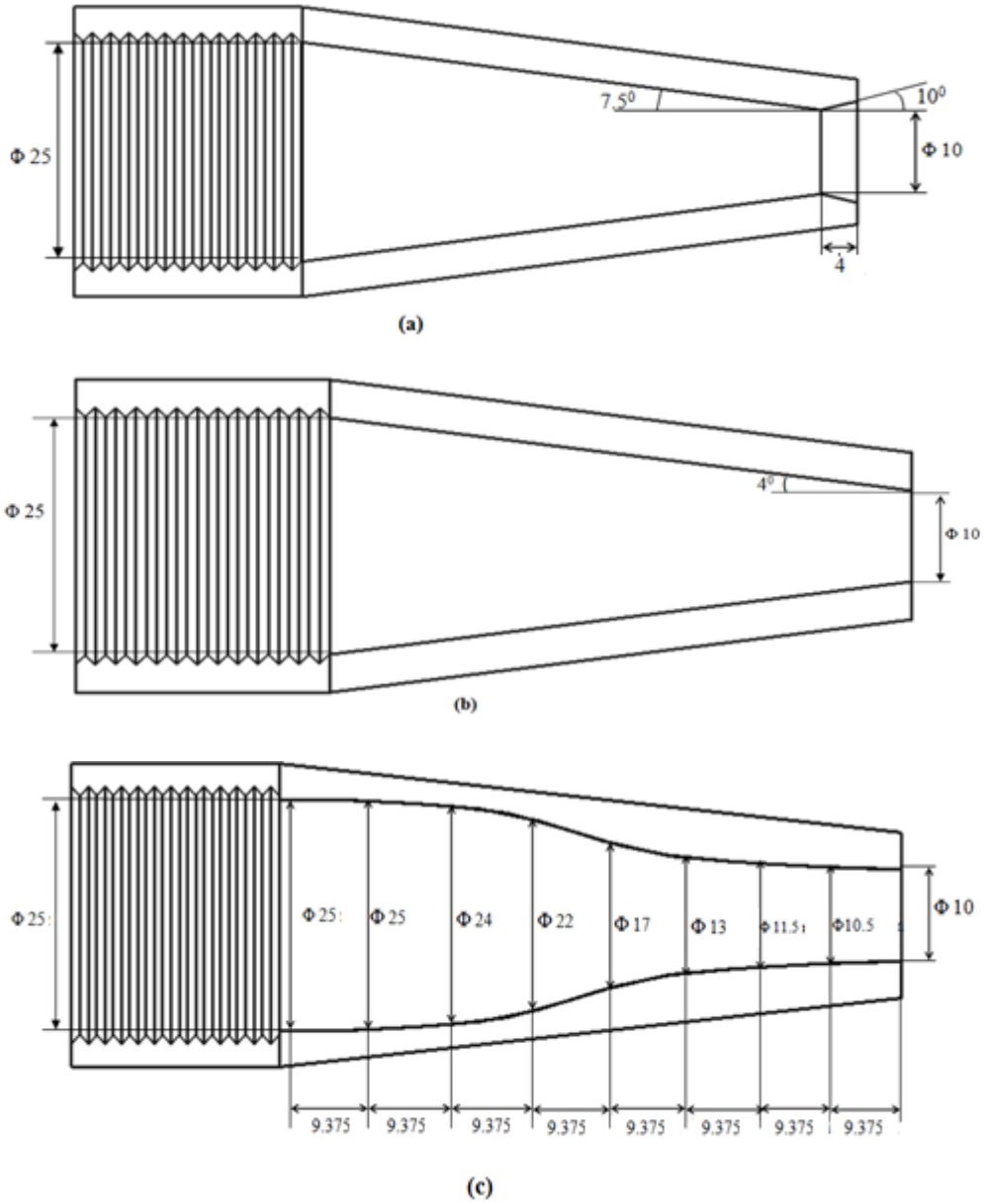

Figure 4.25: Geometrical diagrams of (a) Convergent Divergent nozzle (b) Taper nozzle (c) Spline Nozzle (All dimensions in mm)

4.3 GRINDING PROCESS SIMULATION

After finalizing the nozzles for further simulation and experimentation work, taguchi's orthogonal array technique is used to carry out the grinding process simulation and experimentation. In grinding process simulation grinding wheel of 300 mm diameter workpiece of 17.750 mm diameter are considered which are rotating at different speeds. An air environment is created around the grinding wheel, workpiece and nozzle. Multi-fluid simulation (air in environment and water in nozzles) is done. The behaviour of coolant flow through nozzle in grinding zone is measured in terms of velocity. According to the degree of freedom of all the factors (wheel speed, workpiece speed, nozzle angle, nozzle tip distance) the most suitable orthogonal array L9 is selected that can be used for this experiment, for each nozzle geometry. Grinding process simulation is done according to the L_9 orthogonal array using multi-fluid (air as environment and water as coolant) simulation. Velocities are found out in the contact region (of grinding wheel and workpiece) in each L_9 case. After finding out the velocity in grinding region of each experiment for each nozzle ANOVA is applied to work out the analysis.

4.3.1 Grinding Process Simulations for Convergent Divergent Nozzle

According to L_9 orthogonal array nine grinding process simulation are carried out for convergent divergent nozzle. For all nine experiments of L_9 velocity vector diagrams are described in figure 4.26 (a to i). In these figures the behaviour of fluid flow through nozzle in grinding zone is shown. The resulting velocity for each experiment is shown in table 4.6.

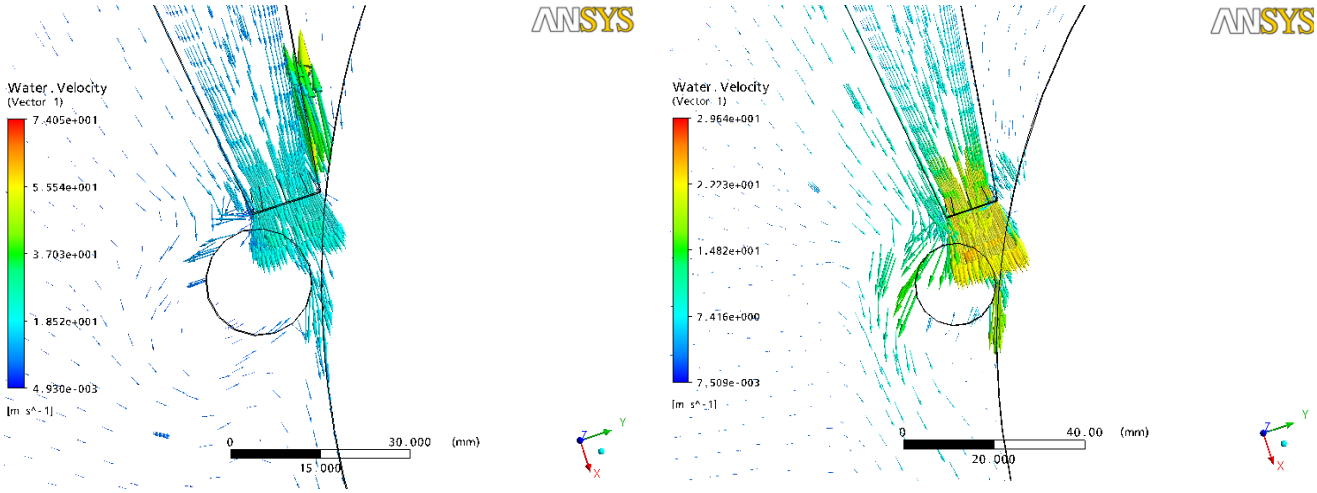

(a) **(b)**

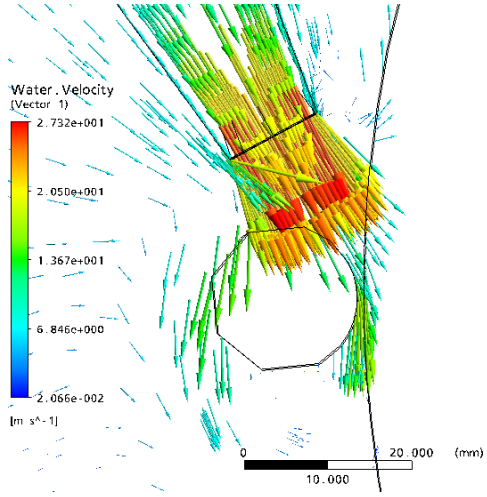
Water . Velocity
(Vector 1)
2.732e+001
2.050e+001
1.367e+001
6.846e+000
2.066e-002
[m s^-1]
0
20.000
(mm)
10.000

(c)

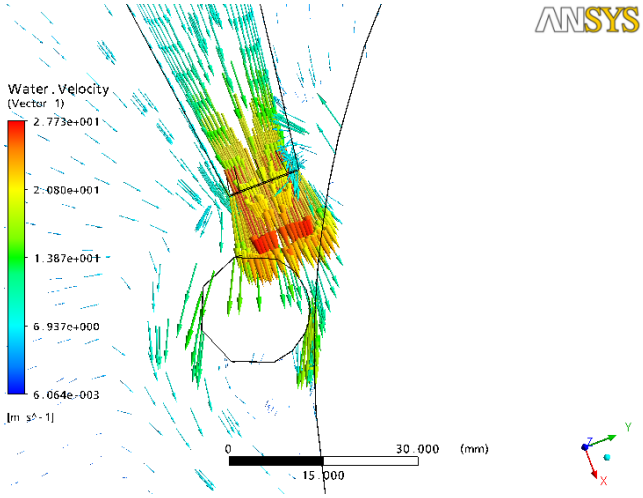
Water . Velocity
(Vector 1)
2.773e+001
2.080e+001
1.387e+001
6.937e+000
6.064e-003
[m s^-1]
0
30.000
(mm)
15.000

(d)

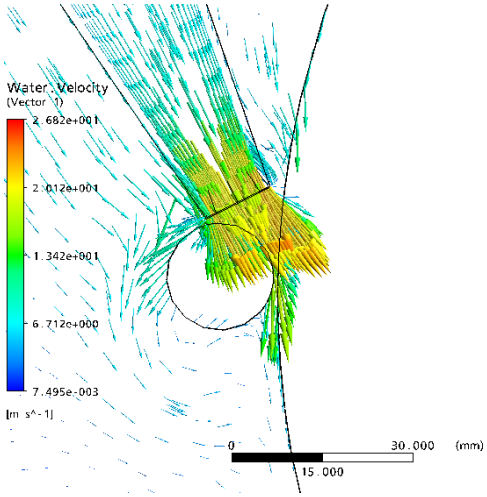
Water . Velocity
(Vector 1)
2.682e+001
2.012e+001
1.342e+001
6.712e+000
7.495e-003
[m s^-1]
0
30.000
(mm)
15.000

(e)

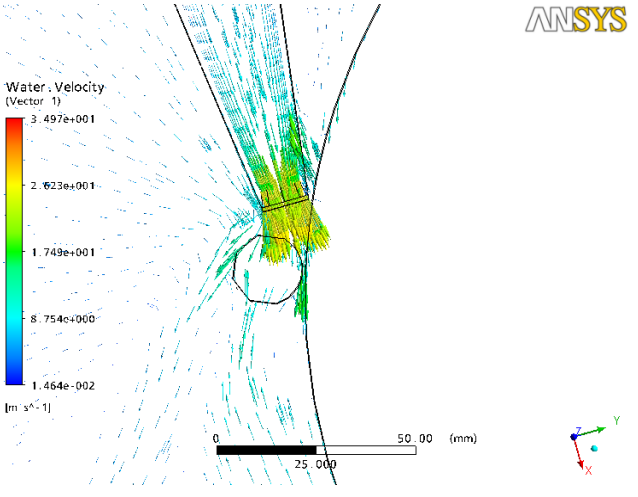
Water . Velocity
(Vector 1)
3.497e+001
2.623e+001
1.749e+001
8.754e+000
1.464e-002
[m s^-1]
0
50.00
(mm)
25.000

(f)

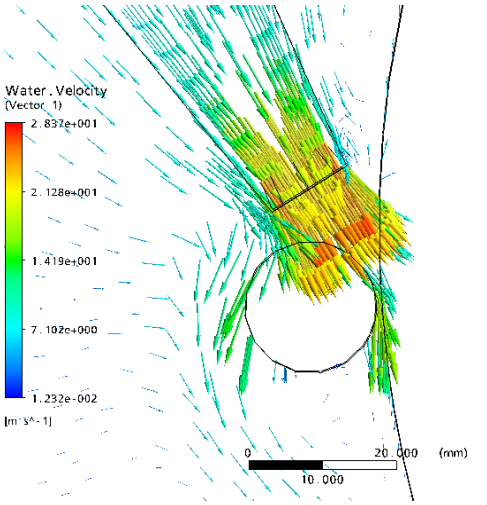
Water . Velocity
(Vector 1)
2.837e+001
2.128e+001
1.419e+001
7.102e+000
1.232e-002
[m s^-1]
0
20.000
(mm)
10.000

(g)

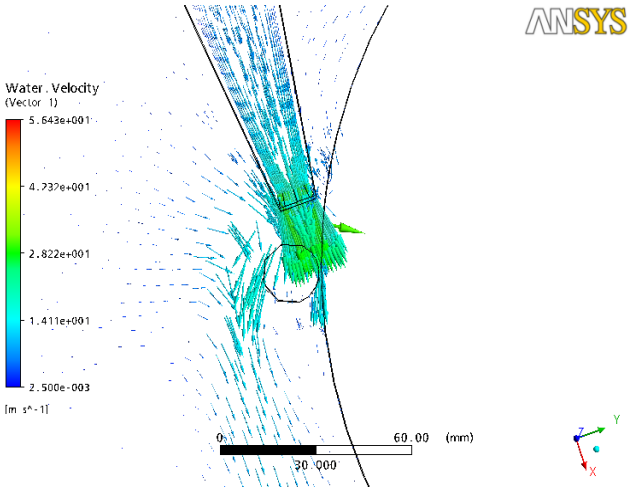
Water . Velocity
(Vector 1)
5.643e+001
4.232e+001
2.822e+001
1.411e+001
2.500e-003
[m s^-1]
0
60.00
(mm)
30.000

(h)

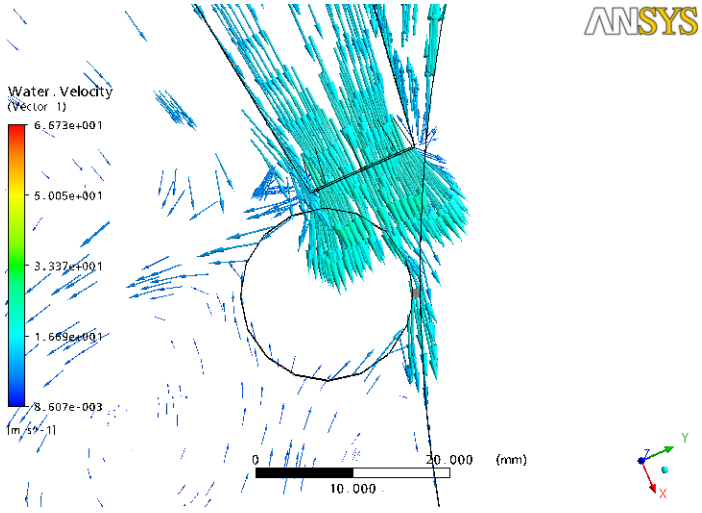

(i)

Figure 4.26: Velocity vector diagrams (a to i) of all nine grinding processes (Experiment no 1 to 9 respectively) with convergent divergent nozzle

4.3.2 Grinding Process Simulations for Taper Nozzle

According to L9 orthogonal array nine grinding process simulation are carried out for taper nozzle. For all nine experiments of L_9 velocity vector diagrams are described in figure 4.27 (a to i). In these figures the behaviour of fluid flow through nozzle in grinding zone is shown. The resulting velocity for each experiment is shown in table 4.11.

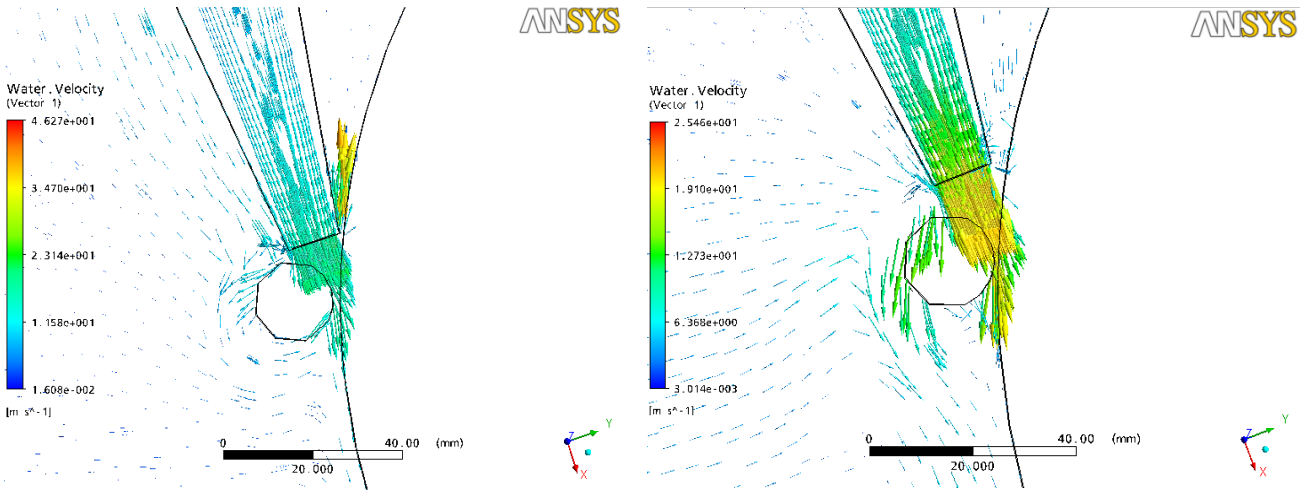

(a) **(b)**

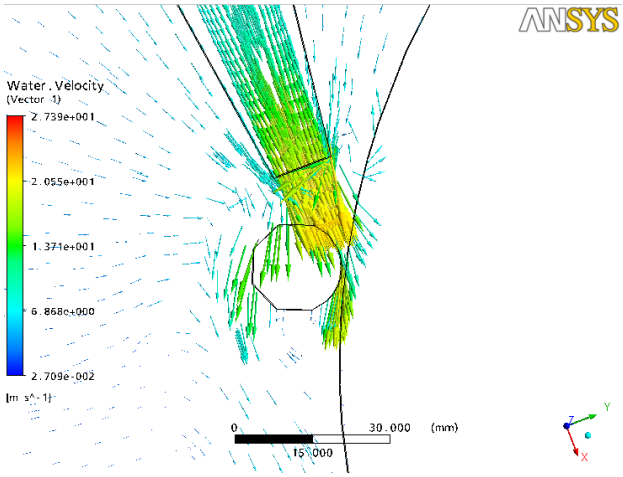
ANSYS
Water . Velocity
(Vector 1)
2.739e+001
2.055e+001
1.371e+001
6.868e+000
2.709e-002
[m s^-1]
0
30.000
(mm)
15.000
Y
Z
X

(c)

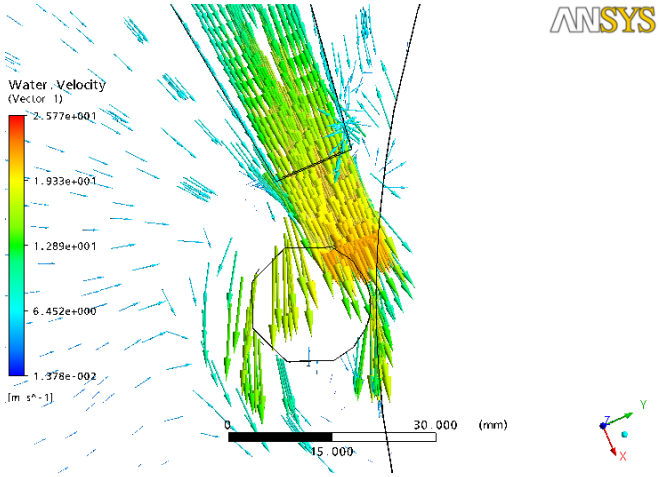
ANSYS
Water . Velocity
(Vector 1)
2.577e+001
1.933e+001
1.289e+001
6.452e+000
1.378e-002
[m s^-1]
0
30.000
(mm)
15.000
Y
Z
X

(d)

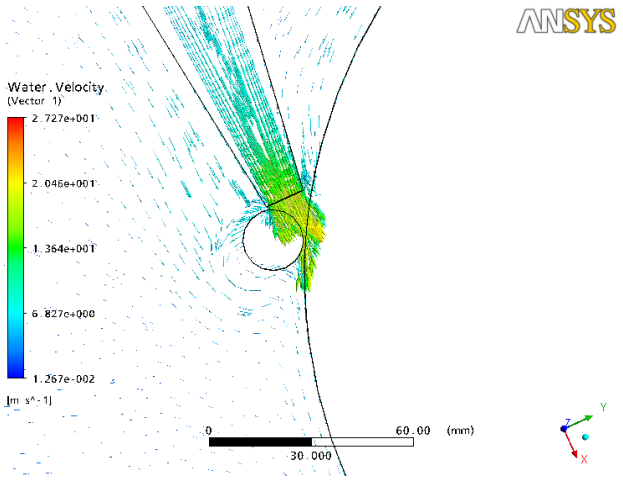
ANSYS
Water . Velocity
(Vector 1)
2.727e+001
2.046e+001
1.364e+001
6.827e+000
1.267e-002
[m s^-1]
0
60.00
(mm)
30.000
Y
Z
X

(e)

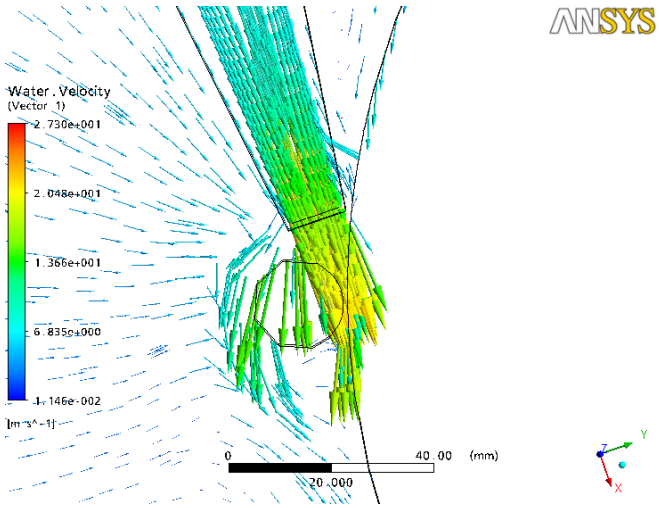
ANSYS
Water . Velocity
(Vector 1)
2.730e+001
2.048e+001
1.366e+001
6.835e+000
1.146e-002
[m s^-1]
0
40.00
(mm)
20.000
Y
Z
X

(f)

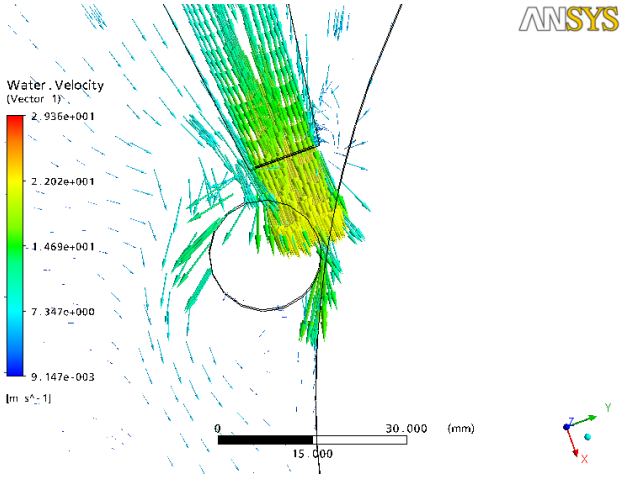
ANSYS
Water . Velocity
(Vector 1)
2.936e+001
2.202e+001
1.469e+001
7.347e+000
9.147e-003
[m s^-1]
0
30.000
(mm)
15.000
Y
Z
X

(g)

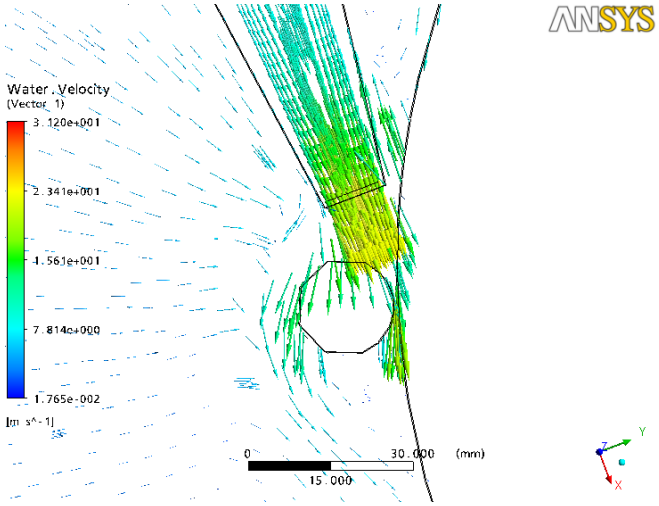
ANSYS
Water . Velocity
(Vector 1)
3.120e+001
2.341e+001
1.561e+001
7.814e+000
1.765e-002
[m s^-1]
0
30.000
(mm)
15.000
Y
Z
X

(h)

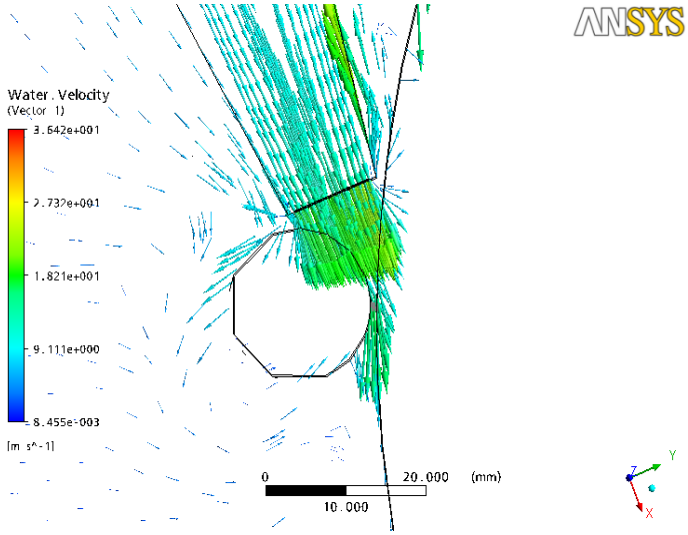

(i)

Figure 4.27: Velocity vector diagrams (a to i) of all nine grinding processes (Experiment no 1 to 9 respectively) with taper nozzle

4.3.3 Grinding Process Simulations for Spline Nozzle

According to L9 orthogonal array nine grinding process simulation are carried out for taper nozzle. For all nine experiments of L_9 velocity vector diagrams are described in figure 4.28 (a to i). In these figures the behaviour of fluid flow through nozzle in grinding zone is shown. The resulting velocity for each experiment is shown in table 4.16.

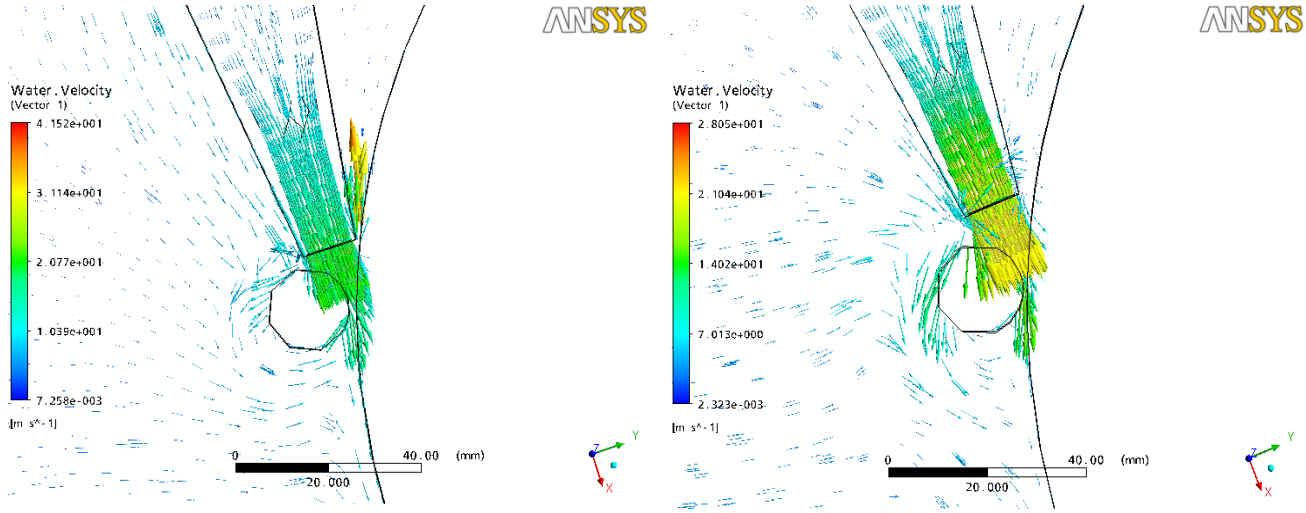

(a) **(b)**

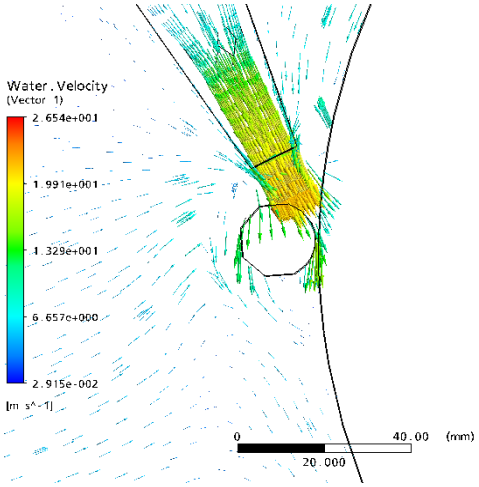
Water . Velocity
(Vector 1)
2.654e+001
1.991e+001
1.329e+001
6.657e+000
2.915e-002
[m s^-1]
0
40.00
(mm)
20.000

(c)

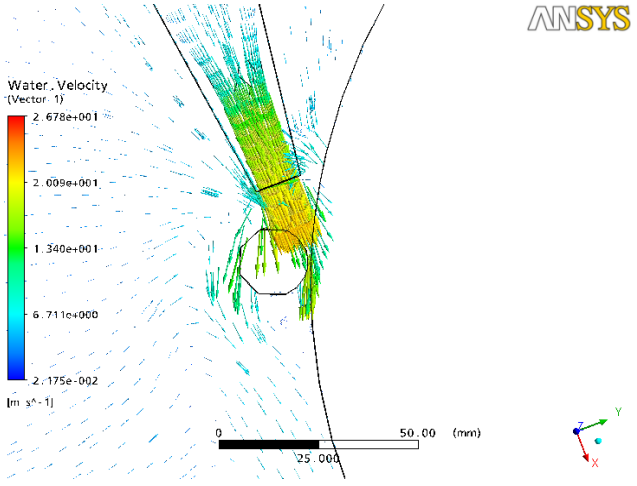
Water . Velocity
(Vector 1)
2.678e+001
2.009e+001
1.340e+001
6.711e+000
2.175e-002
[m s^-1]
0
50.00
(mm)
25.000

(d)

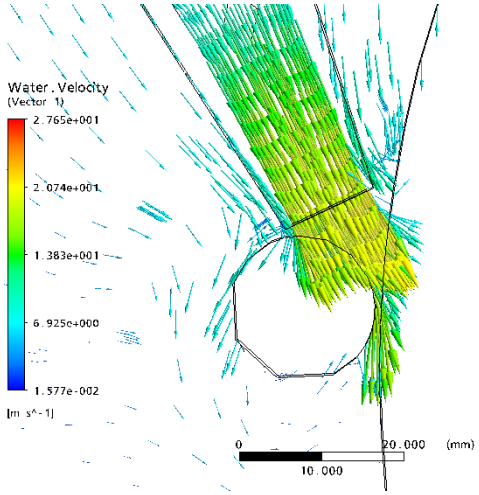
Water . Velocity
(Vector 1)
2.765e+001
2.074e+001
1.383e+001
6.925e+000
1.577e-002
[m s^-1]
0
20.000
(mm)
10.000

(e)

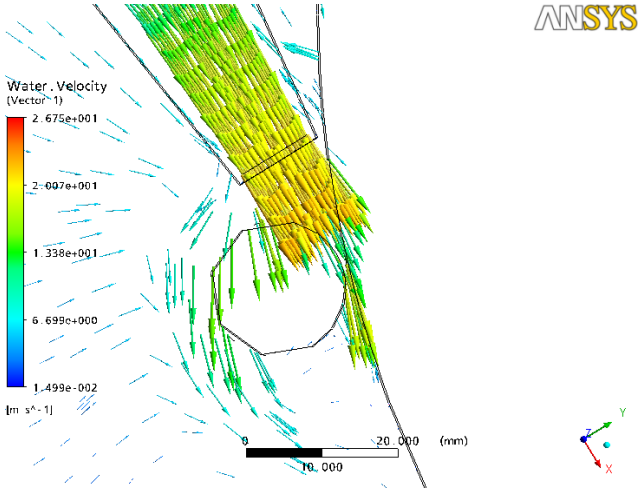
Water . Velocity
(Vector 1)
2.675e+001
2.007e+001
1.338e+001
6.699e+000
1.499e-002
[m s^-1]
0
20.000
(mm)
10.000

(f)

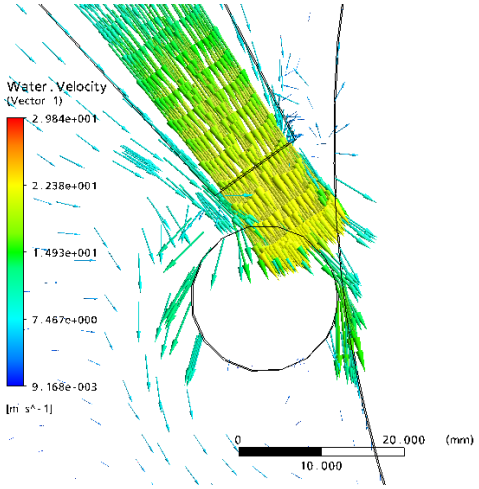
Water . Velocity
(Vector 1)
2.984e+001
2.238e+001
1.493e+001
7.467e+000
9.168e-003
[m s^-1]
0
20.000
(mm)
10.000

(g)

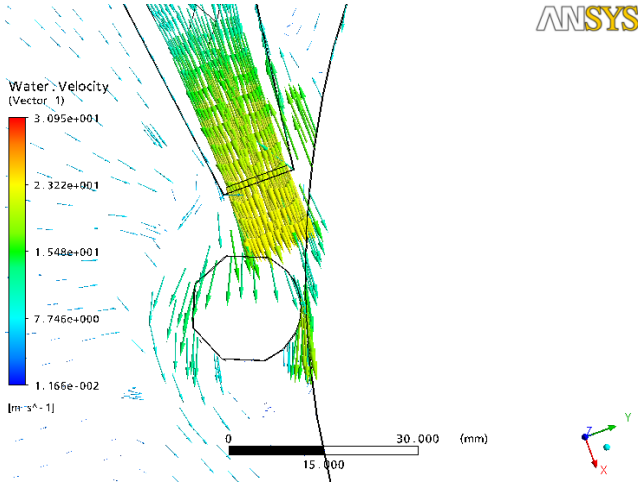
Water . Velocity
(Vector 1)
3.095e+001
2.322e+001
1.548e+001
7.746e+000
1.166e-002
[m s^-1]
0
30.000
(mm)
15.000

(h)

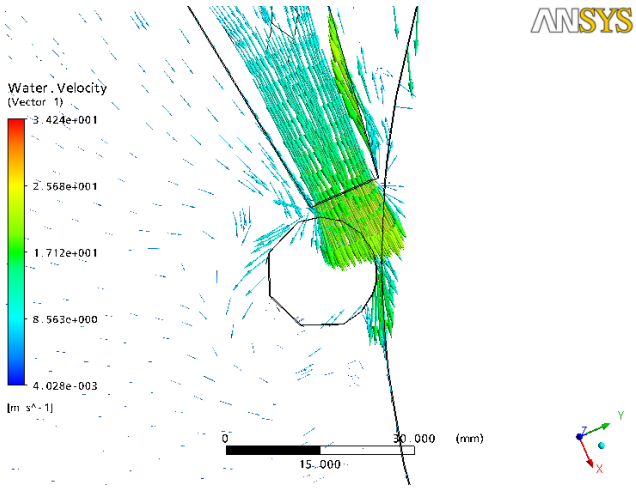

(i)

Figure 4.28: Velocity vector diagrams (a to i) of all nine grinding processes (Experiment no 1 to 9 respectively) with spline nozzle

4.4 ANALYSIS OF VARIANCE (ANOVA)

It is an analysis method to analyse the results obtained from different experiments. ANOVA allows calculating the significance of input parameters for any desired response function. It tells about the most significant parameter/factor. It is done by calculating F value and comparing it with critical F value (α=0.1).ANOVA has been used to study the responses of

1. Velocity
2. Dimension control
3. Hardness
4. Surface cracks

4.5 ANALYSIS OF VARIANCE FOR VELOCITIES OF EACH NOZZLE

The results of velocities from grinding process simulations are observed. Analysis of variance is used to analyse the results for each nozzle to find out the most significant parameter which affect the output response. Means and S/N ratio are calculated. To calculate the S/N ratio 'Larger is better' algorithm is used.

$$S/N = -10\log[(\frac{1}{r}\sum_{i=1}^{r} 1/y^2{}_i)$$

4.6 ANOVA FOR VELOCITIES OF CONVERGENT DIVERGENT NOZZLE

Results of velocities of all nine experiments of convergent divergent nozzles are shown in table 4.6. Signal to noise ratio and ANOVA of mean are calculated. The F value shown in the fifth column of each ANOVA table gives the significance of parameters of desired response.

Table 4.6: Results for Velocities of convergent divergent Nozzle

Exp. No.	Wheel Speed (rpm)	Workpiece Speed (rpm)	Nozzle Angle (degree)	Nozzle Tip Distance (mm)	Velocity (m/s)
1	1628	245	18	14	18.25
2	1628	375	23	18	18.40
3	1628	545	28	22	16.34
4	1795	245	23	22	17.31
5	1795	375	28	14	17.08
6	1795	545	18	18	17.24
7	1921	245	28	18	17.08
8	1921	375	18	22	15.31
9	1921	545	23	14	15.93

4.6.1 ANOVA for Means

ANOVA of means is shown in table 4.7 and its response table is shown in table 4.8. F value and percentage contribution of each factor are calculated. Percentage contribution explains how much a factor is responsible for the variation in desired output response.

Table 4.7 ANOVA for means of velocity of convergent divergent nozzle

Source	DF	SS	MS	F	Order of Significance	Percentage contribution
Wheel Speed	2	3.84607	1.92303	16.5208	1	47.34
Work piece Speed	2	1.65087	0.82543	7.0913	3	20.32
Nozzle Angle	2	0.23280	0.11640	-	-	-
Nozzle Tip Distance	2	2.39547	1.19773	10.2897	2	29.48
Total	8	8.12520				100
E pooled	2	0.23280	0.11640			2.87

Table 4.8: Response table for means of velocity of convergent divergent nozzle

Level	Wheel Speed (rpm)	Work piece Speed (rpm)	Nozzle Angle (degree)	Nozzle Tip Distance (mm)
1	17.66	17.55	16.93	17.09
2	17.21	16.93	17.21	17.57
3	16.11	16.50	16.83	16.32
Delta	1.56	1.04	0.38	1.25
Rank	1	3	4	2

Main effect Plot for S/N ratio of convergent divergent nozzle is shown in figure 4.29. In this plot abscissa represents the three levels of each parameter and ordinate represents the change in result response. In the main effects plot it is shown that wheel speed at level 1 i.e 1628 rpm is most significant factor followed by nozzle tip distance level two 18 mm, because at 1628 rpm wheel speed the velocity of air around the wheel is less and the coolant jet injected through the nozzle from 18 mm distance can easy displace this layer and also swirl of air produced due to displacement enhances the speed of coolant.

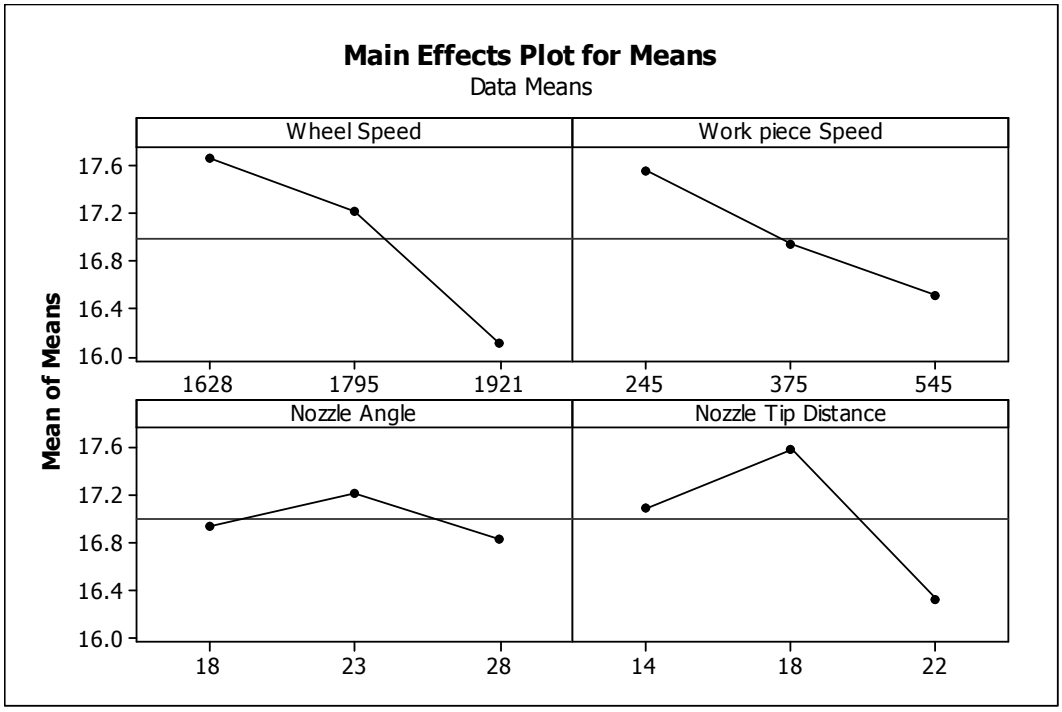

Figure 4.29: Main effect plot for means for velocity of convergent divergent nozzle

4.6.2 ANOVA for S/N Ratio

Signal to noise ratio is a ratio of number of replicas which have variations. It is used to know how much variation is there in results calculated in the taguchi design array Table 4.9 shows the Analysis of variance for S/N ratio. S/N ratio table shows that wheel speed is a most significant factor followed by nozzle tip distance. Response table for S/N ratio is shown in table 4.10.

Table 4.9: ANOVA for S/N ratio of velocity of convergent divergent nozzle

Source	DF	SS	MS	F	Order of Significance
Wheel Speed	2	1.02325	0.511624	18.2143	1
Work piece Speed	2	0.43556	0.217782	7.7532	3
Nozzle Angle	2	0.05618	0.028089	-	-
Nozzle Tip Distance	2	0.64173	0.320865	11.4	2
Total	8	2.15672			
E pooled	2	0.05618	0.028089		

Table 4.10 Response table for S/N ratios for velocity of convergent divergent nozzle

Level	Wheel Speed (rpm)	Work piece Speed (rpm)	Nozzle Angle (degree)	Nozzle Tip Distance (mm)
1	24.93	24.88	24.55	24.64
2	24.72	24.55	24.70	24.89
3	24.13	24.35	24.52	24.24
Delta	0.80	0.53	0.18	0.65
Rank	1	3	4	2

Main effect Plot for S/N ratio of convergent divergent nozzle is shown in figure 4.30. This plot explains the variation in velocity with change in parameters (wheel speed, workpiece speed, nozzle angle, nozzle tip distance). In this plot abscissa represents the three levels of each parameter and ordinate represents the change in result response.

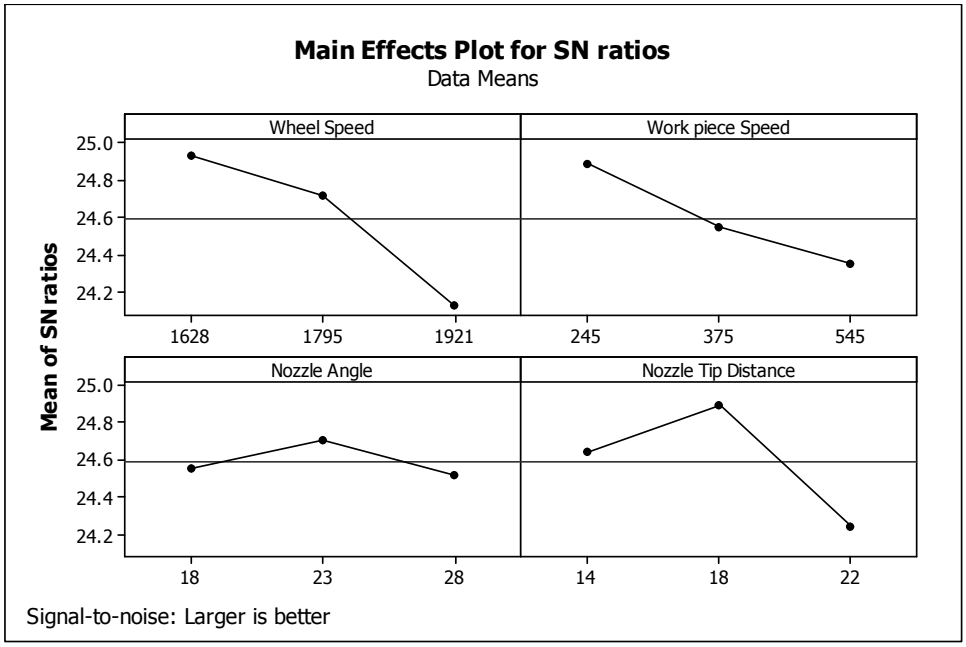

Figure 4.30: Main effect plot for S/N ratio for velocity of convergent divergent nozzle

4.6.3 Optimal Design

Velocity should be higher for desired response. Main effects plot shown in figure 4.29 shows that Wheel speed and Nozzle tip distance has most significant effect on velocity. For optimal design Wheel speed 1628 rpm and Nozzle tip distance 18mm are selected because they have effect on variation of output response. Table 4.11 shows order of significant factors that affect velocity response after completion of S/N ratio and ANOVA for means analysis.

Table 4.11: Order of significant factors for velocity of convergent divergent Nozzle

Factor	Significance order of factors in ANOVA	Significance order of factors in S/N ratio
Wheel speed	1	1
Workpiece speed	3	3
Nozzle angle	No	No
Nozzle tip distance	2	2

Estimating the Confidence Interval for Velocity

Mean value for Velocity

$\mu_{A_1D_2} = \overline{A_1} + \overline{D_2} - \overline{T}$

$\mu_{A_1B_2} = 17.66 + 17.57 - 16.99 = 18.24$

Confidence Interval:

$$CI_1 = \sqrt{\frac{F_{\alpha,v_1,v_2} V_e}{n_{eff}}} \quad \text{Where} \quad F_{\alpha v_1 v_2} = F\ ratio$$

α = risk (0.1) confidence= 1- α

ν_1= *dof* for means which is always 1

ν_2= *dof* for error

$$V_e = \frac{\text{sum of square of e pooled}}{\text{degree of freedom of e pooled}} = 0.1164$$

n_{eff} = Number of tests under that condition using the participating factors

$$n_{eff} = \frac{N}{1 + dof_{A,B}} = \frac{9}{1 + 2 + 2} = 1.8$$

$$CI_1 = \sqrt{\frac{F_{\alpha,v_1,v_2} V_e}{n_{eff}}} = \sqrt{\frac{8.52 \times 0.1164}{1.8}} = 0.7422$$

So the confidence interval around the estimated velocity is 18.24 ± 0.7422 m/s.

4.7 ANALYSIS FOR VELOCITY OF TAPER NOZZLE

Results of velocities of all nine experiments of Taper nozzle are shown in table 4.12. Signal to noise ratio and mean are calculated. The F value and percentage contribution shown in the following ANOVA tables gives the significance of parameters of desired response.

Table 4.12: Results for Velocities of Taper Nozzle

Exp. No.	Wheel Speed (rpm)	Workpiece Speed (rpm)	Nozzle Angle (degree)	Nozzle Tip Distance (mm)	Velocity (m/s)
1	1628	245	18	14	18.53
2	1628	375	23	18	18.92
3	1628	545	28	22	18.35
4	1795	245	23	22	16.77
5	1795	375	28	14	17.62
6	1795	545	18	18	17.75
7	1921	245	28	18	16.01
8	1921	375	18	22	18.74
9	1921	545	23	14	16.67

4.7.1 ANOVA for Means

ANOVA of means is shown in table 4.13 and its response table is shown in table 4.14. F value and percentage contribution of each factor is calculated. It shows that wheel speed and workpiece speed have significant effect on velocity. Main effect plot is shown in figure 4.31.

Table 4.13: ANOVA for means of velocity of taper nozzle

Source	DF	SS	MS	F	Order of significance	Percentage contribution
Wheel Speed	2	3.67760	1.83880	13.2736	1	43.41
Work piece Speed	2	2.68807	1.34403	9.7020	2	31.73
Nozzle Angle	2	1.82907	0.91453	6.6016	3	21.59
Nozzle Tip Distance	2	0.27707	0.13853	-	-	-
Total	8	8.4718				100
E pooled	2	0.27707	0.13853			3.27

Table4.14: Response table for means of velocity of taper nozzle

Level	Wheel Speed (rpm)	Work piece Speed (rpm)	Nozzle Angle (degree)	Nozzle Tip Distance (mm)
1	18.60	17.10	18.34	17.61
2	17.38	18.43	17.45	17.56
3	17.14	17.59	17.33	17.95
Delta	1.46	1.32	1.01	0.39
Rank	1	2	3	4

In the main effects plot (figure 4.31) it is shown that wheel speed at level 1 i.e 1628 rpm is most significant factor followed by Workpiece speed Level two i.e 375 rpm, because at 1628 rpm wheel speed the velocity of air around the wheel is less and the coolant jet injected through the nozzle can easy displace this layer and also swirl of air produced due to displacement enhances the speed of coolant. Workpiece speed also helps in getting the coolant in grinding zone quickly.

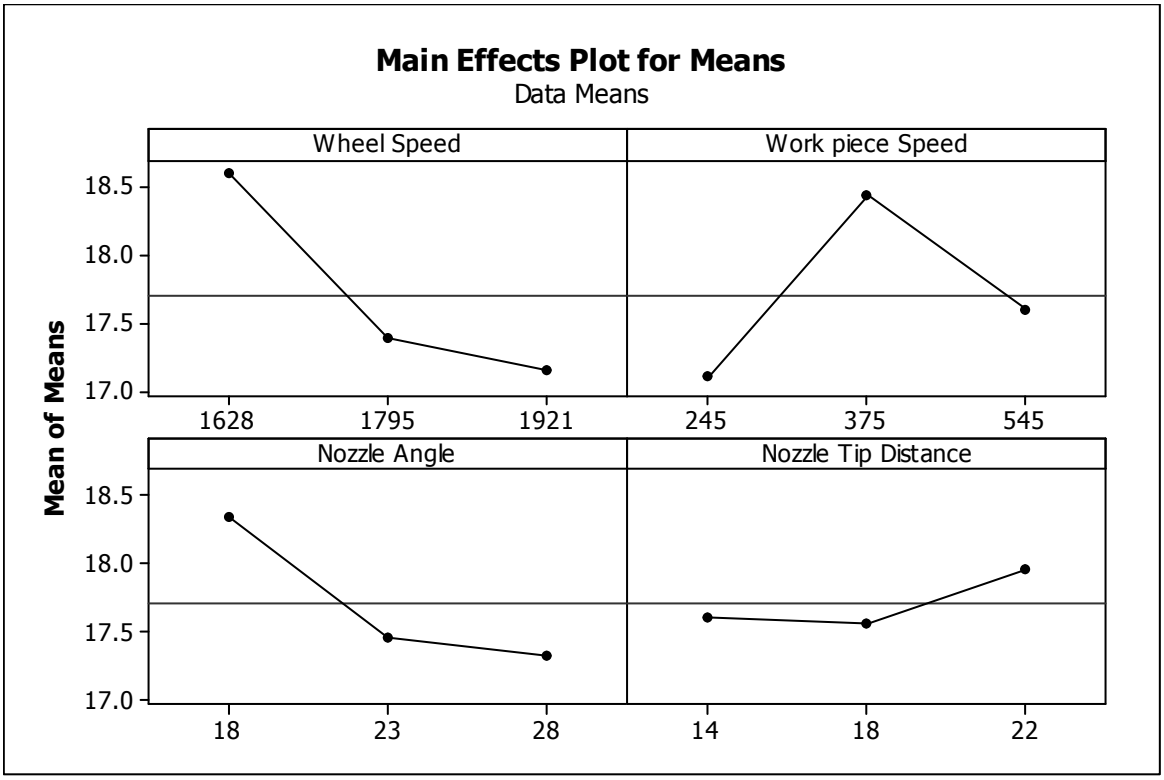

Figure 4.31: Main effect plot for means for velocity of Taper nozzle

4.7.2 Analysis for S/N Ratio

Signal to noise ratio tells about the variation present in the process. In this design response of velocity for S/N ratio is taken as 'Larger is better'. Table 4.15 shows the Analysis of variance for S/N ratio. And response table for S/N ratio is shown in table 4.16. Tables show that wheel speed and workpiece speed are most significant factors for desired response.

Table 4.15: ANOVA for S/N ratio for velocity of taper nozzle

Source	DF	SS	MS	F	Order of significance
Wheel Speed	2	0.89988	0.44994	12.7733	1
Work piece Speed	2	0.66375	0.33187	9.4215	2
Nozzle Angle	2	0.45559	0.22779	6.4668	3
Nozzle Tip Distance	2	0.07045	0.03522	-	-
Total	8	2.08967			
E pooled	2	0.07045	0.03522		

Table4.16: Response table for S/N ratio of velocity of taper nozzle

Level	Wheel Speed (rpm)	Work piece Speed (rpm)	Nozzle Angle (degree)	Nozzle Tip Distance (mm)
1	25.39	24.65	25.27	24.91
2	24.80	25.30	24.82	24.87
3	24.66	24.90	24.76	25.07
Delta	0.73	0.66	0.51	0.20
Rank	1	2	3	4

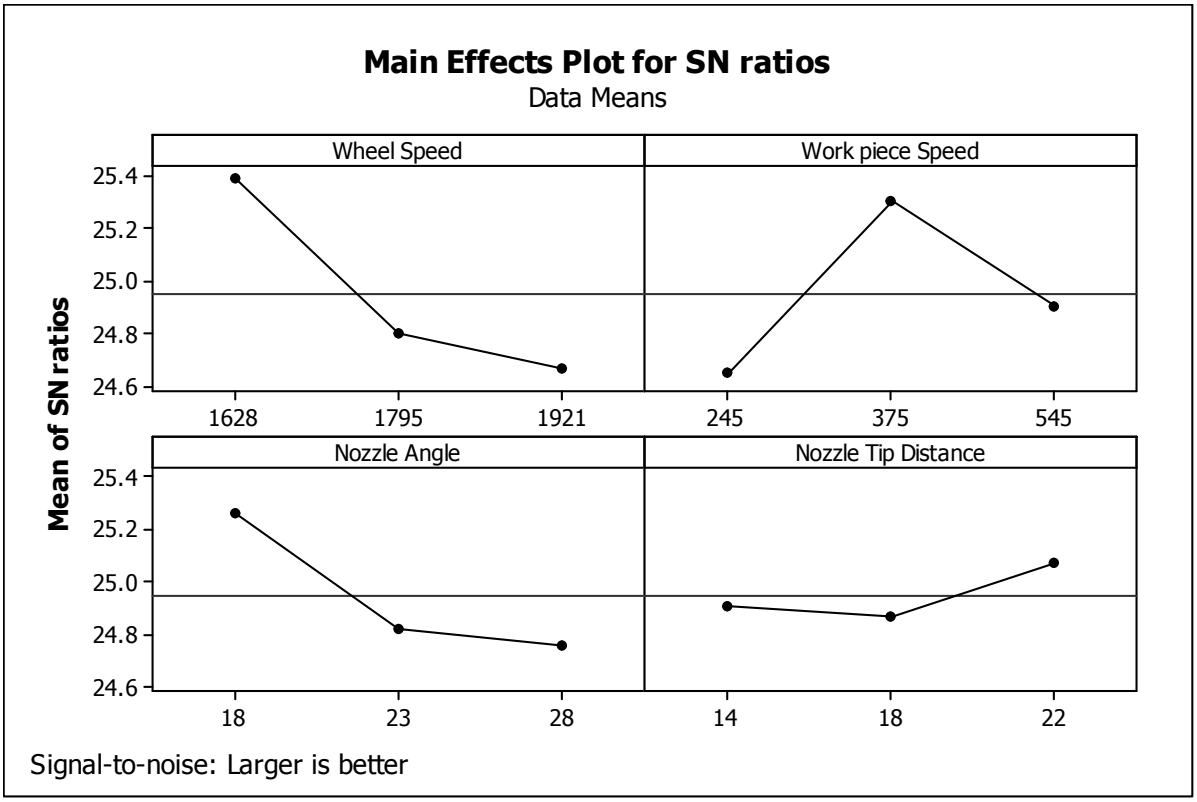

Figure 4.32: Main effect plot for signal to noise ratio for velocity of taper nozzle

4.7.3 Optimal Design

Velocity should be higher for desired response. Main effects plot shown in figure 4.31 shows that Wheel speed and workpiece speed has most significant effect on velocity. For optimal design Wheel speed 1628 rpm and workpiece speed 375 rpm are selected because they have effect on variation of output response. Table 4.17 shows the order of significant factors that affect velocity response after completion of S/N and ANOVA of means analysis.

Table 4.17: Order of significant factors for velocity response of taper Nozzle

Factor	Significance order of factors in ANOVA	Significance order of factors in S/N ratio
Wheel speed	1	1
Workpiece speed	2	2
Nozzle angle	3	3
Nozzle tip distance	No	No

Estimating the Confidence interval for velocity

Mean value for Velocity

$\mu_{A_1B_2} = \overline{A_1} + \overline{B_2} - \overline{T}$

$\mu_{A_1B_2} = 18.60 + 18.43 - 17.70 = 19.33$

Confidence Interval:

$$CI_1 = \sqrt{\frac{F_{\alpha,v_1,v_2} V_e}{n_{eff}}} \quad \text{Where} \quad F_{\alpha v_1 v_2} = F\ ratio$$

α = risk (0.1) confidence= 1- α

ν_1= *dof* for means which is always 1

ν_2= *dof* for error

$$Varience = V_e = \frac{sum\ of\ square\ of\ e\ pooled}{degree\ of\ freedom\ of\ e\ pooled} = 0.1385$$

n_{eff} = Number of tests under that condition using the participating factors

$$n_{eff} = \frac{N}{1 + dof_{A,B}} = \frac{9}{1 + 2 + 2} = 1.8$$

$$CI_1 = \sqrt{\frac{F_{\alpha,v_1,v_2} V_e}{n_{eff}}} = \sqrt{\frac{8.52 \times 0.1385}{1.8}} = .8096$$

,

So the confidence interval around the estimated velocity is 19.33 ± 0.8096 m/s.

4.8 ANALYSIS OF VELOCITY FOR SPLINE NOZZLE

Results of velocities of all nine experiments of spline nozzle are shown in table 4.18. Signal to noise ratio and mean are calculated. The F value and percentage contribution shown in the ANOVA tables gives the significance of parameters for desired output.

Table 4.18: Results for Velocities of Spline Nozzle

Exp. No.	Wheel Speed (rpm)	Workpiece Speed (rpm)	Nozzle Angle (degree)	Nozzle Tip Distance (mm)	Velocity (m/s)
1	1628	245	18	14	18.04
2	1628	375	23	18	16.35
3	1628	545	28	22	15.28
4	1795	245	23	22	17.59
5	1795	375	28	14	16.63
6	1795	545	18	18	17.40
7	1921	245	28	18	15.79
8	1921	375	18	22	18.61
9	1921	545	23	14	16.58

4.8.1 ANOVA for Means

ANOVA of means is shown in table 4.19 and its response table is shown in table 4.20.from these tables according to the F value and percentage contribution most effecting factor which is responsible for variation in output response is examined. In S/N ratio table it is shown that Nozzle angle has significant effect on velocity of spline nozzle. Main effect plot is shown in figure 4.33.

Table 4.19: ANOVA for means of velocity of spline nozzle

Source	DF	SS	MS	F	Order of significance	Percentage Contribution
Wheel Speed	2	0.65869	0.32934	-	-	-
Work piece Speed	2	1.12482	0.56241	1.7076	2	12.12
Nozzle Angle	2	6.74842	3.37421	10.246	1	72.71
Nozzle Tip Distance	2	0.74896	0.37448	1.1370	3	8.07
Total	8	9.28089				100
E pooled	2	0.65869	0.32934			7.10

Table 4.20: Response table for means of velocity of spline nozzle

Level	Wheel Speed (rpm)	Work piece Speed (rpm)	Nozzle Angle (degree)	Nozzle Tip Distance (mm)
1	16.56	17.14	18.02	17.08
2	17.21	17.20	16.84	16.51
3	16.99	16.42	15.90	17.16
Delta	0.65	0.78	2.12	0.65
Rank	3	2	1	3

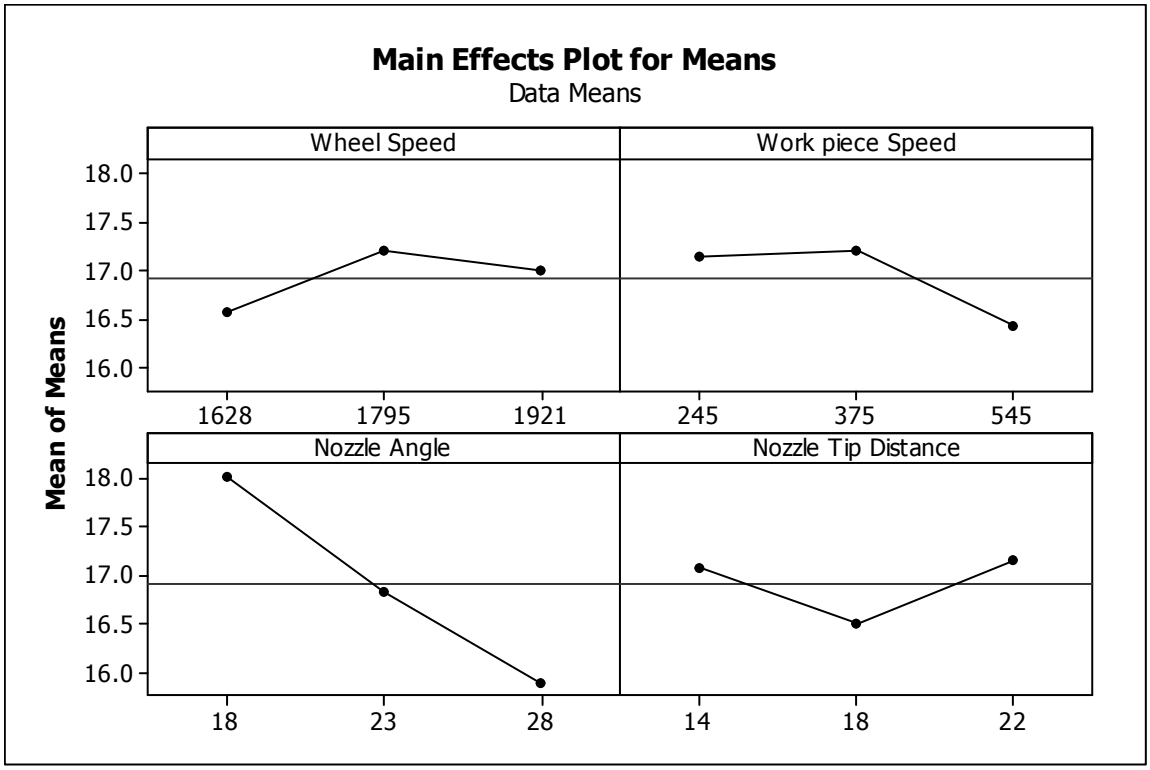

Figure 4.33: Main effect plot for means of velocity of spline nozzle

In the main effects plot for means shows that nozzle angle has significant effect on velocity of coolant jet in grinding zone. Due to the shape of spline nozzle the coolant jet coming out of nozzle outlet does not scatter in larger area and impact layer of air with higher velocity abd replaces it.

4.8.2 Analysis of S/N Ratio

In this design response of velocity for S/N ratio is taken as 'Larger is better'. Table 4.21 shows the Analysis of variance for S/N ratio. And response table for S/N ratio is shown in table 4.22. It is shown that nozzle angle is making the maximum contribution in affecting output response. Main effect plot for S/N ratio is shown in figure 4.34.

Table 4.21: ANOVA for S/N ratio of velocity of spline nozzle

Source	DF	SS	MS	F	Order of Significance
Wheel Speed	2	0.19096	0.095480	1.0366	3
Work piece Speed	2	0.29780	0.148902	1.6166	2
Nozzle Angle	2	1.77806	0.889029	9.6521	1
Nozzle Tip Distance	2	0.18421	0.092107	-	-
Total	8	2.45103			
E pooled	2	0.18421	0.092107		

Table 4.22: Response table for S/N ratio of velocity of spline nozzle

Level	Wheel Speed (rpm)	Work piece Speed (rpm)	Nozzle Angle (degree)	Nozzle Tip Distance (mm)
1	24.36	24.67	25.11	24.64
2	24.71	24.69	24.52	24.17
3	24.58	24.30	24.02	24.66
Delta	0.35	0.40	1.09	0.31
Rank	3	2	1	4

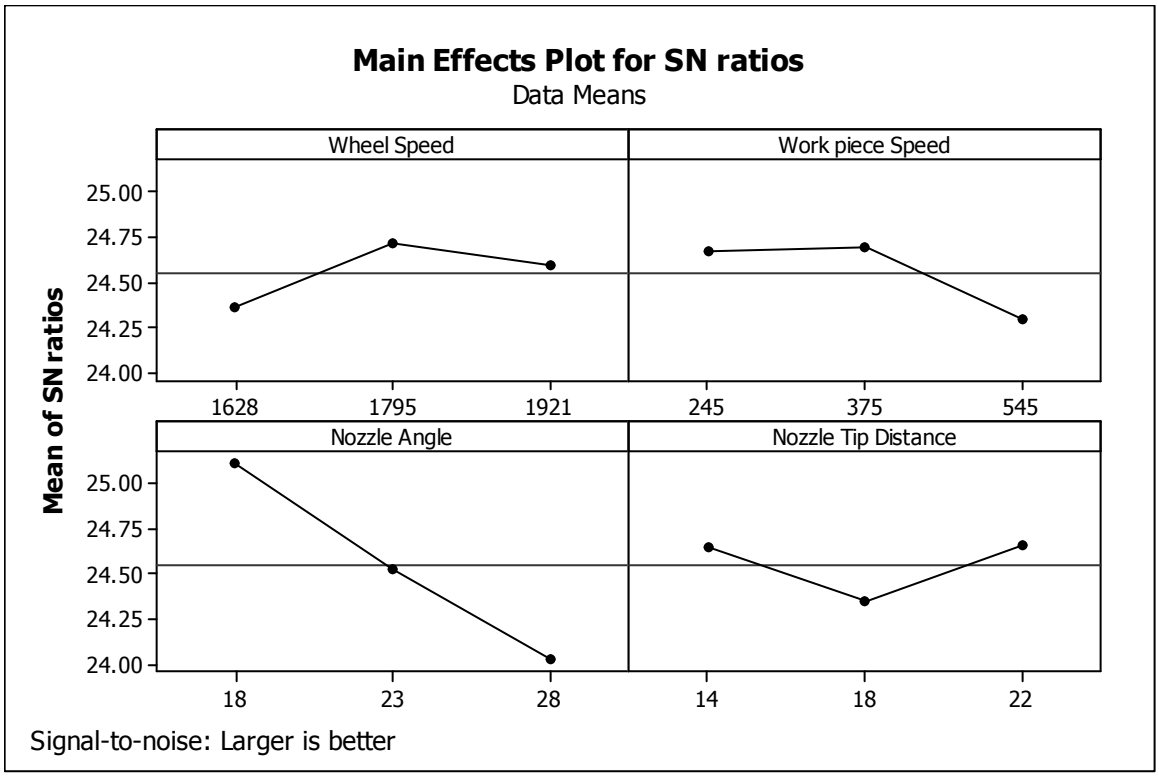

Figure 4.34: Main effect plot for S/N ratio for velocity of Spline nozzle

4.8.3 Optimal Design

Velocity should be higher for desired response. Main effects plot shown in figure 4.33 shows Nozzle angle has most significant effect on velocity. For optimal design Nozzle angle 18^0 is selected because it has effect on variation of output response. Table 4.23 shows order of significant factors that affect velocity response after completion of S/N and ANOVA of means analysis.

Table 4.23: Order of significant factors for velocity response of taper nozzle

Factor	Significance order of factors in ANOVA	Significance order of factors in S/N ratio
Wheel speed	No	3
WorkPiece speed	2	2
Nozzle angle	1	1
Nozzle tip distance	3	No

4.9 EXPERIMENTAL RESULTS AND ANALYSIS

Experimentation is done to validate the simulation. In experimentation three selected nozzles are manufactured and grinding process is performed on work piece (material: mild steel rod) of initial diameter 17.750 mm, varying four input parameters. Results are measured in terms of dimensional accuracy, surface hardness and surface cracks. Analysis of these results is done using ANOVA.

4.10 ANALYSIS OF SURFACE HARDNESS

Surface hardness is measured for all nozzles for all four input parameters using L_9 orthogonal array. Coolant delivery has major effect on hardness of workpiece material because due to high temperature in grinding zone can cause recrystallisation of work piece material grains Surface hardness is measured with Vickers Hardness Tester. A diamond pyramid shaped indenter is used to make indent impression on workpiece. Load applied and dwell time for indention is 50 kgf and 20 seconds respectively. Diagonal length of indent is measured upto 1 μm accuracy. Then this value is converted into converted in to VHN with the help of formulation:

$$VHN= (1.8544 * Load)/y^2$$

Here y is diagonal length of indent.

S/N ratio for Vickers Hardness Number (VHN) is calculated considering ‘smaller is better’ algorithm with the target value of 140 VHN.

$$S/N_{LB} = -10\log[(\frac{1}{r}\sum_{i=1}^{r} y^2{}_i)$$

4.11 ANALYSIS OF SURFACE HARDNESS FOR CONVERGENT DIVERGENT NOZZLE

ANOVA is applied nine trials of convergent divergent nozzle according to L_9 array. In table 4.24 three replicas of VHN are shown. ANOVA for means and its response table is given in table 4.25 and table 4.26. ANOVA of S/N ratio and its response table are shown in table 4.27 and table 4.28.

Table 4.24: Results for Surface hardness of convergent divergent nozzle

Exp. No.	Wheel Speed (rpm)	Work-piece Speed (rpm)	Nozzle Angle (degree)	Nozzle Tip Distance (mm)	Vickers hardness Number (VHN)			Mean of VHN
					1	2	3	
1	1628	245	18	14	148.191	149.321	150.082	149.198
2	1628	375	23	18	148.333	148.782	149.963	149.026
3	1628	545	28	22	155.575	152.01	153.184	153.590
4	1795	245	23	22	152.01	151.234	150.465	151.236
5	1795	375	28	14	157.61	155.575	156.791	156.658
6	1795	545	18	18	150.082	151.234	150.849	150.722
7	1921	245	28	18	153.184	150.082	152.01	151.759
8	1921	375	18	22	173.516	165.276	167.505	168.766
9	1921	545	23	14	175.43	179.356	177.868	177.552

4.11.1 ANOVA for Means

ANOVA of means is shown in table 4.25 and its response table is shown in table 4.26. F value and percentage contribution gives the most contributing factor which effects variation in output response. Wheel sped comes out to be most significant factor. Main effects plot is shown in figure 4.35. Plot shows that the significant level of wheel speed is level 3 i.e. 1921 rpm.

Table 4.25: ANOVA for means of surface hardness for convergent divergent nozzle

Source	DF	SS	MS	F	Order of significance	Percentage contribution
Wheel Speed	2	415.950	207.975	9.9087	1	52.33
Work piece Speed	2	158.961	79.481	3.7867	3	20.00
Nozzle Angle	2	41.978	20.989	-	-	-
Nozzle Tip Distance	2	177.980	88.990	4.2398	2	22.39
Total	8	794.869				100
E pooled	2	41.978	20.989			5.28

Table 4.26: Response table for mean of hardness for convergent divergent nozzle

Level	Wheel Speed (rpm)	Work piece Speed (rpm)	Nozzle Angle (degree)	Nozzle Tip Distance (mm)
1	150.6	150.7	156.2	161.1
2	152.9	158.7	159.3	150.5
3	166.0	160.6	154.0	157.9
Delta	15.4	9.9	5.3	10.6
Rank	1	3	4	2

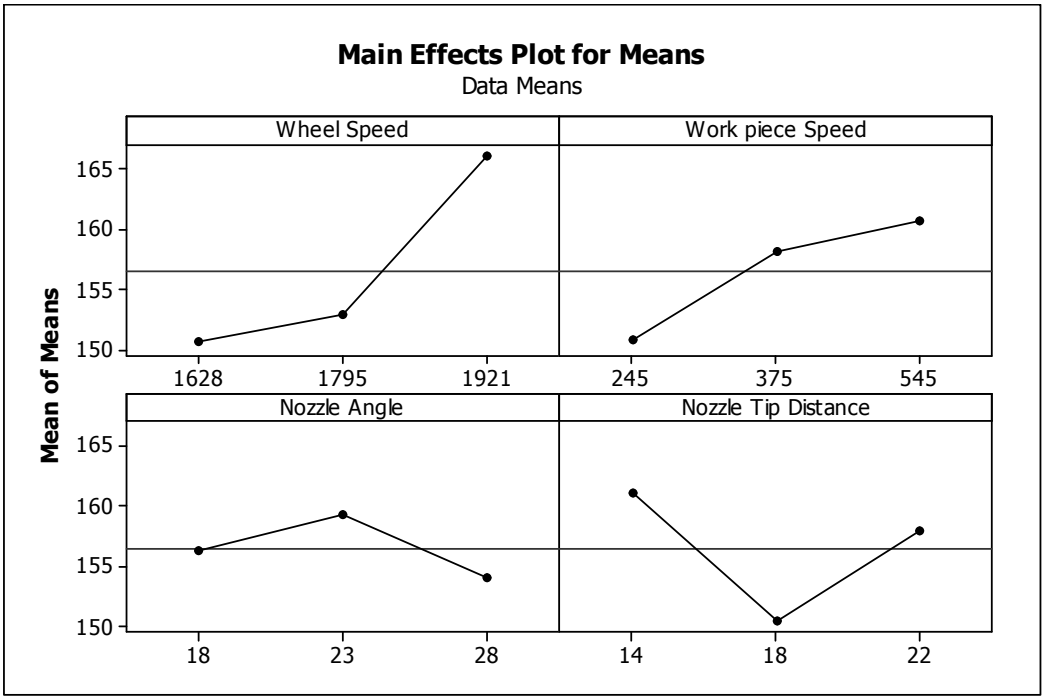

Figure 4.35: Main effect plot for Means of surface hardness for convergent divergent nozzle

4.11.2 Analysis of S/N Ratio

Table 4.27 shows the Analysis of variance for S/N ratio. And response table for S/N ratio is shown in table 4.28. F value shows the most significant factor effecting variation of output response. Wheel speed is most significant factor. Main effect plot for S/N ratio is shown in figure 4.36.

Table 4.27: ANOVA for S/N ratio for surface hardness of convergent divergent nozzle

Source	DF	SS	MS	F	Order of significance
Wheel Speed	2	1.19403	0.597016	11.2290	1
Work piece Speed	2	0.45939	0.229695	4.3202	3
Nozzle Angle	2	0.10633	0.053167	-	-
Nozzle Tip Distance	2	0.51553	0.257765	4.8482	2
Total	8	2.27529			
E pooled	2	0.10633	0.053167		

Table 4.28: Response table for S/N ratio for surface hardness of convergent divergent nozzle

Level	Wheel Speed (rpm)	Work piece Speed (rpm)	Nozzle Angle (degree)	Nozzle Tip Distance (mm)
1	-43.56	-43.56	-43.86	-44.12
2	-43.69	-43.97	-44.01	-43.55
3	-44.39	-44.09	-43.75	-43.96
Delta	0.83	0.53	0.27	0.57
Rank	1	3	4	2

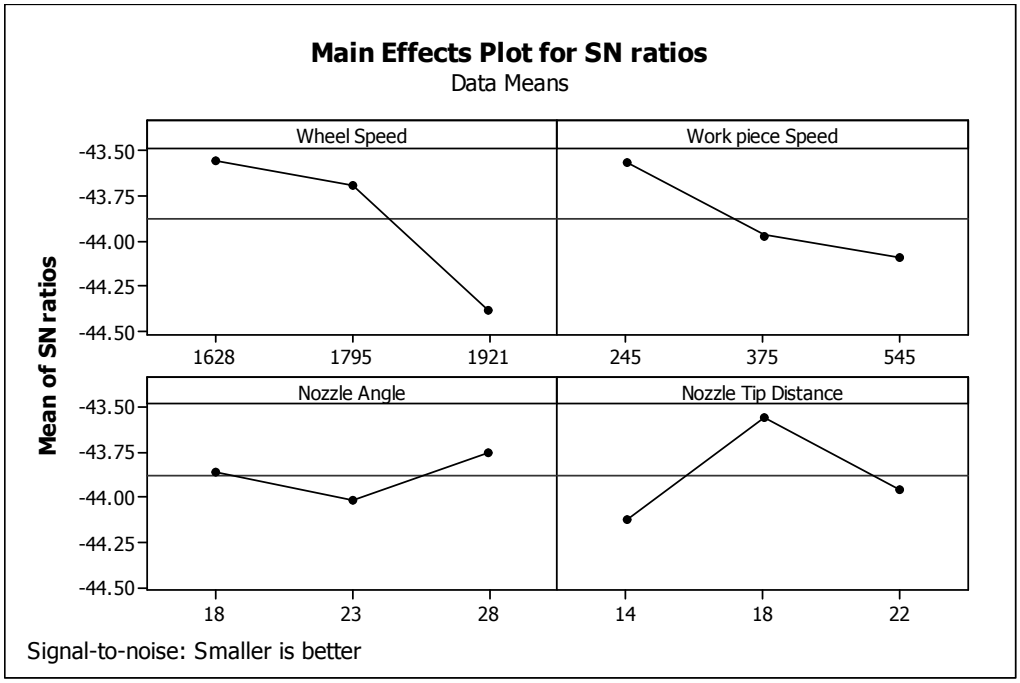

Figure 4.36: Main effect plot for S/N ratio for surface hardness of convergent divergent nozzle

4.11.3 Optimal Design

Hardness Number should be lower for desired response. Main effects plot shown in figure 4.35 shows that Wheel speed has most significant effect on hardness number. But also nozzle tip distance is has small effect. For optimal design Wheel speed 1921 rpm is selected because it has significant effect on variation of output response. Table 4.29 shows order of significant factors that affect VHN response after completion of S/N and ANOVA of means analysis.

Table 4.29: Order of Significant factors for surface hardness of convergent divergent nozzle

Factor	Significance of factors in ANOVA	Significance of factors in S/N ratio
Wheel speed	1	1
WorkPiece speed	3	3
Nozzle angle	No	No
Nozzle tip distance	2	2

4.12 ANALYSIS OF SURFACE HARDNESS FOR TAPER NOZZLE

ANOVA is applied nine trials of taper nozzle. Table 4.30 shows VHN values for all experiments. ANOVA for means and ANOVA of S/N ratio are shown in tables 4.31 and table 4.33.

Table 4.30: Results for Surface hardness number for taper nozzle

Exp. No.	Wheel Speed (rpm)	Work-piece Speed (rpm)	Nozzle Angle (degree)	Nozzle Tip Distance (mm)	Vickers hardness Number (VHN)			Mean of VHN
					1	2	3	
1	1628	245	18	14	154.772	151.234	153.184	153.063
2	1628	375	23	18	148.191	150.082	149.701	149.324
3	1628	545	28	22	150.465	149.701	152.01	150.725
4	1795	245	23	22	157.199	159.266	158.85	158.439
5	1795	375	28	14	154.772	153.184	154.373	154.110
6	1795	545	18	18	153.579	149.701	155.575	152.951
7	1921	245	28	18	160.251	161.256	160.062	160.523
8	1921	375	18	22	150.465	148.618	149.012	149.365
9	1921	545	23	14	153.949	154.850	156.105	154.968

4.12.1 ANOVA for Means

ANOVA of means is shown in table 4.31 and its response table is shown in table 4.32. F value and percentage contribution are calculated. Table for means shows that Work piece speed is most significant factor and wheel speed is second significant factor. Main effect plot is shown in figure 4.37.

Table 4.31: ANOVA for Means of surface hardness for taper nozzle

Source	DF	SS	MS	F	Order of significance	Percentage contribution
Wheel Speed	2	32.417	16.2085	9.2428	2	27.35
Work piece Speed	2	64.760	32.3801	18.3779	1	54.63
Nozzle Angle	2	17.832	8.9160	5.0604	3	15.04
Nozzle Tip Distance	2	3.524	1.7619	-	-	-
Total	8	118.533				100
E pooled	2	3.524	1.7619			2.97

Table 4.32: Response table for means of surface hardness for taper nozzle

Level	Wheel Speed (rpm)	Work piece Speed (rpm)	Nozzle Angle (degree)	Nozzle Tip Distance (mm)
1	151.0	157.3	151.8	154.0
2	155.2	150.9	154.2	154.3
3	155.0	152.9	155.1	152.8
Delta	4.1	6.4	3.3	1.4
Rank	2	1	3	4

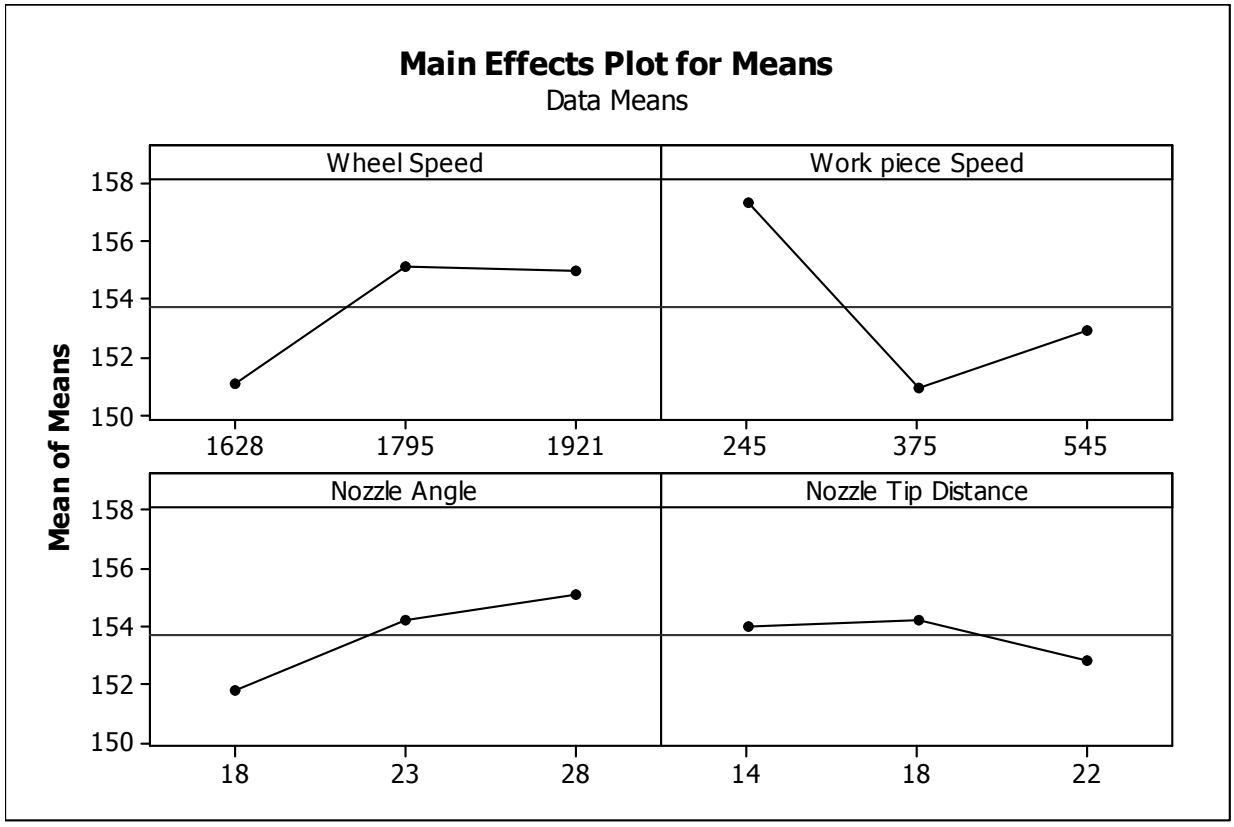

Figure 4.37: Main effect plot for Means of Surface hardness with Taper Nozzle

4.12.2 Analysis for S/N Ratio

Table 4.33 shows the Analysis of variance for S/N ratio. And response table for S/N ratio is shown in table 4.34. Workpiece speed and wheel speed has significant effect on surface hardness. Main effect plot for S/N ratio is shown in figure 4.38.

Table 4.33: ANOVA for S/N ratio of surface hardness for taper nozzle

Source	DF	SS	MS	F	Order of significance
Wheel Speed	2	0.102774	0.051387	8.9900	2
Work piece Speed	2	0.204187	0.102094	17.8610	1
Nozzle Angle	2	0.055708	0.027854	5.8729	3
Nozzle Tip Distance	2	0.011433	0.005716	-	-
Total	8	0.374102			
E pooled	2	0.011433	0.005716		

Table 4.34: Response table for S/N ratio of surface hardness for taper nozzle

Level	Wheel Speed (rpm)	Work piece Speed (rpm)	Nozzle Angle (rpm)	Nozzle Tip Distance (mm)
1	-43.58	-44.94	-43.62	-43.75
2	-43.81	-43.57	-43.76	-43.76
3	-43.80	-43.69	-43.81	-43.68
Delta	0.23	0.36	0.19	0.08
Rank	2	1	3	4

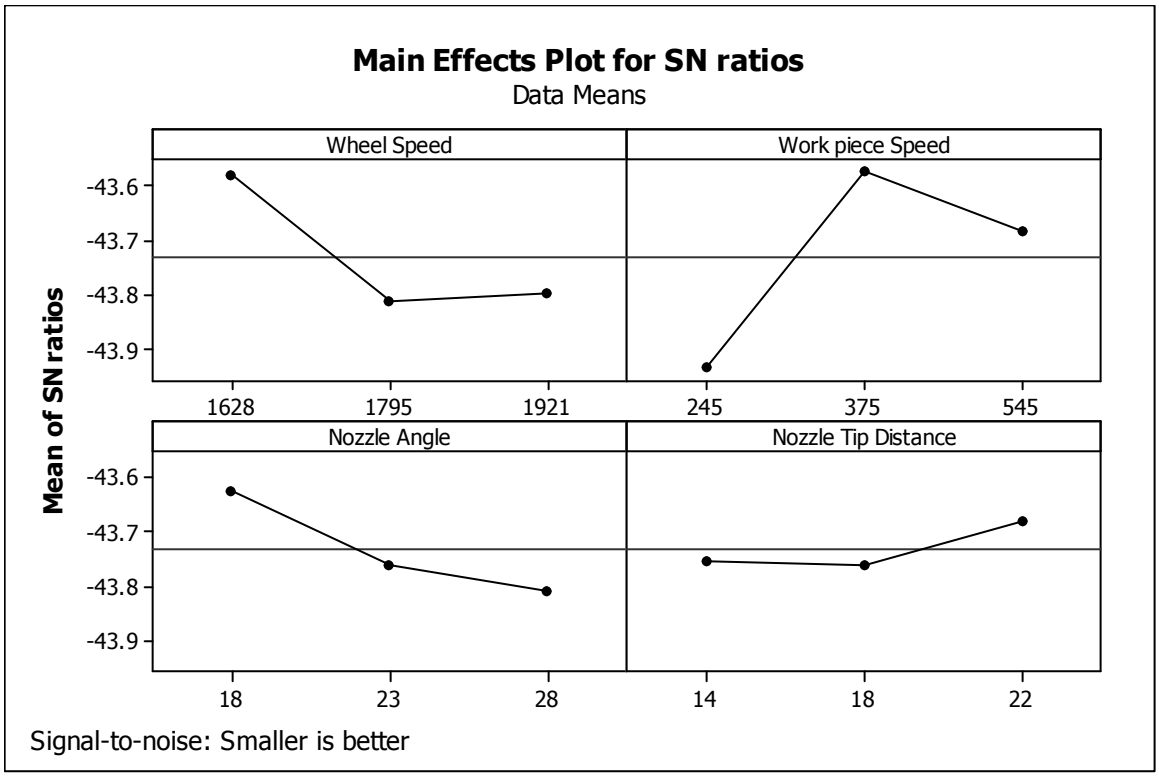

Figure 4.38: Main effects plot for S/N ratio of hardness for taper nozzle

4.12.3 Optimal Design

Hardness number is the output response and it should be smaller for desired response. Main effects plot shown in figure 4.31 shows that Wheel speed and workpiece speed has most significant effect on hardness number. For optimal design Wheel speed 1628 rpm and workpiece speed 375 rpm are selected.. Table 4.35 shows order of significant factors that affect surface hardness response after completion of S/N and ANOVA of means analysis.

Table 4.35: Order of significant factors for surface hardness for taper nozzle

Factor	Significance order of factors in ANOVA	Significance order of factors in S/N ratio
Wheel speed	2	2
Workpiece speed	1	1
Nozzle angle	3	3
Nozzle tip distance	No	No

Estimation of Means of Surface Hardness Number (VHN)

Mean value for VHN

$\mu_{A_1B_2} = \overline{A_1} + \overline{B_2} - \overline{T}$

$\mu_{A_1B_2} = 151 + 150.9 - 153.7083 = 148.19$

Confidence Interval around the estimated VHN

$$CI_1 = \sqrt{\frac{F_{\alpha,v_1,v_2} V_e}{n_{eff}}} \quad \text{Where} \quad F_{\alpha v_1 v_2} = F\ ratio$$

α = risk (0.1) confidence= 1- α

v_1= *dof* for means always 1 v_2= *dof* for error

$$Varienc = V_e = \frac{sum\ of\ square\ of\ e\ pooled}{degree\ of\ freedom\ of\ e\ pooled} = 1.762$$

n_{eff} = Number of tests under that condition using the participating factors

$$n_{eff} = \frac{N}{1 + dof_{A,B}} = \frac{9}{1 + 2 + 2} = 1.8$$

$$CI_1 = \sqrt{\frac{F_{\alpha,v_1,v_2} V_e}{n_{eff}}} = \sqrt{\frac{8.52 \times 1.762}{1.8}} = 2.88$$

Confidence Interval around the estimated surface harness number is 148.19 ± 2.88 VHN.

4.13 ANALYSIS OF SURFACE HARDNESS FOR SPLINE NOZZLE

ANOVA is applied nine trials of spline nozzle. Table 4.36 shows three Vickers hardness number values for each experiment. Mean of these values in taken. ANOVA for means and ANOVA of S/N ratio is done.

Table 4.36: Results for Surface hardness number for spline nozzle

Exp. No.	Wheel Speed (rpm)	Work-piece Speed (rpm)	Nozzle Angle (degree)	Nozzle Tip Distance (mm)	Vickers hardness Number (VHN)			Mean of VHN
					1	2	3	
1	1628	245	18	14	152.01	151.234	152.791	152.012
2	1628	375	23	18	165.718	167.056	165.276	166.017
3	1628	545	28	22	165.718	165.276	169.321	166.772
4	1795	245	23	22	155.172	156.791	158.435	156.799
5	1795	375	28	14	159.266	157.61	160.105	158.994
6	1795	545	18	18	156.791	156.791	155.978	156.520
7	1921	245	28	18	161.375	164.397	162.66	162.810
8	1921	375	18	22	152.791	149.701	151.621	151.371
9	1921	545	23	14	157.61	157.199	159.685	158.165

4.13.1 ANOVA for Means

ANOVA of means is shown in table 4.37 and its response table is shown in table 4.38. F value and percentage contribution tells most significant factor and contribution of each factor which effects variation in output response. Main effect plot is shown in figure 4.39.

Table 4.37: ANOVA for means of surface hardness for spline nozzle

Source	DF	SS	MS	F	Order of significance	Percentage contribution
Wheel Speed	2	34.558	17.2791	2.14295	3	14.24408
Work piece Speed	2	16.126	8.0632	-	-	-
Nozzle Angle	2	147.12	73.5598	9.12290	1	60.63978
Nozzle Tip Distance	2	44.809	22.4043	2.77858	2	18.46933
Total	8	242.613				100
E pooled	2	16.126	8.0632			6.6468

Table 4.38: Response table for means of surface hardness for spline nozzle

Level	Wheel Speed (rpm)	Work piece Speed (rpm)	Nozzle Angle (degree)	Nozzle Tip Distance (mm)
1	161.6	157.2	153.3	156.4
2	157.4	158.8	160.3	161.8
3	157.4	160.5	162.9	158.3
Delta	4.2	3.3	9.6	5.4
Rank	3	4	1	2

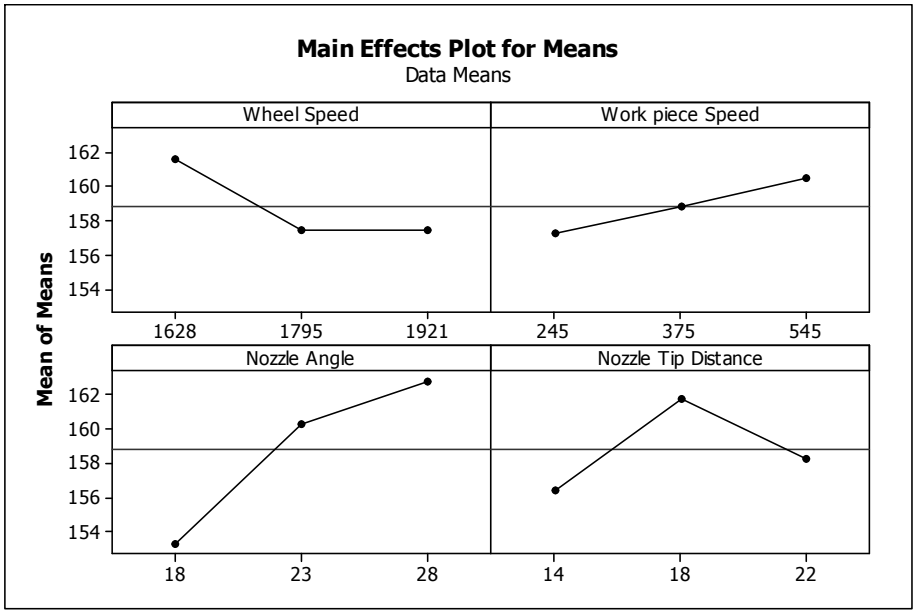

Figure 4.39: Main effects plot for means of surface hardness for spline nozzle

4.13.2 Analysis of S/N Ratio

Table 4.39 shows the Analysis of variance for S/N ratio. And response table for S/N ratio is shown in table 4.40. Nozzle angle is significant factor for surface hardness with spline nozzle Main effect plot for S/N ratio is shown in figure 4.40.

Table 4.39: ANOVA for S/N ratio of surface hardness number for spline nozzle

Source	DF	SS	MS	F	Order of significance
Wheel Speed	2	0.097323	0.048662	2.01549	3
Work piece Speed	2	0.048288	0.024144	-	-
Nozzle Angle	2	0.444158	0.222079	9.198103	1
Nozzle Tip Distance	2	0.133488	0.066744	2.764414	2
Total	8	0.723257			
e-pool	2	0.048288	0.024144		

Table 4.40: Response table for S/N ratio of surface hardness number for spline nozzle

Level	Wheel Speed (rpm)	Work piece Speed (rpm)	Nozzle Angle (rpm)	Nozzle Tip Distance (mm)
1	-44.16	-43.93	-43.71	-43.88
2	-43.94	-44.01	-44.1	-44.18
3	-43.94	-44.11	-44.23	-43.98
Delta	0.22	0.18	0.52	0.29
Rank	3	4	1	2

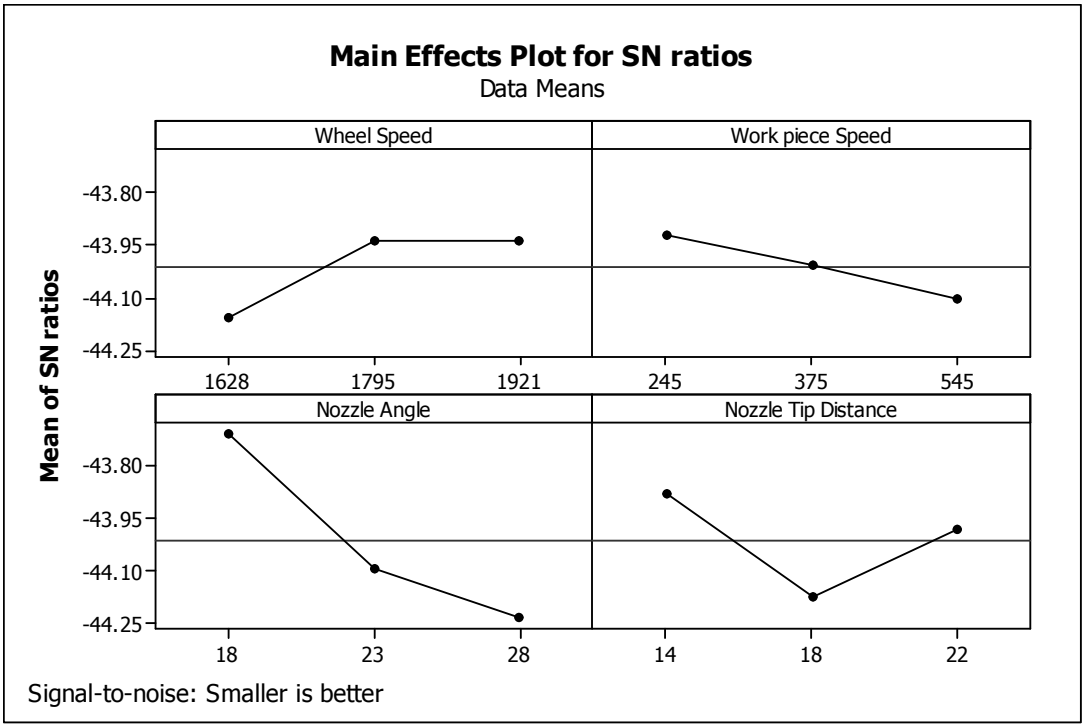

Figure 4.40: Main effect plot for S/N ratio of surface hardness for spline nozzle

4.13.3 Optimal Design

Main effects plot shown in figure 4.39 shows that Nozzle angle has significant effect surface hardness. Hardness number should be smaller for desired response. Nozzle angle 18^0 is the effecting level. Table 4.31 shows order of significant factors that affect surface hardness number after completion of S/N and ANOVA of means analysis. This table shows that in both ANOVA and S/N ration analysis Nozzle angle is most significant.

Table 4.41: Order of significant factors for surface hardness number for spline nozzle

Factors	Significance order of factors in ANOVA	Significance order of factors in S/N ratio
Wheel Speed	3	3
Workpiece speed	No	No
Nozzle angle	1	1
Nozzle tip distance	2	2

4.14 ANALYSIS OF DIMENSIONAL ACCURACY

Dimensional accuracy for all three Nozzles is measured. For each of nine trials, dimension is measured with six replications. For all these six replicas C_p is calculated.

C_p for dimensional control is

$$C_p = \frac{T}{6\sigma}$$

T is the tolerance and it is taken as ± 5 µ.

σ is Standard deviation of six replications on each work-piece

$$\sigma = \sqrt{\frac{1}{N}\sum_{i=1}^{6} f_i\left(x_i - \bar{x}\right)^2}$$

N is the number of replications

$x_i \mid f_i$ is the frequency distribution

$\bar{x}$ is the arithmetic mean

The calculated value of C_p has been used for analysis. Two cuts are made on each workpiece which have initial diameter of 17.750 mm. First cut is of 100 µm and second cut is of 50 µm. Both S/N ratio and mean is calculated using ANOVA and on the bases of results most contributing factor for variation is found out. For this response 'Larger is better' algorithm for S/N ratio is used.

$$S/N = -10\log[(\frac{1}{r}\sum_{i=1}^{r} 1/y^2{}_i)$$

4.15 ANALYSIS OF DIMENSIONAL ACCURACY OF CONVERGENT DIVERGENT NOZZLE

ANOVA is applied nine trials of convergent divergent nozzle. Table 4.42 shows the six replicas of dimension values for each trial. C_p is calculated for all six replicas. ANOVA for S/N ratio and ANOVA for means are done as shown in following tables.

Table 4.42: Results for dimensional accuracy for convergent divergent nozzle

Exp. No.	Wheel Speed (rpm)	Work-piece Speed (rpm)	Nozzle Angle (degree)	Nozzle Tip Distance (mm)	Dimensional Control (mm)						C_p
					1	2	3	4	5	6	
1	1628	245	18	14	17.601	17.600	17.600	17.600	17.601	17.601	3.0429
2	1628	375	23	18	17.601	17.601	17.600	17.600	17.600	17.601	3.0429
3	1628	545	28	22	17.597	17.596	17.596	17.595	17.595	17.598	1.4256
4	1795	245	23	22	17.598	17.599	17.597	17.598	17.596	17.598	1.6137
5	1795	375	28	14	17.604	17.603	17.601	17.605	17.603	17.606	0.9517
6	1795	545	18	18	17.599	17.599	17.598	17.598	17.596	17.597	1.4256
7	1921	245	28	18	17.605	17.603	17.604	17.603	17.603	17.605	1.6951
8	1921	375	18	22	17.598	17.597	17.598	17.599	17.603	17.602	0.6861
9	1921	545	23	14	17.606	17.608	17.609	17.608	17.605	17.604	0.8475

4.15.1 ANOVA for Means

ANOVA of means is shown in table 4.43 and its response table is shown in table 4.44. F value and percentage contribution are calculated to find out most contributing factor which effects variation in output response. Table shows that wheel speed affects more. Main effect plot is shown in figure 4.41.

Table 4.43: ANOVA for means of dimensional accuracy for convergent divergent nozzle

Source	DF	SS	MS	F	Order of significance	Percentage contribution
Wheel Speed	2	3.47936	1.73968	9.3672	1	57.57
Work piece Speed	2	1.19936	0.59968	3.2289	2	19.85
Nozzle Angle	2	0.3714	0.18572	-	-	-
Nozzle Tip Distance	2	0.99310	0.49655	2.67364	3	16.43
Total	8	6.04325				100
E pooled	2	0.3714	0.18572			6.15

Table 4.44: Response table for means of dimensional accuracy for convergent divergent nozzle

Level	Wheel Speed (rpm)	Work piece Speed (rpm)	Nozzle Angle (degree)	Nozzle Tip Distance (mm)
1	2.504	2.117	1.718	1.614
2	1.330	1.560	1.835	2.055
3	1.076	1.233	1.358	1.242
Delta	1.428	0.884	0.477	0.813
Rank	1	2	4	3

Main effect plot for means shows that, at speed 1628 rpm dimensional accuracy is more. Because the Velocity of air around grinding wheel is slower than other levels so nozzle coolant can cut the air layer easily and get in the grinding zone and remove the chips so that dimensional accuracy is maintained.

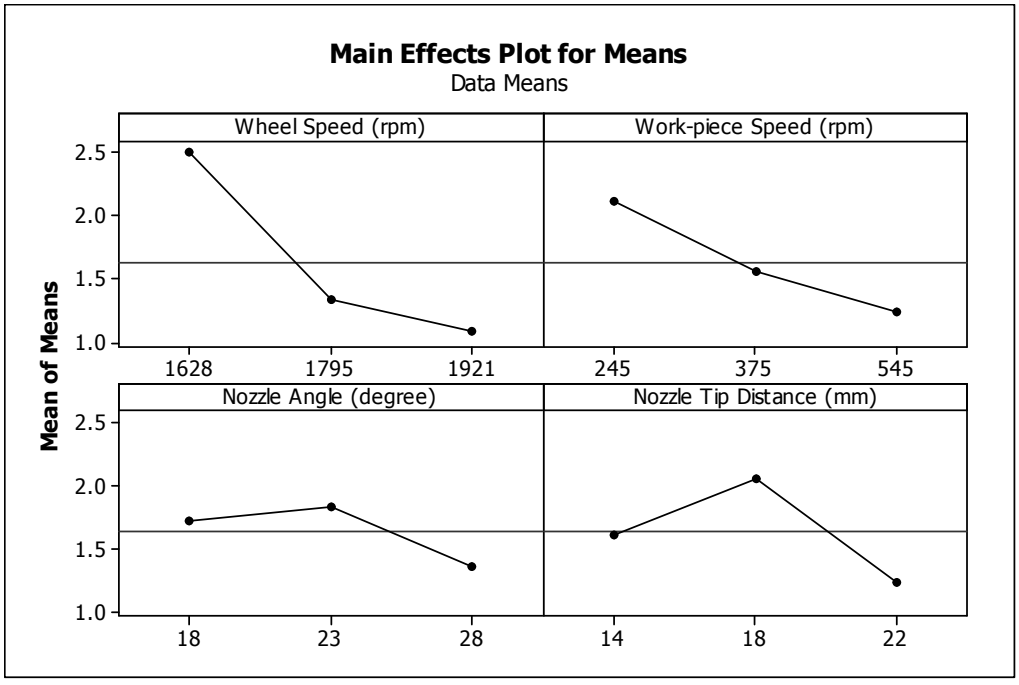

Figure 4.41: Main effects plot for means of dimensional accuracy with convergent divergent nozzle

4.15.2 Analysis for S/N Ratio

Table 4.45 shows the Analysis of variance for S/N ratio. Response table for S/N ratio is shown in table 4.46. Main effect plot for S/N ratio is shown in figure 4.42. The table and plot shows that wheel speed has significant effect on dimensional accuracy.

Table 4.45: ANOVA for S/N ratio of dimensional accuracy for convergent divergent nozzle

Source	DF	SS	MS	F	Order of Significance
Wheel Speed	2	88.822	44.4108	19.9706	1
Work piece Speed	2	38.172	19.0862	8.5826	2
Nozzle Angle	2	4.448	2.2238	-	-
Nozzle Tip Distance	2	31.573	15.7863	7.0987	3
Total	8	163.014			
e-pool	2	4.448	2.2238		

Table 4.46: Response table for S/N ratio of dimensional accuracy for convergent divergent nozzle

Level	Wheel Speed (rpm)	Work piece Speed (rpm)	Nozzle Angle (degree)	Nozzle Tip Distance (mm)
1	7.413	7.173	4.786	2.567
2	4.459	2.758	5.428	7.589
3	1.650	3.592	3.308	3.366
Delta	5.763	4.415	2.120	5.022
Rank	1	3	4	2

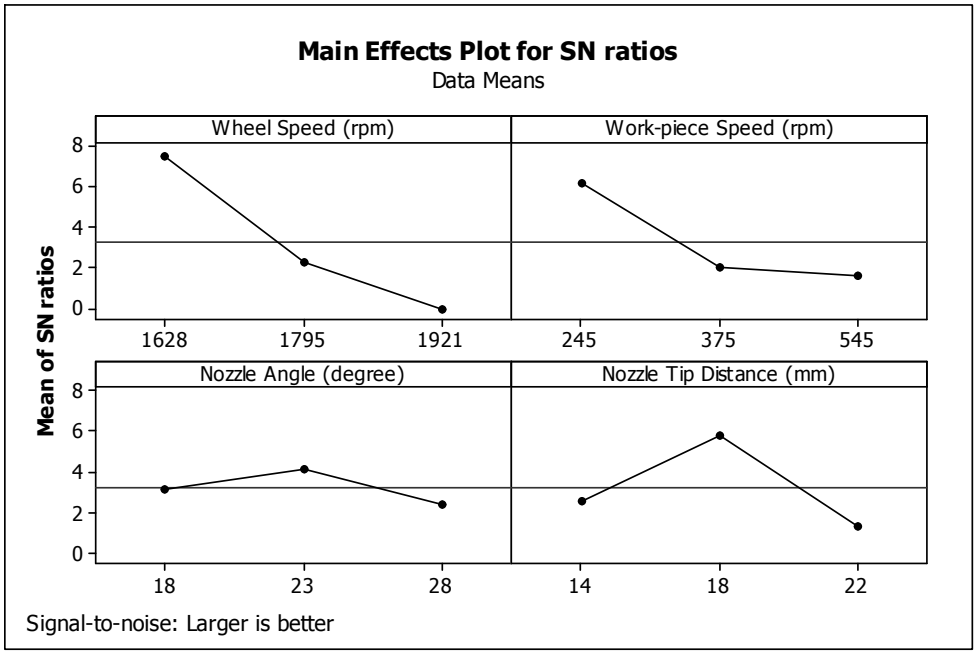

Figure 4.42: Main effect plot for S/N ratio of dimensional accuracy for convergent divergent nozzle

4.15.3 Optimal Design

In dimensional accuracy desired output response is C_p and larger C_p is desired. Main effects plot shown in figure 4.41 shows that Wheel speed has most significant effect on C_p. For optimal design Wheel speed 1628 rpm is selected because it has effect on variation of output response. Table 4.47 shows order of significant factors that affect C_p response after completion of S/N and ANOVA of means analysis.

Table 4.47: Order of significant factors for C_p for convergent divergent nozzle

Factor	Significance order of factors in ANOVA	Significance order of factors in S/N ratio
Wheel speed	1	1
Workpiece speed	2	2
Nozzle angle	No	No
Nozzle tip distance	3	3

4.16 ANALYSIS OF DIMENSIONAL ACCURACY OF TAPER NOZZLE

ANOVA is applied nine trials of Taper nozzle. Table 4.48 shows the six replicas of dimension values for each trial. ANOVA of S/N ratio and ANOVA for means is calculated and is given in following tables.

Table 4.48: Results for dimensional accuracy for taper nozzle

Exp. No.	Wheel Speed (rpm)	Work-piece Speed (rpm)	Nozzle Angle (degree)	Nozzle Tip Distance (mm)	Dimensional Control (mm)						C_p
					1	2	3	4	5	6	
1	1628	245	18	14	17.600	17.601	17.601	17.602	17.601	17.601	2.6352
2	1628	375	23	18	17.601	17.601	17.602	17.601	17.601	17.602	3.2274
3	1628	545	28	22	17.604	17.605	17.604	17.604	17.603	17.605	2.2140
4	1795	245	23	22	17.595	17.597	17.595	17.596	17.593	17.592	0.8951
5	1795	375	28	14	17.603	17.602	17.604	17.602	17.605	17.603	1.4256
6	1795	545	18	18	17.591	17.592	17.594	17.594	17.594	17.593	1.3176
7	1921	245	28	18	17.606	17.608	17.605	17.605	17.603	17.603	0.8784
8	1921	375	18	22	17.594	17.595	17.595	17.594	17.594	17.594	3.2274
9	1921	545	23	14	17.596	17.596	17.595	17.596	17.594	17.592	1.0403

4.16.1 ANOVA for Means

ANOVA for means of taper nozzle is shown in table 4.49 and its response table is shown in table 4.50.F value and percentage contribution is calculated for all factors. Table shoes that Wheel speed and workpiece speed contribute maximum in effecting output response. Main effect plot is shown in figure 4.43.

Table 4.49: ANOVA for means of dimensional accuracy for taper nozzle

Source	DF	SS	MS	F	Order of significance	Percentage Contribution
Wheel Speed	2	3.39559	1.69779	12.4025	1	45.19
Work piece Speed	2	2.55863	1.27932	9.3456	2	34.05
Nozzle Angle	2	1.28590	0.64295	4.6968	3	17.11
Nozzle Tip Distance	2	0.27379	0.13689	-	-	-
Total	8	8.57089				100
e-pool	2	0.27379	0.13689			3.64

Table 4.50: Response table for means of dimensional accuracy for taper nozzle

Level	Wheel Speed (rpm)	Work piece Speed (rpm)	Nozzle Angle (rpm)	Nozzle Tip Distance (mm)
1	2.692	1.470	2.393	1.700
2	1.213	2.627	1.721	1.808
3	1.715	1.524	1.506	2.112
Delta	1.479	1.157	0.887	0.412
Rank	1	2	3	4

Main effect plot for means shows that, at speed 1628 rpm and workpiece speed 375 rpm dimensional accuracy is more. Because the Velocity of air around grinding wheel is slower at 1628 rpm than other levels so nozzle coolant can cut the air layer easily work piece speed helps the coolant to get in the grinding zone and remove the chips so that dimensional accuracy is maintained.

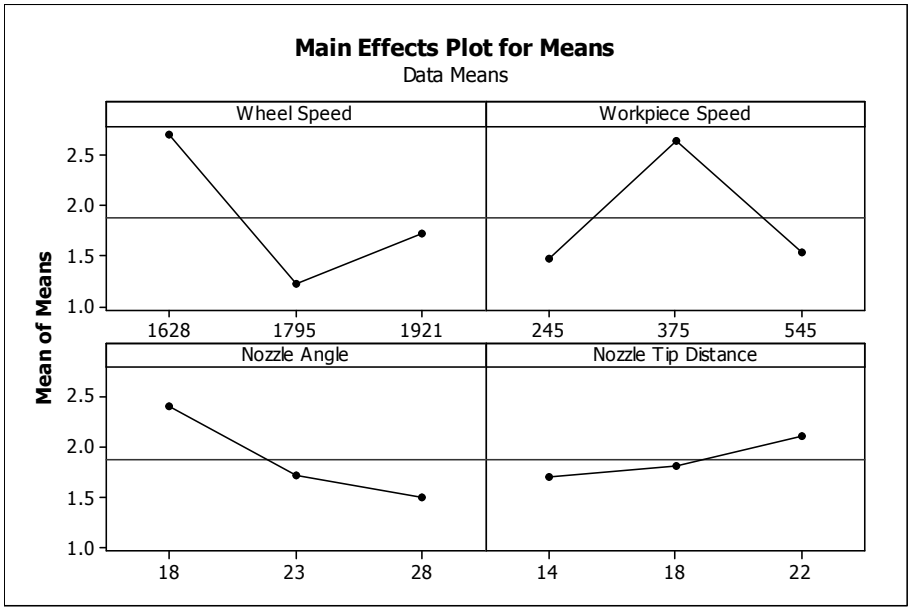

Figure 4.43: Main effects plot for Means of dimensional accuracy for taper nozzle

4.16.2 Analysis for S/N Ratio

Table 4.51 shows the Analysis of variance for S/N ratio. And response table for S/N ratio is shown in table 4.42. Wheel speed and workpiece speed came out to be most significant factor for output response. Main effect plot for S/N ratio is shown in figure 4.44.

Table 4.51: ANOVA for S/N ratio of dimensional accuracy for taper nozzle

Source	DF	SS	MS	F	Order of significance
Wheel Speed	2	80.380	40.1902	17.9556	1
Work piece Speed	2	54.872	27.4362	12.2576	2
Nozzle Angle	2	30.926	15.4628	6.9082	3
Nozzle Tip Distance	2	4.477	2.2383	-	-
Total	8	170.655			
E pooled	2	4.477	2.2383		

Table 4.52: Response table for S/N ratio of dimensional accuracy for taper nozzle

Level	Wheel Speed (rpm)	Work piece Speed (rpm)	Nozzle Angle (degree)	Nozzle Tip Distance (mm)
1	8.499	2.109	6.996	3.947
2	1.505	7.812	3.186	3.816
3	3.132	3.214	2.953	5.373
Delta	6.994	5.702	4.044	1.557
Rank	1	2	3	4

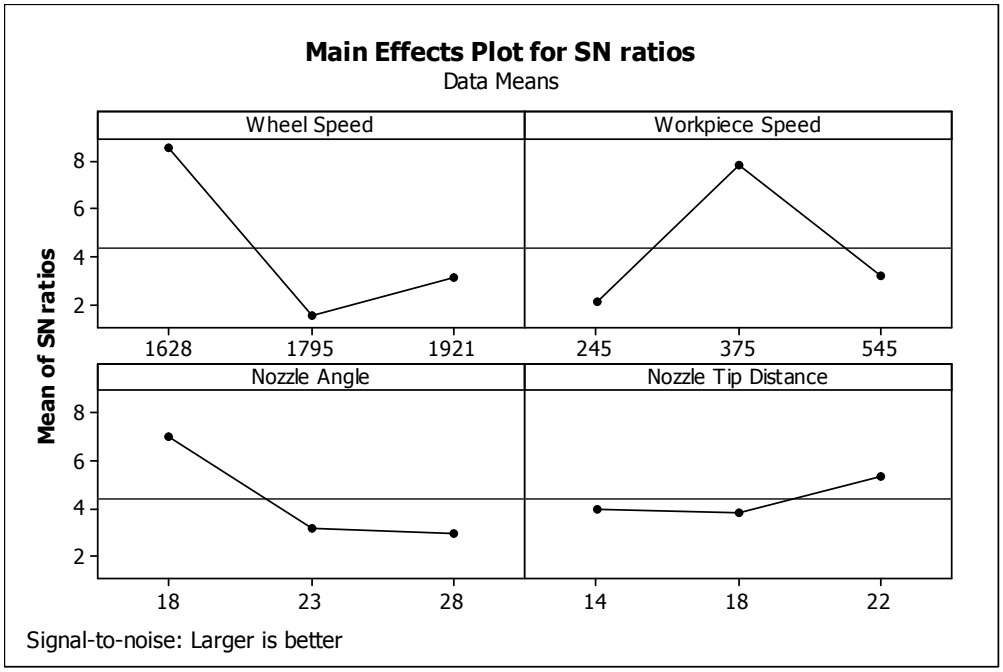

Figure 4.44: Main effect plot for S/N ratio of dimensional accuracy for taper nozzle

4.16.3 Optimal Design

Main effects plot shown in figure 4.43 shows that Wheel speed and workpiece speed has most significant effect on dimensional accuracy. C_p is desired response and it should be higher. For optimal design Wheel speed 1628 rpm and workpiece speed 375 rpm are selected because they have most effect on variation of output response. Table 4.53 shows order of significant factors that affect dimensional accuracy response after completion of S/N and ANOVA of means analysis.

Table 4.53: Order of significant factors for dimensional accuracy for taper nozzle

Factor	Significance order of factors in ANOVA	Significance order of factors in S/N ratio
Wheel speed	1	1
Workpiece speed	2	2
Nozzle angle	3	3
Nozzle tip distance	No	No

Estimating the Mean Value of C_p for Dimensional Accuracy

Mean value for C_p for dimensional accuracy

$\mu_{A_1B_2} = \overline{A_1} + \overline{B_2} - \overline{T}$

$\mu_{A_1B_2} = 2.692 + 2.627 - 1.873 = 3.446$

Confidence Interval around the estimated C_p

$$CI_1 = \sqrt{\frac{F_{\alpha,v_1,v_2} V_e}{n_{eff}}}$$ Where $F_{\alpha v_1 v_2} = F\ ratio$

α = risk (0.1) confidence= 1- α

ν_1= *dof* for means which is always 1

ν_2= *dof* for error

$$V_e = \frac{sum\ of\ square\ of\ e\ pooled}{degree\ of\ freedom\ of\ e\ pooled} = 0.1368$$

n_{eff} = Number of tests under that condition using the participating factors

$$n_{eff} = \frac{N}{1 + dof_{A,B}} = \frac{9}{1 + 2 + 2} = 1.8$$

$$CI_1 = \sqrt{\frac{F_{\alpha,v_1,v_2} V_e}{n_{eff}}} = \sqrt{\frac{8.52 \times 0.1368}{1.8}} = 0.8046$$

,

So the confidence interval around the estimated C_p is 3.446± 0.8046.

4.17 ANALYSIS OF DIMENSIONAL ACCURACY OF SPLINE NOZZLE

ANOVA is applied nine trials of Spline nozzle. Table 4.54 shows the six replicas of dimension values and also C_p is shown. ANOVA of S/N ratio and ANOVA for means are calculated and are given in following.

Table 4.54: Results for dimensional accuracy of Spline nozzle

Exp. No.	Wheel Speed (rpm)	Work-piece Speed (rpm)	Nozzle Angle (degree)	Nozzle Tip Distance	Dimensional Control (mm)						C_p
					1	2	3	4	5	6	
1	1628	245	18	14	17.601	17.602	17.602	17.602	17.601	17.601	3.0429
2	1628	375	23	18	17.601	17.599	17.599	17.599	17.601	17.601	1.5214
3	1628	545	28	22	17.596	17.597	17.596	17.598	17.596	17.599	1.3176
4	1795	245	23	22	17.598	17.597	17.598	17.599	17.598	17.598	2.6352
5	1795	375	28	14	17.593	17.594	17.594	17.593	17.595	17.595	1.8633
6	1795	545	18	18	17.602	17.602	17.603	17.603	17.604	17.603	2.2140
7	1921	245	28	18	17.604	17.606	17.607	17.604	17.603	17.602	0.8951
8	1921	375	18	22	17.602	17.602	17.602	17.603	17.603	17.602	3.2274
9	1921	545	23	14	17.603	17.604	17.603	17.601	17.603	17.603	1.6951

4.17.1 ANOVA for Means

ANOVA of means is shown in table 4.55 and its response table is shown in table 4.56. F value and percentage contribution are calculated. Nozzle angle came out to be most significant factor which affects output response. Main effect plot is shown in figure 4.45.

Table 4.55: ANOVA for Means of dimensional accuracy of spline nozzle

Source	DF	SS	MS	F	Order of significance	Percentage contribution
Wheel Speed	2	0.16611	0.08305	-	-	-
Work piece Speed	2	0.41491	0.20745	2.4978	3	8.21
Nozzle Angle	2	3.27961	1.63981	19.7448	1	64.92
Nozzle Tip Distance	2	1.19113	0.59557	7.17122	2	23.58
Total	8	5.05176				100
E pooled	2	0.16611	0.08305			3.29

Table 4.56: Response table for means of dimensional accuracy of spline nozzle

Level	Wheel Speed (rpm)	Work piece Speed (rpm)	Nozzle Angle (degree)	Nozzle Tip Distance (mm)
1	1.961	2.191	2.828	2.200
2	2.238	2.204	1.951	1.544
3	1.939	1.742	1.359	2.393
Delta	0.298	0.462	1.469	0.850
Rank	4	3	1	2

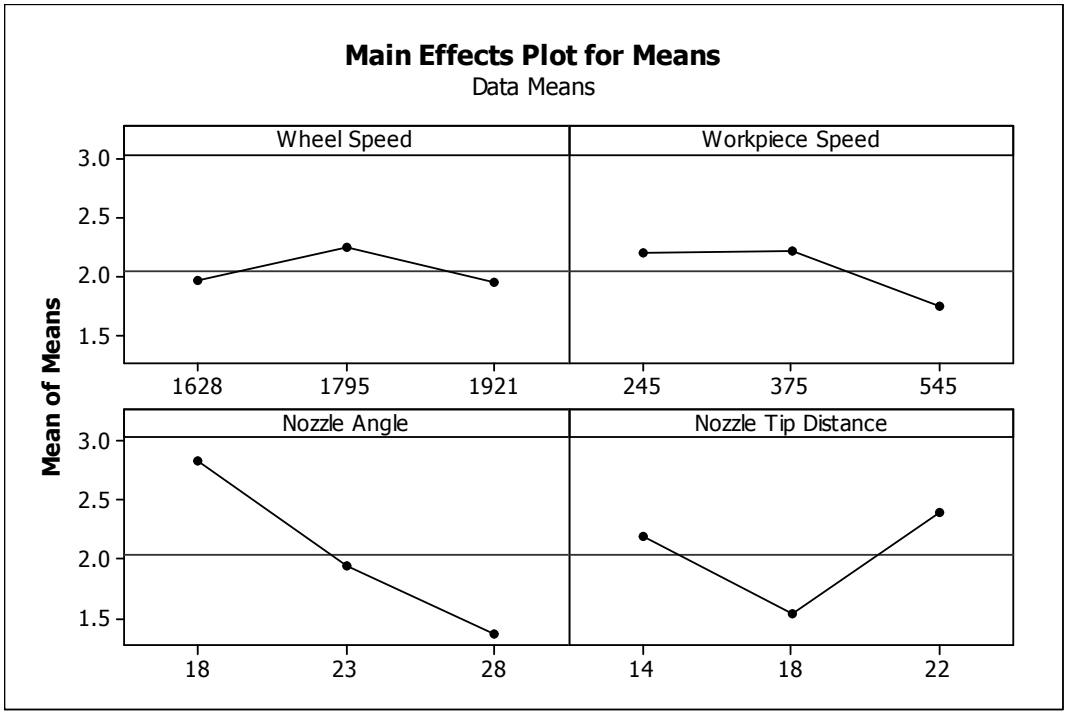

Figure 4.45: Main effects plot for means of dimensional accuracy of spline nozzle

In case of spline as it is shown in velocity response analysis nozzle angle is most significant for achieving the higher velocity in grinding zone, and for dimensional accuracy velocity of coolant should be high to remove the chips from grinding wheel , there for nozzle angle has significant effect on achieving dimensional accuracy. Nozzle tip distance also gives some significance at 22 mm.

4.17.2 Analysis of S/N Ratio

Table 4.57 shows the Analysis of variance for S/N ratio. And response table for S/N ratio is shown in table 4.58. Main effects plot for S/N ratio is shown in figure 4.46.

Table 4.57: ANOVA for S/N ratio of dimensional accuracy of spline nozzle

Source	DF	SS	MS	F	Order of significance
Wheel Speed	2	8.535	4.2674	1.7663	3
Work piece Speed	2	4.832	2.4159	-	-
Nozzle Angle	2	66.053	33.0266	13.6705	1
Nozzle Tip Distance	2	25.910	12.9551	5.3624	2
Total	8	105.330			
E pooled	2	4.832	2.4159		

Table 4.58: Response table for S/N ratio of dimensional accuracy of spline nozzle

Level	Wheel Speed (rpm)	Work piece Speed (rpm)	Nozzle Angle (degree)	Nozzle Tip Distance (mm)
1	5.236	5.707	8.916	6.552
2	6.909	6.410	5.549	3.196
3	4.600	4.628	2.280	6.996
Delta	2.309	1.782	6.636	3.801
Rank	3	4	1	2

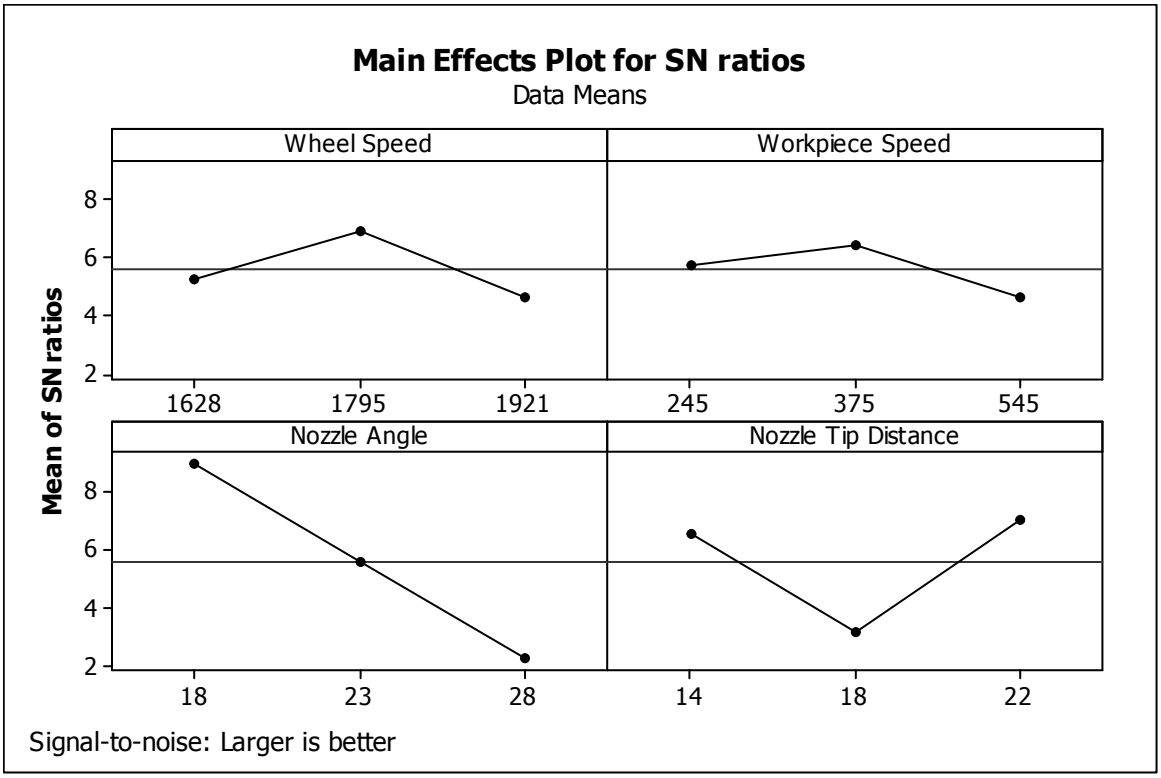

Figure 4.46: Main effect plot for S/N ratio of dimensional accuracy of spline nozzle

4.17.3 Optimal Design

Main effects plot shown in figure 4.45 shows that Nozzle angle has significant effect on dimensional accuracy. In dimensional accuracy desired output response is C_p and larger C_p is desired. Nozzle angle 18^0 in Nozzle angle graph has highest mean value. Workpiece speed is almost straight line so it is least significant factor Table 4.59 shows order of significant factors that affect dimensional accuracy after completion of S/N and ANOVA of means analysis. This table shows that in both ANOVA and S/N ration analysis Nozzle angle is most significant.

Table 4.59: Order of significant factors for dimensional accuracy of spline nozzle

Factors	Significance order of factors in ANOVA	Significance order of factors in S/N ratio
Wheel Speed	No	3
Workpiece speed	3	No
Nozzle angle	1	1
Nozzle tip distance	2	2

4.18 ANALYSIS OF SURFACE CRACKS

Surface Cracks are measured with the help of metallurgical microscope. Severity of cracks is checked and number of cracks is estimated. According to these parameters Cracks on each workpiece are categorized as in following table 4.60 and ranks to each workpiece are given accordingly. Higher rank is desirable for better surface.

Table 4.60: Severity level classification of cracks

Severity Level	Rank
Sever	1
Less sever	2
Significant	3
Negligible	4

S/N ratio algorithm used for this analysis is 'Larger is better'.

$$S/N = -10\log[(\frac{1}{r}\sum_{i=1}^{r} 1/y^2{}_i)$$

4.19 ANALYSIS OF SURFACE CRACKS FOR CONVERGENT DIVERGENT NOZZLE

ANOVA is applied nine trials of convergent divergent nozzle. Table 4.61 shows Cracks severity level ranks according to L_9 array. ANOVA of S/N ratio and ANOVA for means is given as following.

Table 4.61: Results for ranks of surface cracks of convergent divergent nozzle

Exp. No.	Wheel Speed (rpm)	Work-piece Speed (rpm)	Nozzle Angle (degree)	Nozzle Tip Distance (mm)	Rank of severity
1	1628	245	18	14	4
2	1628	375	23	18	3
3	1628	545	28	22	4
4	1795	245	23	22	2
5	1795	375	28	14	4
6	1795	545	18	18	3
7	1921	245	28	18	4
8	1921	375	18	22	2
9	1921	545	23	14	3

4.19.1 ANOVA for Means

ANOVA of means is shown in table 4.62 and its response table is shown in table 4.63. F value and percentage contribution are calculated. Nozzle angle comes out to be most significant factor affecting output response. Main effect plot is shown in figure 4.45.

Table 4.62: ANOVA for means of rank of surface cracks for convergent divergent nozzle

Source	DF	SS	MS	F	Order of significance	Percentage contribution
Wheel Speed	2	0.88889	0.44444	4.0	3	16.00
Work piece Speed	2	0.22222	0.11111	-	-	-
Nozzle Angle	2	2.88889	1.44444	13.0	1	52.00
Nozzle Tip Distance	2	1.55556	0.77778	7.0	2	28.00
Total	8	5.55556				100
E pooled	2	0.22222	0.11111			4.00

Table 4.63: Response table for means of rank of cracks for convergent divergent nozzle

Level	Wheel Speed (rpm)	Work piece Speed (rpm)	Nozzle Angle (degree)	Nozzle Tip Distance (mm)
1	3.667	3.333	3.000	3.667
2	3.000	3.000	2.667	3.333
3	3.000	3.333	4.000	2.667
Delta	0.667	0.333	1.333	1.000
Rank	3	4	1	2

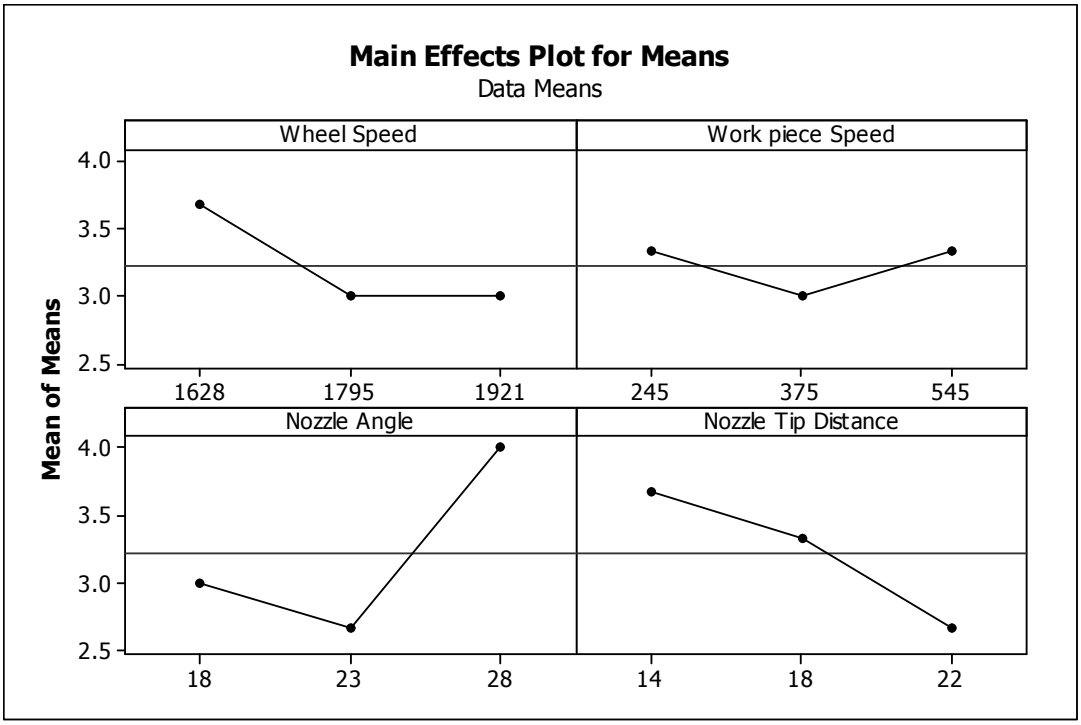

Figure 4.47: Main effect plot for means of rank of cracks for convergent divergent nozzle

Main effect plot showed that nozzle angle 28^0 is significant factor for improving surface crack rank. Because at of that angle and due to high peak velocity of convergent divergent nozzle heat elimination is fast, reducing the severity of cracks on the surface.

4.19.2 Analysis of S/N Ratio

Table 4.64 shows the Analysis of variance for S/N ratio. And response table for S/N ratio is shown in table 4.65. Main effects plot for S/N ratio is shown in figure 4.48. ANOVA table and response table shows that nozzle angle is most significant factor and level of significance is third.

Table 4.64: ANOVA for S/N ratio of rank of cracks for convergent divergent nozzle

Source	DF	SS	MS	F	Order of significance
Wheel Speed	2	8.0550	4.0275	3.68	3
Work piece Speed	2	2.1882	1.0941	-	-
Nozzle Angle	2	22.2470	11.1235	10.17	1
Nozzle Tip Distance	2	16.3239	8.1619	7.46	2
Total	8	48.8141			
E pooled	2	2.1882	1.0941		

Table 4.65: Response table for S/N ratio of rank of surface cracks for convergent divergent nozzle

Level	Wheel Speed (rpm)	Work piece Speed (rpm)	Nozzle Angle (rpm)	Nozzle Tip Distance (mm)
1	11.208	10.034	9.201	11.208
2	9.201	9.201	8.368	10.375
3	9.201	10.375	12.041	8.027
Delta	2.007	1.174	3.673	3.181
Rank	3	4	1	2

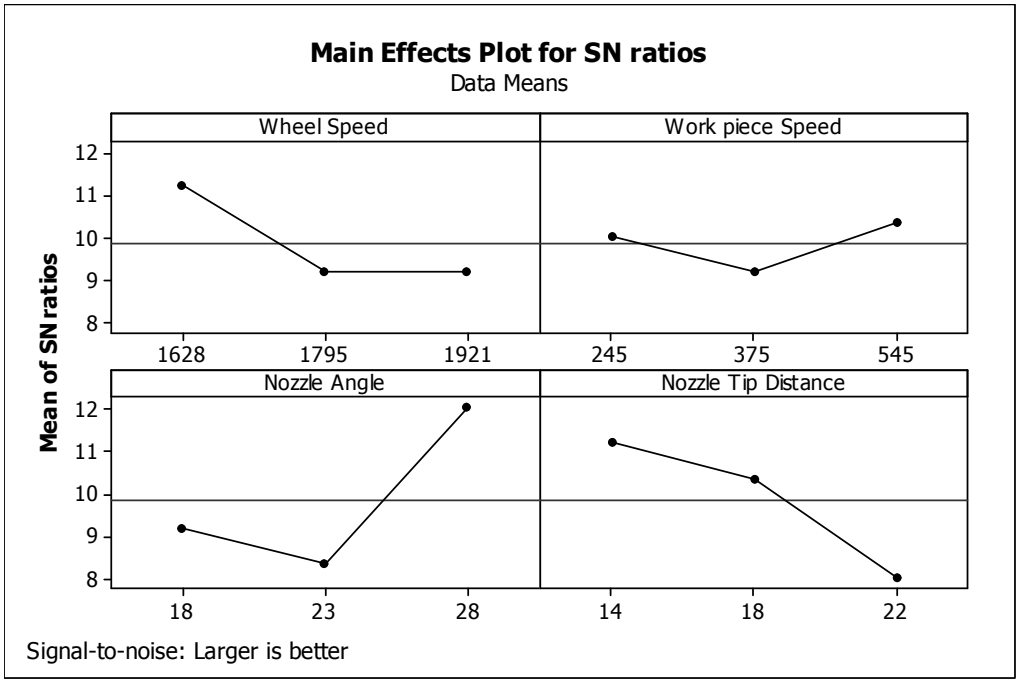

Figure 4.48: Main effect plot for S/N ratio of rank of surface cracks for convergent divergent nozzle

4.19.3 Optimal Design

Desired output response is Rank of severity level of cracks. Larger rank is desired because least severity level has highest rank (Table 3.60). Main effects plot for means shown in figure 4.47 shows that, most significant factor which affects surface cracks is Nozzle angle. Nozzle angle Graph shows that third level i.e. angle 28^0 is most significant. Table 6.66 shows order of significant factors that affect severity level of cracks after completion of S/N and ANOVA of means analysis. This table shows that in both ANOVA and S/N ration analysis Nozzle angle is most significant.

Table 6.66: Order of significant factors for surface cracks for convergent divergent nozzle

Factors	Significance order of factors in ANOVA	Significance order of factors in S/N ratio
Wheel Speed	3	3
Workpiece speed	No	No
Nozzle angle	1	1
Nozzle tip distance	2	2

4.20 ANALYSIS OF SURFACE CRACKS FOR TAPER NOZZLE

ANOVA is applied nine trials of Taper nozzle. Table 4.67 shows cracks severity level ranks for each experiment. ANOVA for S/N and ANOVA for means are given in following tables.

Table 4.67: Results for ranks of surface cracks for taper nozzle

Exp. No.	Wheel Speed (rpm)	Work-piece Speed (rpm)	Nozzle Angle (degree)	Nozzle Tip Distance (mm)	Rank of severity
1	1628	245	18	14	3
2	1628	375	23	18	4
3	1628	545	28	22	2
4	1795	245	23	22	3
5	1795	375	28	14	2
6	1795	545	18	18	3
7	1921	245	28	18	1
8	1921	375	18	22	3
9	1921	545	23	14	2

4.20.1 ANOVA for Means

ANOVA of means is shown in table 4.68 and its response table is shown in table 4.69. According to the F value and percentage contribution most contributing factor which effects variation in output response is calculated. Main effect plot is shown in figure 4.49. In table order of significance shows that Nozzle and wheel speed are significant factors. Main effective plot shoes that level of significance for nozzle angle is 18^0 and level of significance for wheel speed is 1628 rpm.

Table 4.68: ANOVA for means of ranks of surface cracks for taper nozzle

Source	DF	SS	MS	F	Order of significance	Percentage contribution
Wheel Speed	2	1.55556	0.7777	7.0001	2	25.00
Work piece Speed	2	0.88889	0.4444	4.0000	3	14.29
Nozzle Angle	2	3.55556	1.7777	16.0002	1	57.14
Nozzle Tip Distance	2	0.22222	0.1111	-	-	-
Total	8	6.22222				100
E pool	2	0.22222	0.1111			3.57

Table 4.69: Response table for means of ranks of surface cracks for taper nozzle

Level	Wheel Speed (rpm)	Work piece Speed (rpm)	Nozzle Angle (degree)	Nozzle Tip Distance (mm)
1	3.000	2.333	3.000	2.333
2	2.667	3.000	3.000	2.667
3	2.000	2.333	1.667	2.667
Delta	1.000	0.667	1.333	0.333
Rank	2	3	1	4

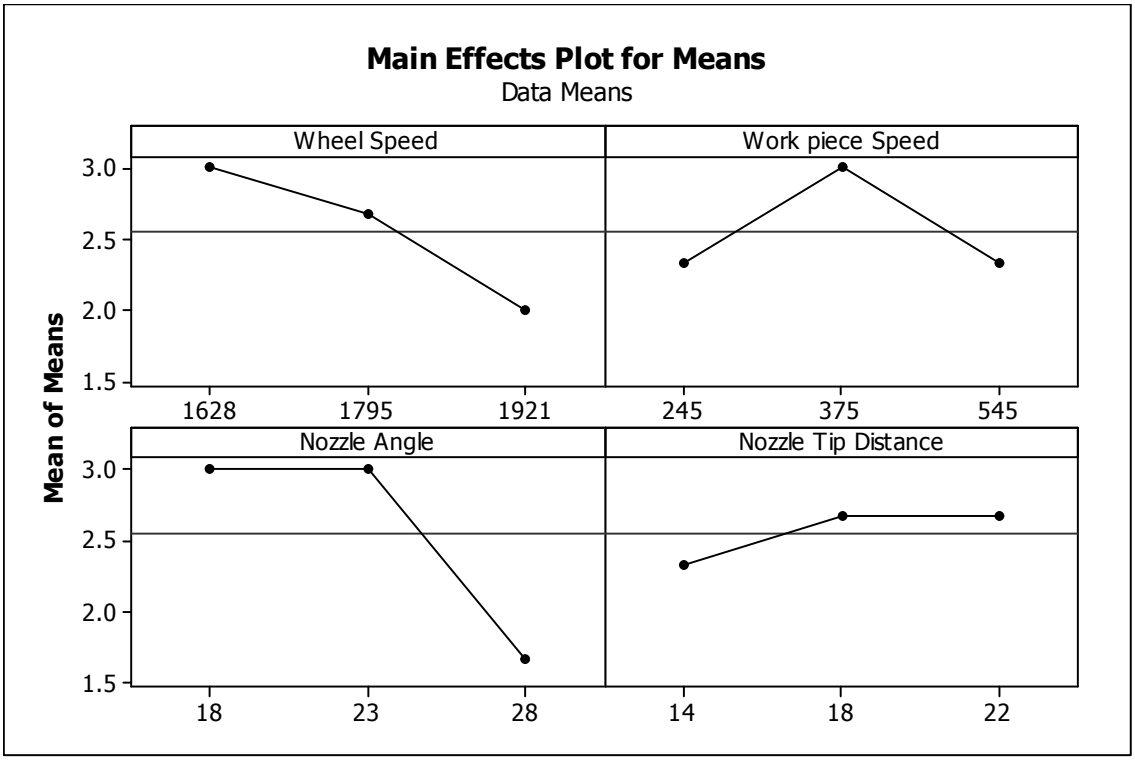

Figure 4.49: Main effect plot for means of ranks of surface cracks for taper nozzle

4.20.2 Analysis of S/N Ratio

Table 4.70 shows the Analysis of variance for S/N ratio. And response table for S/N ratio is shown in table 4.71. Main effects plot for S/N ratio is shown in figure 4.50. In table order of significance shows that Nozzle and wheel speed are significant factors. Main effective plot shoes that level of significance for nozzle angle is 18^0 and level of significance for wheel speed is 1628 rpm.

Table 4.70: ANOVA for S/N ratio of ranks of surface cracks for taper nozzle

Source	DF	SS	MS	F	Order of significance
Wheel Speed	2	26.921	13.4607	9.7675	2
Work piece Speed	2	12.786	6.3928	4.6388	3
Nozzle Angle	2	57.595	28.7973	20.8963	1
Nozzle Tip Distance	2	2.756	1.3781	-	-
Total	8	100.058			
E pooled	2	2.756	1.3781		

Table 4.71: Response table for S/N ratio of ranks of surface cracks for taper nozzle

Level	Wheel Speed (rpm)	Work piece Speed (rpm)	Nozzle Angle (degree)	Nozzle Tip Distance (mm)
1	9.201	6.362	9.542	7.195
2	8.368	9.201	9.201	7.195
3	5.188	7.195	4.014	8.368
Delta	4.014	2.840	5.529	1.174
Rank	1	4	2	3

Main effect plot (figure 4.50) shows that nozzle angle and wheel speed are contributing factors for improving surface crack rank. Because varying the nozzle angle and wheel speed the heat generated in grinding zone is quickly extracted, and reduces the effect of heat on surface of workpiece, reducing the severity of cracks on the surface.

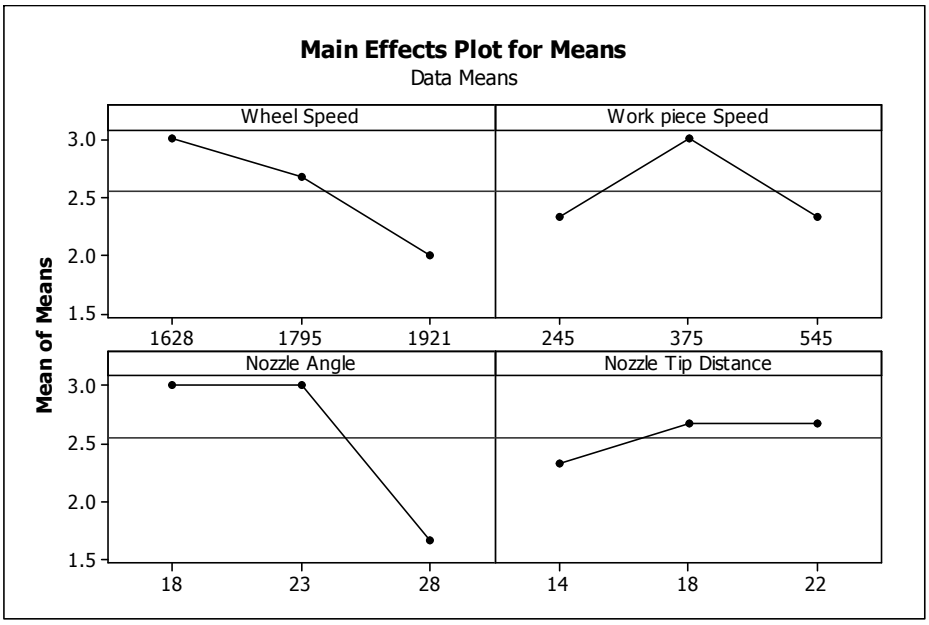

Figure 4.50: Main effect plot for S/N ratio of ranks of surface cracks for taper nozzle

4.20.3 Optimal Design

Desired output response is Rank of severity level of cracks. Larger rank is desired because least severity level has highest rank (Table 3.60). Main effects plot for means shown in figure 4.49 shows that, most significant factor which affects surface cracks is Nozzle angle. Nozzle angle Graph shows that first level i.e 18^0 is most significant. Wheel speed also has some contribution for desired response at 1628 rpm. Table 6.72 shows order of significant factors

that affect severity level rank of cracks after completion of S/N and ANOVA of means analysis.

Table 6.72: Order of significant factors for rank of surface cracks for taper nozzle

Factors	Significance level for ANOVA	Significance level for S/N ratio
Wheel Speed	2	2
Workpiece speed	3	3
Nozzle angle	1	1
Nozzle tip distance	No	No

4.21 ANALYSIS OF SURFACE CRACKS FOR SPLINE NOZZLE

ANOVA is applied on nine trials of Spline nozzle. Table 4.73 shows cracks severity level rank values for severity of cracks. ANOVA of S/N ratio and ANOVA for means is given in following tables.

Table 4.73: Results for rank of surface cracks for spline nozzle

Exp. No.	Wheel Speed (rpm)	Work-piece Speed (rpm)	Nozzle Angle (degree)	Nozzle Tip Distance (mm)	Rank of severity
1	1628	245	18	14	2
2	1628	375	23	18	4
3	1628	545	28	22	1
4	1795	245	23	22	4
5	1795	375	28	14	2
6	1795	545	18	18	4
7	1921	245	28	18	1
8	1921	375	18	22	2
9	1921	545	23	14	2

4.21.1 ANOVA for Means

ANOVA of means is shown in table 4.74 and its response table is shown in table 4.75.from these tables according to the F value and percentage contribution most effecting factor which effects variation in output Wheel Speed and Nozzle angle are significant factors for desired response. Main effect plot is shown in figure 4.51.

Table 4.74: ANOVA for means of rank of surface cracks for Spline nozzle

Source	DF	SS	MS	F	Order of significance	Percentage contribution
Wheel Speed	2	4.2222	2.11111	19.0001	2	34.55
Work piece Speed	2	0.2222	0.11111	-	-	-
Nozzle Angle	2	6.2222	3.11111	28.0007	1	50.91
Nozzle Tip Distance	2	1.5556	0.77778	7.0000	3	12.73
Total	8	12.2222				100
E pooled	2	0.2222	0.11111			1.82

Table 4.75: Response table for means of ranks of surface cracks for Spline nozzle

Level	Wheel Speed (rpm)	Work piece Speed (rpm)	Nozzle Angle (rpm)	Nozzle Tip Distance (mm)
1	2.333	2.333	2.667	2.000
2	3.333	2.667	3.333	3.000
3	1.667	2.333	1.333	2.333
Delta	1.667	0.333	2.000	1.000
Rank	2	4	1	3

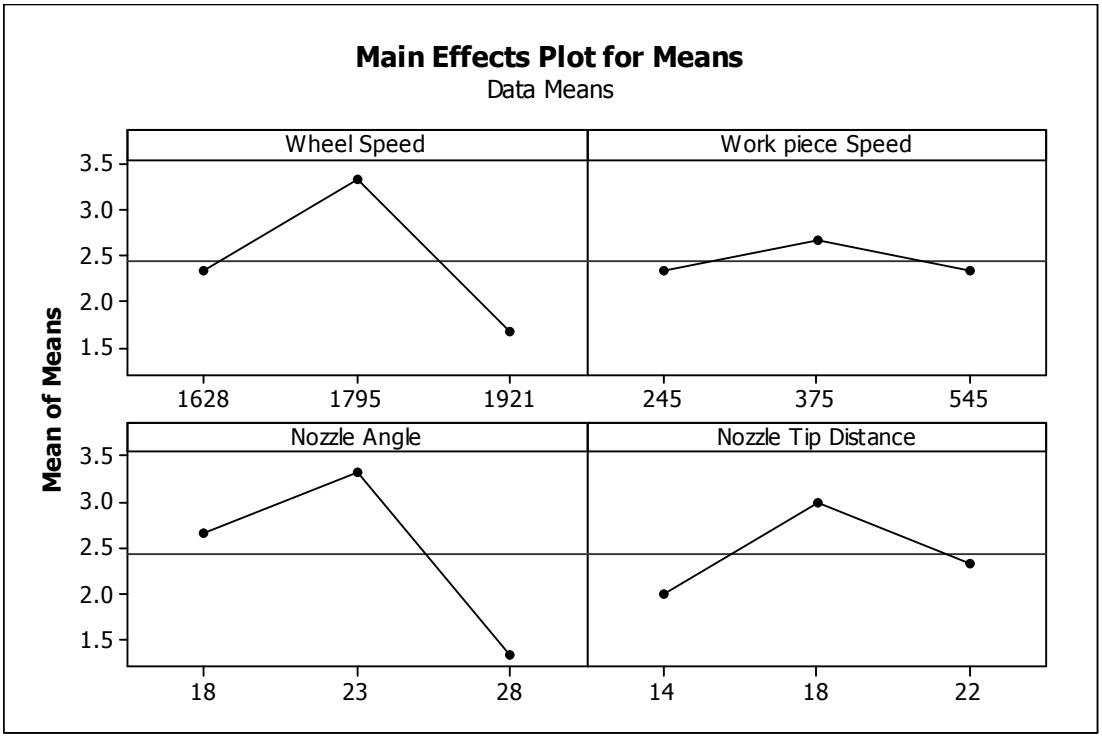

Figure 4.51: Main effects plot for means of ranks of surface cracks for spline nozzle

In case of Spline nozzle angle is most effective in achieving the highest velocity as shown in velocity response tables, so heat can be removed easily also wheel speed is contributing as the swirl of displaced air around the wheel generated due to coolant velocity pushes the coolant in grinding zone and effectively removing heat and improves severity levels of cracks.

4.21.2 Analysis of S/N Ratio

Table 4.76 shows the Analysis of variance for S/N ratio. And response table for S/N ratio is shown in table 4.77. It is shown in table 4.76 nozzle angle comes out to be most significant factors which affect severity level of surface cracks. Main effects plot for S/N ratio is shown in figure 4.52.

Table 4.76: ANOVA for S/N ratio of ranks of surface cracks for Spline nozzle

Source	DF	SS	MS	F	Order of significance
Wheel Speed	2	56.385	28.1926	7.0000	2
Work piece Speed	2	8.055	4.0275	-	3
Nozzle Angle	2	104.715	52.3577	13.0000	1
Nozzle Tip Distance	2	8.055	4.0275	-	-
Total	8	177.211			
E pool	2	8.055	4.0275		

Table 4.77: Response table for S/N ratio of ranks of surface cracks for Spline nozzle

Level	Wheel Speed (rpm)	Work piece Speed (rpm)	Nozzle Angle (degree)	Nozzle Tip Distance (mm)
1	6.021	6.021	8.027	6.021
2	10.034	8.027	10.034	8.027
3	4.014	6.021	2.007	6.021
Delta	6.021	2.007	8.027	2.007
Rank	2	3	1	4

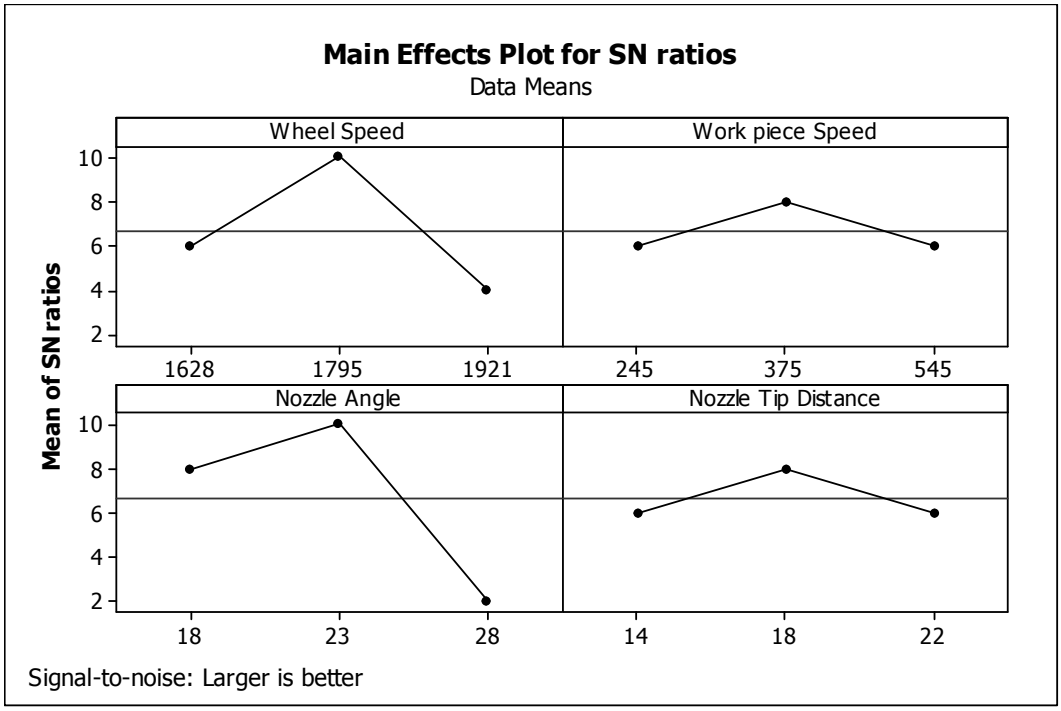

Figure 4.52: Main effects plot for S/N ratio of ranks of surface cracks for Spline nozzle

4.21.3 Optimal Design

Desired output response is Rank of severity level of cracks. Larger rank is desired because least severity level has highest rank (Table 3.60). Main effects plot for means shown in figure 4.51 shows that, most significant factor which affects surface cracks are Nozzle angle and wheel speed. Nozzle angle Graph shows that second level i.e angle 23^0 is most significant. Wheel speed also has significance at level second i.e 1795 rpm for desired response. Table 6.78 shows significant factors that affect severity level of cracks after completion of S/N and ANOVA of means analysis.

Table 6.78: Order of significant factors for ranks of surface cracks for spline nozzle

Factors	Significance level for ANOVA	Significance level for S/N ratio
Wheel Speed	2	2
Workpiece speed	3	No
Nozzle angle	1	1
Nozzle tip distance	No	3

CHAPTER 5
CONCLUSION

5.1 Flow of Work Done

The present thesis work is carried out to optimize the coolant flow in grinding zone and improve the performance of grinding process. Performance of grinding process is evaluated with the effect of process parameters (wheel speed, workpiece speed, nozzle angle and nozzle tip distance) on the quality of ground workpiece.

First of all simulation work is done on ANSYS CFX. Simulation of Fluid flow through different Nozzles is done. Three nozzles convergent divergent nozzle (convergent angle7.5^0 divergent angle 10^0 and divergent length of 4 mm), taper nozzle (taper angle 4^0) and a spline profile nozzle are selected by observing their peak velocity and according to length of peak velocity region. Taguchi technique is then applied design the experimentation L9 orthogonal array is defined for four process parameters to analyse their effect on coolant velocity, surface hardness, dimensional accuracy, surface cracks. Grinding process simulation is then carried out for three selected nozzles to measure the velocity response. Experimental setup is done on cylindrical grinding process and total 27 experiments are carried out (9 for each nozzle). After experimentation testing of ground workpiece is done, measuring dimensional accuracy, Vickers hardness number and surface cracks. ANOVA and S/N ratio analysis of all the response parameters is done with MINITAB. And it is checked that which factor has significant effect and its percentage contribution.

5.2 RESULTS

Selecting best nozzles: Five types of nozzles (Convergent divergent, taper, splines, round and step) are simulated, varying their dimensions. From distance versus velocity graphs, Three Nozzles with highest velocity and longest peak velocity region are selected. These nozzles are convergent divergent nozzle (convergent angle7.5^0 divergent angle 10^0 and divergent length of 4 mm), taper nozzle (taper angle 4^0) and a spline profile nozzle.

Effect of input parameter on Velocity: In the results chapter it is shown that wheel speed is found as most significant factors for convergent and divergent nozzle, Taper nozzle, while for spline nozzle angle is most significant factor.

Effect of input parameter on surface hardness: Results of ANOVA for surface hardness showed that Wheel speed and workpiece speed contribute more than any other factor for

convergent and divergent nozzle, Taper nozzle. Results for surface roughness due to Spline nozzle, nozzle angle is most significant factor for desired hardness number.

Effect of input parameters on dimensional Accuracy: Results of ANOVA for dimensional accuracy shows that Wheel speed and workpiece speed are most significant factors which affects the dimensional accuracy for all of the nozzles.

Effect of input parameters on surface cracks: Nozzle angle has shown maximum significance for desired (improved) surface rank for all of the nozzles

5.3 CONCLUSION

Simulation results of fluid flow through nozzles shows that convergent divergent nozzle achieved highest peak velocity of 24.505 m/s followed by spline nozzle (22.20 m/s) then taper nozzle (21.76 m/s). Grinding process simulation shows that adjusting the appropriate wheel speed, work piece speed and nozzle angle optimal delivery of coolant in grinding zone can be achieved. Grinding process simulation shows that peak velocity achieved by at grinding point taper nozzle is 18.92m/s, by convergent divergent nozzle is 18.40 m/s and by spline nozzle 18.61 m/s. Grinding process Simulation and Experimentation on the bases of Taguchi L9 design have shown that for convergent divergent and taper nozzles parameters wheel speed and workpiece speed, have most significant effect on desired output responses velocity and dimensional accuracy on surface hardness number. For Spline nozzle, nozzle angle has most significant effect on most of the responses. Nozzle angle has shown major contribution for desired response of surface cracks. In whole study it is seen that wheel speed is most significant factor and nozzle tip distance as least significant factor

Circular crossection and rectangular cross section of Nozzles: Nozzles with rectangular crossection are also simulated and their peak velocities came out to be higher that circular crossection. But due to manufacturing difficulty of rectangular crossection circular crossection are considered.

5.4 FUTURE SCOPE

There is lot of scope for research in this area in future. For further research in this area Computer simulation can be used for simulating fluid flow through new nozzle designs. Designs of nozzles can be improved further by changing different crossections like rectangular elliptical etc. and also varying the input parameters. Simulation can be done by changing the type of fluid changing grades of wheels and by changing material of workpiece to analyse the flow behaviour of coolant through grinding zone.

REFERENCES

[1] Rowe W.B. (2009), Principles of Modern Grinding Technology, *William Andrew Applied Science Publishers, First Edition,* pp. 1-9, 25-26, 35-58.

[2] http://www.fischercustomknives.com/images/surface_grinding2.JPG

[3] http://en.wikipedia.org/wiki/Abrasive

[4] Bhattacharya A.(2007), Machining Science – Self Instruction Manual, *Department of Distance Education, Thapar University Patiala*, pp. 105-161.

[5] http://en.wikipedia.org/wiki/Grinding_wheel

[6] http://www.cumi-murugappa.com/useful-articles/grinding-wheels-types.html

[7] www.britannica.com/EBchecked/topic/1651/abrasive

[8] Singh M. (2010), An experimental validation of simulated coolant nozzles and their orientation in a grinding process, *ME Thesis, Thapar University*.

[9] http://en.wikipedia.org/wiki/Grinding_(abrasive_cutting)

[10] http://www.thesurfacegrinder.com/wp-content/uploads/2010/06/surface-grinder14.jpg

[11] http://www.lamottenterprises.com/images/headers/IMG_7019.png

[12] http://www.satbgmbh.de/1_GCX1.jpeg

[13] http://its.fvtc.edu/machshop1/coolant/cutfluids.htm

[14] http://en.wikipedia.org/wiki/Cutting_fluid

[15] http://www.mfg.mtu.edu/testbeds/cfest/fluid.html

[16] Oliveira J.F.G., Silva E.J., Guo C. and Hashimoto F. (2009), Industrial challenges in grinding, *CIRP Annals - Manufacturing Technology,* Volume 58, Issue 2, pp. 663-680.

[17] Malkin S. and Guo C. (2007), Thermal analysis of grinding, *CIRP Annals - Manufacturing Technology*, Volume 56, Issue 2, pp. 760-782.

[18] Jin T. and Stephenson D.J. (2008), A study of the convection heat transfer coefficients of grinding fluids, *CIRP Annals - Manufacturing Technology,* Volume 57, Issue 1, pp. 367-370.

[19] Tawakoli T., Westkaemper E. and Rabiey M. (2007), Dry grinding by special conditioning, *International Journal of Advanced Manufacturing Technology*, Volume 33, pp. 419–424

[20] Schumack M.R., Chung J.B., Schultz W.W., Kannatey-Asibu E. (1991), Analysis of fluid flow under a grinding wheel, *ASME Journal of Engineering for Industry,* Volume 113, Issue 2, pp. 190-197.

[21] Kiyak M. and Cakir O. (2010), Study of surface quality in dry and wet external cylindrical grinding, *International Journal of Computational Materials Science and Surface Engineering,* Volume 3, Issue 1, pp. 12-23.

[22] Ebbrell S., Woolley N. H., Tridimas Y. D., Allanson D. R., Rowe W. B.(*2000*), The effects of cutting fluid application methods on the grinding process, *International Journal of Machine Tools and Manufacture*, Volume 40, Issue 2, Pages 209-223.

[23] Webster J.A., Cui C, Mindek Jr. R.B. and Lindsay R. (1995), Grinding fluid application system design, *CIRP Annals - Manufacturing Technology,* Volume 44, Issue 1, pp. 333-338.

[24] Alves M.C. de S., Bianchi E.C. and de Aguiar P.R. (2008), Grinding of hardened steels using optimized cooling, *Ingeniare. Revista chilena de ingeniería,* Volume 16, Issue 1, pp.195-202.

[25] Cakir O., Yardimeden A., Ozben T. and Kilickap E. (2007), Selection of cutting fluids in machining processes, *Journal of Achievements in Materials and Manufacturing Engineering,* Volume 25, Issue 2, pp. 99-102.

[26] Choi H.Z., Lee S.W., Kim D.J. (2001), Optimization of cooling effect in the grinding with mist type coolant, *American Society for Precision Engineering Proceedings, Crystal City, Virginia*.

[27] Gviniashvili V.K., Woolley N.H. and Rowe W.B. (2004), Useful coolant flowrate in grinding, *International Journal of Machine Tools and Manufacture,* Volume 44, Issue 6, pp. 629-636.

[28] Irani R.A., Bauer R.J. and Warkentin A. (2005), A review of cutting fluid application in the grinding process, *International Journal of Machine Tools and Manufacture*, Volume 45, Issue 15, pp. 1696-1705.

[29] Powell J. W. (1979), The application of grinding fluid in creep feed grinding, *PhD Thesis, University of Bristol*.

[30] Hryniewicz P.,Szeri A.Z. and Jahanmir S. (2001), Application of lubrication theory to fluid flow in grinding: Part I—Flow between smooth surfaces, *Journal of Engineering for Industry Transactions of ASME,* Volume 123, pp. 94-100.

[31] Cameron A., R. Bauer R., Warkentin A. (2010), *An investigation of the effects of wheel-cleaning parameters in creep-feed grinding, International Journal of Machine Tools & Manufacture,* Volume 50, p.p .126–130.

[32] Sinot O., Chevrier P. , Padill P. (2006), Experimental simulation of the efficiency of high speed grinding wheel cleaning, *International Journal of Machine Tools & Manufacture,* Volume 46, pp. 170–175.

[33] Rowe W.B., Ebbrell S. and Morgan M.N. (2004), Process requirements for cost-effective precision grinding, *CIRP Annals - Manufacturing Technology*, Volume 53, Issue 1, pp. 255-258.

[34] Li C.H., Liu G.Y., Hou Y.L., Ding Y.C. and Lu B.H. (2009), Modeling and experimental investigation of useful flow-rate in flood delivery grinding, *Chinese Control and Decision Conference,* pp. 5467-5471.

[35] Monici R.D., Bianchi E.C., Catai R.E. and de Aguiar P.R. (2006), Analysis of the different forms of application and types of cutting fluid used in plunge cylindrical grinding using conventional and superabrasive CBN grinding wheels, *International Journal of Machine Tools and Manufacture,* Volume 46, Issue 2, pp. 122-131.

[36] Morgan M.N., Jackson A.R., Wu H., Baines-Jones V., Batako A., Rowe W.B. (2008), Optimization of fluid application in Grinding, *CIRP Annals - Manufacturing Technology,* Volume 57, Issue 1, pp. 363-366.

[37] Salonitis K. and Chryssolouris G. (2007), Cooling in grind-hardening operations, *International Journal on Advanced Manufacturing Technology,* Volume 33, pp. 285–297.

[38] Engineer F., Guo C. and Malkin S. (1992), Experimental measurement of fluid flow through the grinding zone**,** *Journal of Engineering for Industry, Americal Society of Mechanical Engineers. 114*, pp. 61–66

[39] Brinksmeier E., Tonshoff H. K., Czenkusch C. and Heinzel C. (1998), Modeling and optimization of grinding processes, *Journal of Intelligent Manufacturing,* Volume 9, Issue 4, pp. 303-314 .

[40] Sakakuraa M., Tsukamotob S., Fujiwarac T. and Inasakid I. (2006), Visual simulation of grinding process, *Intelligent Production Machines and Systems-2nd PROMS Virtual International Conference,* pp. 107-112.

[41] Nguyen T.A. and Butler D.L. (2005), Simulation of precision grinding process, part 1: generation of the grinding wheel surface, *International Journal on Machine Tools and Manufacture,* Volume 45, Issue 11, pp. 1321-1328.

[42] Singh M., Bhattacharya A., Batish A. and Singla V.K. (2010), Computational fluid simulation of coolant flow behaviour through different nozzles for effective cooling in

surface grinding*, 2nd National Conference on Precision Metrology,* SLIET Longowal, pp.18.

[43] Devillez A., Dudzinski D., Chevrier P., High speed grinding: An industrial research on lubrication parameters, *Laboratoire de Physique et Mecanique des Materiaux* UMR CNRS7554, ISGMP, Ile du Saulcy 57045 METZ cedex 01, France.

[44] Chryssolouris G., Tsirbas K.and Salonitis K. (2005), An analytical, numerical and experimental approach to grind hardening, *Journal of Manufacturing Processes,* Volume 7/ No. 1, pp. 1-9.

[45] Banerjee S., Ghosal S. and Dutta T. (2008), Development of a simple technique for improving the efficacy of fluid flow through the grinding zone, *Journal of Materials Processing Technology,* Volume 197, Issue 1-3, pp. 306-313.

[46] Baines-Jones V.A., Morgan M.N., Allanson D.R. , A.D.L Batako A.D.L , Grinding fluid delivery system design-Nozzle Optimization, *European Research Council Grant No: GR/S82350/01.*

[47] Shin'ichi N., Shin'ichi T (2000), Development of coolant method applied formed grinding. Test and performance evaluation of floating nozzle, *Journal of the Japan Society for Precision Engineering,* Volume 66, Issue 6, pp**.** 865-870.

[48] Morgan M. N. and Baines-Jones V. (2009), On the Coherent Length of Fluid Nozzles in Grinding, Key Engineering Materials-Progress in Abrasive and Grinding Technology, Volume 404, pp. 61-67.

[49] Webster J. A. (2006), Storrs, CT (US), *Coherent jet nozzles for grinding applications*, *US Patent Application Publication*, Publication number: US2006/7086930 B2, Saint-Gobain Abrasives, Inc..

[50] Ross P.J., Taguchi Techniques for Quality Engineering, *Mc Graw-Hill Book Company, Second Edition*, 1988.